Chem

CellPress

Article

Photochemical Perfluoroalkylation with Pyridine *N*-Oxides: Mechanistic Insights and Performance on a Kilogram Scale

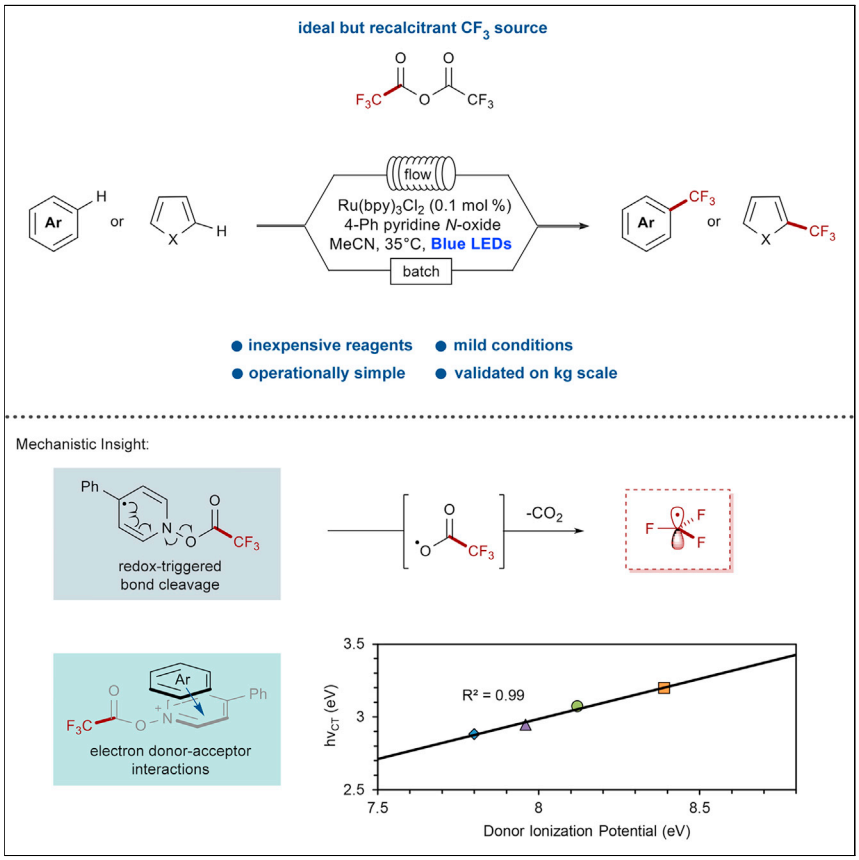

Fluorine incorporation has become a highly important feature of drug-synthesis technology in recent decades. Although a multitude of methods have been developed for small-scale discovery efforts, direct, truly scalable perfluoroalkylation has been generally limited to reactions involving superstoichiometric amounts of copper. In an effort to minimize the associated environmental cost of these processes, Stephenson and colleagues demonstrate an improved perfluoroalkylation method requiring minimal catalyst loadings and utilizing visible light on a kilogram scale.

Joel W. Beatty, James J. Douglas, Richard Miller, Rory C. McAtee, Kevin P. Cole, Corey R.J. Stephenson

crjsteph@umich.edu

HIGHLIGHTS

A range of electron-rich heterocycles are perfluoroalkylated in good yields

Mechanistic insights include the formation of electron donor-acceptor complexes

This inexpensive process has been validated on a kilogram scale in a flow reactor

Beatty et al., Chem *1*, 1–17
September 8, 2016 © 2016 Elsevier Inc.
http://dx.doi.org/10.1016/j.chempr.2016.08.002

Please cite this article in press as: Beatty et al., Photochemical Perfluoroalkylation with Pyridine *N*-Oxides: Mechanistic Insights and Performance on a Kilogram Scale, Chem (2016), http://dx.doi.org/10.1016/j.chempr.2016.08.002

Chem

CellPress

Article

Photochemical Perfluoroalkylation with Pyridine *N*-Oxides: Mechanistic Insights and Performance on a Kilogram Scale

Joel W. Beatty,[1] James J. Douglas,[2] Richard Miller,[2] Rory C. McAtee,[1] Kevin P. Cole,[2] and Corey R.J. Stephenson[1,3,*]

SUMMARY

The direct trifluoromethylation of (hetero)arenes is a process of high importance to the pharmaceutical industry. Many reagents exist for this purpose and have found widespread use in discovery efforts; however, the step-intensive preparation of these reagents and their corresponding cost have resulted in minimal use of these methods in large-scale applications. For the ready transition of direct trifluoromethylation methodologies to large-scale application, the further development of processes utilizing inexpensive CF_3 sources available on a metric ton scale is highly desirable. We report the use of pyridine *N*-oxide derivatives in concert with trifluoroacetic anhydride to promote a high-yielding and scalable trifluoromethylation reaction. Key mechanistic insights include the observation of electron donor-acceptor complexes in solution as well as a high dependence on photon flux. These observations have culminated in the application of this chemistry on a kilogram scale, demonstrating the utility of this reagent combination for preparative applications.

INTRODUCTION

The unique influence of fluorine incorporation on metabolic stability, lipophilicity, and pharmacokinetics has elevated organofluorine chemistry to a central role in the design of pharmaceuticals[1] and agrochemicals.[2] Since the late 1950s, fluorinated drugs have consisted of roughly 5%–15% of newly launched pharmaceuticals on a yearly basis,[3] and about 200 fluorine-containing drugs have been approved to date.[4] Commodity trifluoromethylated arenes are produced industrially through direct halogen-fluoride exchange of benzotrichlorides; however, this process is limited to methylated arenes of significant oxidative and thermal stability, which are chlorinated before being subjected to anhydrous hydrogen fluoride at elevated temperatures.[5] Alternative strategies are required to produce electron-rich and acid-sensitive benzotrifluorides, and halogen-fluoride exchange is not effective for higher-order perfluoroalkyl groups such as C_2F_5. Because of the challenges and limited substrate scope associated with direct C–F bond formation, many reagents for the direct incorporation of fluorinated groups have found widespread synthetic utility and strategic relevance.[6] This is particularly true for trifluoromethylation reagents,[7] which can be used to accomplish fluoroalkylations through nucleophilic,[8–15] electrophilic,[16–20] or radical[21–36] additions of CF_3 and are likewise used broadly in cross-coupling applications.[37–43]

Despite the undeniable value and utility of these compounds for discovery research, the use of many of these reagents in large-scale applications becomes less

The Bigger Picture

Perfluoroalkyl-containing compounds constitute an essential component for advancements in modern health care and the physical and life sciences, as demonstrated by an impressive cohort of fluorinated pharmaceuticals currently on the market. Current state-of-the-art methods for their manufacture require the use of complex, expensive, or environmentally damaging reagents such as fluoroform (a potent greenhouse gas). To facilitate the large-scale production of high-value fluorochemicals, the development of technologies that utilize inexpensive and environmentally benign fluorocarbon sources is essential. Furthermore, expanding the toolbox of methods for the synthesis of fluorine-containing molecules will facilitate their continued diversity, providing new functionality from this prominent class of compounds. This article details the use of perfluoroacid anhydrides in concert with sustainable visible light, thereby demonstrating a truly scalable alternative to current methods.

Please cite this article in press as: Beatty et al., Photochemical Perfluoroalkylation with Pyridine *N*-Oxides: Mechanistic Insights and Performance on a Kilogram Scale, Chem (2016), http://dx.doi.org/10.1016/j.chempr.2016.08.002

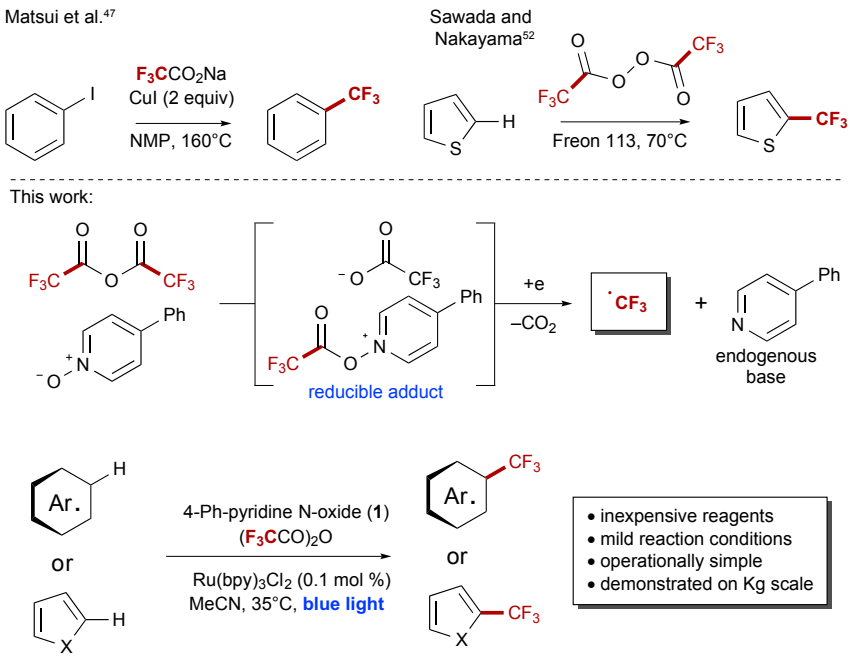

Scheme 1. Strategies for the Decarboxylation of Trifluoroacetate Derivatives

A notable precedent for the decarboxylation of trifluoroacetate derivatives includes the use of superstoichiometric copper and bis(trifluoroacetyl)peroxide. Freon 113 = 1,1,2-trichloro-1,2,2-trifluoroethane.

appealing when issues of reagent cost, environmental impact, and material sourcing are considered. Trifluoroacetic acid (TFA) and fluoroform (HCF_3) are the most attractive CF_3 source materials in these respects because they are inexpensive and available in large quantities; furthermore, the majority of reagents for trifluoromethylation are prepared from these materials, and the environmental impact of the direct use of TFA or HCF_3 is consequently minimal in comparison. The use of HCF_3 has been pioneered by Grushin for the preparation of $CuCF_3$ in high yields; it can be used in a mild, room-temperature trifluoromethylation of both halides and boronic acids.[39,44,45] Conversely, a broadly applicable and mild utilization of TFA as a CF_3 source has been slower to develop, given that forcing conditions have traditionally been required to promote this reactivity.

The ability to directly oxidize trifluoroacetate has yet to be accomplished by redox-based photocatalysis; this is a result of the high oxidation potential of trifluoroacetate, which is observed for the sodium salt at potentials greater than +2.4 V versus saturated calomel electrode (SCE) in MeCN.[46] These electrochemical potentials limit the compatibility of direct TFA oxidation with many substrates and solvents, and an alternative strategy is required for true synthetic utility. Matsui was the first to report the trifluoromethylation of aryl halides using sodium trifluoroacetate and superstoichiometric copper and noted that the polar decarboxylation of this salt was observed at temperatures above 140°C in the presence of CuI (Scheme 1).[47] Subsequent work by Buchwald has demonstrated that this reactivity can be accelerated significantly at increased temperatures.[48] Open-shell pathways for decarboxylation through oxidation to the corresponding carboxyl radical have been accomplished with relatively few reagents, including XeF_2,[49] mixtures of silver salts and persulfate,[50] and the UV-promoted decarboxylation of silver trifluoroacetate.[51] The requisite strength of these oxidants has limited the substrate scope of such

[1]Department of Chemistry, University of Michigan, Ann Arbor, MI 48109, USA

[2]Small Molecule Design and Development, Lilly Research Laboratories, Eli Lilly and Company, Indianapolis, IN 46285, USA

[3]Lead Contact

*Correspondence: crjsteph@umich.edu

http://dx.doi.org/10.1016/j.chempr.2016.08.002

Please cite this article in press as: Beatty et al., Photochemical Perfluoroalkylation with Pyridine *N*-Oxides: Mechanistic Insights and Performance on a Kilogram Scale, Chem (2016), http://dx.doi.org/10.1016/j.chempr.2016.08.002

transformations to electron-poor compounds to minimize their background degradation. A sole and notable exception to this theme is Sawada's use of bis(trifluoroacetyl) peroxide (Scheme 1), which, despite the use of Freon 113 (1,1,2-trichloro-1,2,2-trifluoroethane) as a solvent, has been shown to be the only TFA derivative capable of trifluoromethylating electron-rich heterocycles such as furans and thiophenes.[52,53]

Visible-light photoredox catalysis has shown remarkable utility for decarboxylative chemistry, with a number of leading examples from MacMillan,[54–60] Wallentin,[61] and Nicewicz[62] demonstrating the feasibility and compatibility of this approach. As a general principal, these methods involve the direct oxidation of a carboxylate by a redox-active photocatalyst and are limited to electron-rich aliphatic carboxylates with minimal exception.[63] Our interest in visible-light-mediated processes led us to pursue a photochemical means for the radical decarboxylation of trifluoroacetate derivatives, which optimally would be safely scalable, promoted within a readily accessible redox window, and occur at ambient temperature. We recently reported such a method through the use of pyridine *N*-oxide as a stoichiometric redox trigger to facilitate the photochemical decarboxylation of trifluoroacetic anhydride (TFAA).[64] As a conceptual alternative to direct carboxylate oxidation, the acylation of a pyridine *N*-oxide derivative allows the reaction manifold to be accessed through a reductive pathway. This design expands the scope of photoredox-mediated decarboxylation to electron-poor carboxylates, and through this method, a number of electron-rich and redox-sensitive substrates have been trifluoromethylated using TFAA. At the outset of this work, the use of pyridine *N*-oxide remained untested for scale-up applications beyond 20 g, and the yields of this process were not competitive with those of popular and established trifluoromethylation methods such as MacMillan's use of trifluoromethanesulfonyl chloride with photoredox catalysis[26] or Baran's $Zn(O_2SCF_3)_2$/tBuOOH system.[29,30] Driven by an improved mechanistic understanding of this process, we have identified 4-phenylpyridine *N*-oxide as an efficient redox trigger with correspondingly improved reaction yields and detail the application of this methodology on a 1.2 kg scale in a photochemical flow reactor.

RESULTS AND DISCUSSION

Optimization of *N*-Oxide Electronics

Although pyridine *N*-oxide is readily available and presents minimal cost when implemented on scale, we recognized that the electronics of the *N*-oxide are influential in determining reactivity. Both the redox potential of the *N*-oxide/TFAA adduct and the affinity of the CF_3 radical for the pyridine byproducts could be tuned through pyridine functionalization, and other mechanistic factors including reaction quantum yield and fluorescence quenching rates are expected to be influenced by these changes. Electron-poor and highly conjugated *N*-oxides are expected to be more readily reduced, and so using mesitylene (**2**) as the model substrate, we began by investigating a number of electronically tuned pyridine *N*-oxides. This process initially yielded mixed results, such that a large number of pyridine derivatives proved less efficient than pyridine *N*-oxide itself (Table 1, entries 1–12). Inclusion of electron-withdrawing substituents did not improve reaction efficiency (entries 2–4), and electron-donating substituents were equally ineffective (entries 5–7). Alkyl pyridines with substituents in the 2 and 4 positions are well-known substrates of the Boekelheide reaction, and as such were excluded from our investigation.[65] Improved results were obtained when 4-phenylpyridine *N*-oxide (**1**) was used, providing 10% more mono-functionalized mesitylene (entry 9). Alternative biaryl *N*-oxides did not perform as efficiently (entries 10–12).

Please cite this article in press as: Beatty et al., Photochemical Perfluoroalkylation with Pyridine *N*-Oxides: Mechanistic Insights and Performance on a Kilogram Scale, Chem (2016), http://dx.doi.org/10.1016/j.chempr.2016.08.002

Table 1. Optimization of *N*-Oxide Electronics

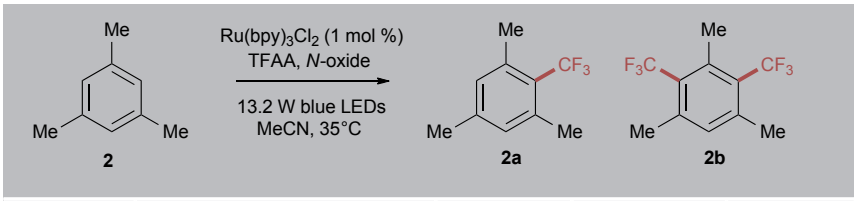

Entry[a]	*N*-Oxide	Equiv[b]	Yield 2a[c]	Yield 2b[c]
1	pyridine	1	44%	<5%
2	4-Cl-pyridine	1	16%	ND
3	4-CN-pyridine	1	25%	<5%
4	4-NO_2-pyridine	1	ND	ND
5	4-^{t}Bu-pyridine	1	27%	ND
6	3,5-dimethoxypyridine	1	<10%	ND
7	4-methoxypyridine	1	<10%	ND
8	quinoline	1	ND	ND
9	4-phenylpyridine (**1**)	1	54%	<5%
10	2-phenylpyridine	1	24%	<5%
11	2,2′-bipyridine monooxide	1	45%	<5%
12	2,2′-bipyridine bisoxide	0.5[d]	29%	<5%
13[e]	pyridine	1	ND	ND
14[e]	**1**	1	<10%	ND
15	pyridine	2	47%	<5%
16	**1**	2	59%	16%
17[f]	pyridine	2	57%	12%
18[f]	**1**	2	62%	16%
19[f,g]	pyridine	2	57%	6%
20[f,g]	**1**	2	65%	14%
21[e,f]	**1**	1	40%	<5%
22[e,f]	**1**	2	55%	<5%
23[e,f,h]	**1**	1	ND	ND
24[e,f,i]	**1**	1	74%	<5%

ND, not detected.
[a]Optimization reactions were performed on a 0.8 mmol scale in 2.0 mL of MeCN for a 12 hr reaction time.
[b]For every X equiv of *N*-oxide, X.1 equiv of TFAA was used.
[c]Yields obtained versus trifluorotoluene as ^{19}F NMR internal standard.
[d]1.1 equiv of TFAA.
[e]No catalyst.
[f]Degassed.
[g]0.1 mol % $Ru(bpy)_3Cl_2$.
[h]Light excluded.
[i]10.0 equiv of mesitylene (**2**).

Exclusion of the catalyst from these reaction conditions was found to provide only trace amounts of **2** when 4-phenylpyridine *N*-oxide was used (entries 13 and 14), and increased equivalents of *N*-oxide and TFAA in the presence of catalyst resulted in improvements to the overall yield, with concomitant increases in the amount of **2b** formed (entries 15 and 16). The formation of **2b** resulted from further functionalization of **2** and as such was not considered a drawback at this point of reaction development. Degassing of the reaction solution was found to improve

Please cite this article in press as: Beatty et al., Photochemical Perfluoroalkylation with Pyridine *N*-Oxides: Mechanistic Insights and Performance on a Kilogram Scale, Chem (2016), http://dx.doi.org/10.1016/j.chempr.2016.08.002

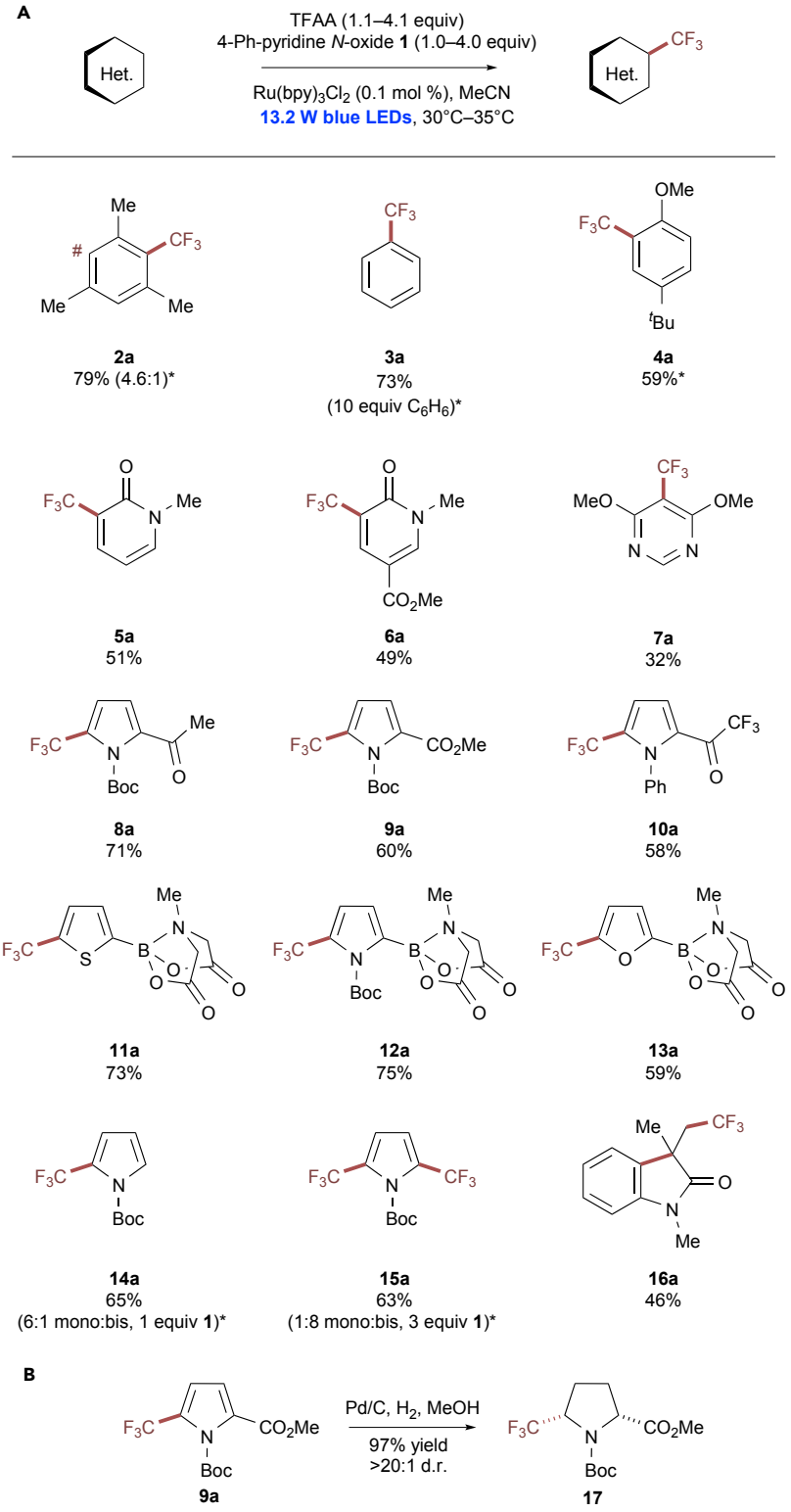

Scheme 2. Trifluoromethylation of (Hetero)arenes with Trifluoroacetic Anhydride

(A) Trifluoromethylation of electron-rich substrates with trifluoroacetic acid. All reactions were performed on a 0.8 mmol scale at 0.4 M concentration. Isolated yields are reported in all cases

Please cite this article in press as: Beatty et al., Photochemical Perfluoroalkylation with Pyridine *N*-Oxides: Mechanistic Insights and Performance on a Kilogram Scale, Chem (2016), http://dx.doi.org/10.1016/j.chempr.2016.08.002

Scheme 2. *Continued*

except for instances of product volatility, in which case yields are reported as ^{19}F NMR internal standard yield. *Internal standard yield. See also Figures S4–S13.

(B) Hydrogenation of pyrrole products can yield high-value perfluoroalkylated pyrrolidines in a diastereoselective fashion. See also Figures S22–S24.

the yield of functionalized mesitylene (entries 17–18); the magnitude of improvement resulting from the exclusion of oxygen has been found to be both *N*-oxide and substrate dependent. Lowering the catalyst loading to 0.1 mol % resulted in comparable yields (entries 19 and 20). Control experiments demonstrated that visible-light irradiation in the absence of oxygen and catalyst promoted an appreciable background reaction with **1** (entries 21 and 22), whereas complete exclusion of light provided no reactivity (entry 23). It should be noted that this background reactivity is predicated on the degassing of the solution (entry 14 versus 21), and background trifluoromethylation is only at trace levels with unfunctionalized pyridine *N*-oxide. It is also clear that the formation of **2b** is an artifact of substrate stoichiometry (entry 24).

Perfluoroalkylations of Electron-Rich (Hetero)arenes

With optimized conditions in hand, the trifluoromethylation of a number of electron-rich arenes and heterocycles was performed using 4-phenylpyridine *N*-oxide (**1**; Scheme 2A). The **1**/TFAA adduct exhibited peak reduction at −0.91 V versus SCE in MeCN, which is 190 mV more positive than the measured reduction potential of the pyridine *N*-oxide adduct (E_{red} = −1.10 V versus SCE in MeCN; see also Figures S34 and S35). Notably, reaction times were significantly shorter when using **1**, and substrate was generally consumed within 2–6 hr. Yields for electron-rich heterocycles were particularly high, and yields of trifluoromethylated products were significantly improved over our previous efforts (up to 28%). Five-membered heterocycles were particularly amenable to the reaction conditions, and acid-labile Boc groups were unaffected by the use of TFAA. In addition, methyliminodiacetic acid (MIDA)-protected boronate esters were well tolerated.[66] The MIDA boronate substrates generally required longer reaction times (12–15 hr) because the conversion of the final 5%–10% of the substrate proceeded slowly. This could be partially overcome through the use of additional equivalents of the *N*-oxide/anhydride reagent. Regardless, remaining starting material for the MIDA boronate substrates invariably co-eluted with the trifluoromethylated products, causing full conversion—and consequently longer reaction times—to be essential for the isolation of clean material. The trifluoromethylated pyrrole **9a** was subjected to an efficient, diastereoselective hydrogenation reaction to provide the trifluoromethylated proline derivative **17** (Scheme 2B), which has been proposed as a potential isostere of pyroglutamic acid.[67]

We next turned our attention to alternative perfluoroalkylation reactions through the use of pentafluoropropionic anhydride (PFPA), which resulted in efficient perfluoroethylation of select substrates in higher yields than the corresponding trifluoromethylations (Scheme 3). Although the reasons behind the differing relative efficiencies of these two processes are not currently understood, the CF_3 and C_2F_5 radicals have been demonstrated to possess surprisingly different kinetic profiles for a number of addition reactions.[68] The reduction potential of the **1**/PFPA adduct was measured to be −0.88 V versus SCE in MeCN, which is not significantly different from the analogous TFAA adduct (see also Figure S36). Most higher-order radical perfluoroalkylation reactions involve the use of perfluoroalkyl iodides,[6] which are generally synthesized from the corresponding fluorinated acids.[69,70]

Please cite this article in press as: Beatty et al., Photochemical Perfluoroalkylation with Pyridine *N*-Oxides: Mechanistic Insights and Performance on a Kilogram Scale, Chem (2016), http://dx.doi.org/10.1016/j.chempr.2016.08.002

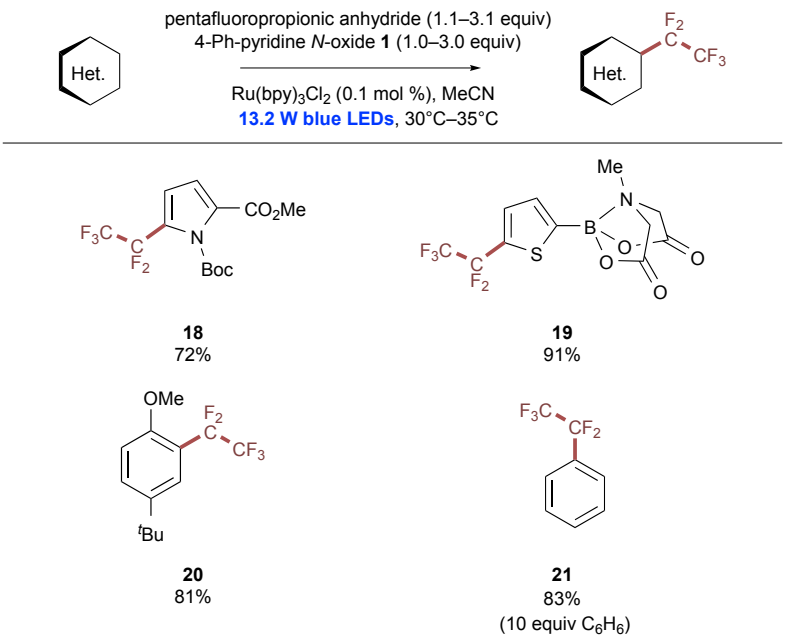

Scheme 3. Pentafluoroethylation of (Hetero)arenes with Pentafluoropropionic Anhydride
All reactions were performed on a 0.8 mmol scale at 0.4 M concentration. Isolated yields are reported in all cases. See also Figures S14–S19.

Expansion of this methodology for the generation of larger perfluoroalkyl radicals predictably becomes less atom-economical as larger and larger acid equivalents are produced as byproducts. Although smaller acid chlorides are volatile (F_3CCOCl bp = –27°C; F_5C_2COCl bp = 7°C–9°C), the use of heptafluorobutyryl chloride **22** in place of its corresponding anhydride **23** (E_{red} of the **1**/**23** adduct = −0.93 V versus SCE in MeCN; see also Figure S37) provided a comparable yield of pyrrole **24** (Scheme 4). The slightly lower yield obtained with the acid chloride can likely be attributed to incomplete solubility of the reagent in solution.

Mechanistic Investigations

With particular interest in elucidating the mechanism of the light-promoted trifluoromethylation background reaction (Table 1, entries 21 and 22), we turned our attention to the absorption of light by other species in solution. At 0.4 M concentration and in the absence of catalyst, the reaction solution containing **1**, TFAA, and mesitylene (**2**) displayed a significant absorbance peak centered at 390 nm, which trailed significantly into the upper 400 nm range (Figure 1A). This absorbance was found to be highly concentration dependent and diminished significantly at lower concentrations (see Supplemental Information). Mesitylene (**2**) and TFAA predictably displayed no absorbance in the visible region of the spectrum, with strictly baseline absorbance above 350 nm. 4-Phenylpyridine *N*-oxide **1** showed an absorbance profile trailing into the visible region, and this absorbance was not significantly altered in the presence of **2**. A mixture of TFAA and **1** in a 1.1:1.0 ratio displayed significant absorbance in the visible region, and a closer analysis provided a number of mechanistically relevant insights.

Because light absorption depends on the presence of TFAA, the relative equivalents of TFAA were varied in the presence of 1.0 equiv of **1** at 0.4 M concentration in MeCN (Figure 1B). The solution displayed the largest absorbance in the visible region when near-equimolar amounts (0.5–1.1 equiv) of TFAA were used and exhibited shifting

Please cite this article in press as: Beatty et al., Photochemical Perfluoroalkylation with Pyridine *N*-Oxides: Mechanistic Insights and Performance on a Kilogram Scale, Chem (2016), http://dx.doi.org/10.1016/j.chempr.2016.08.002

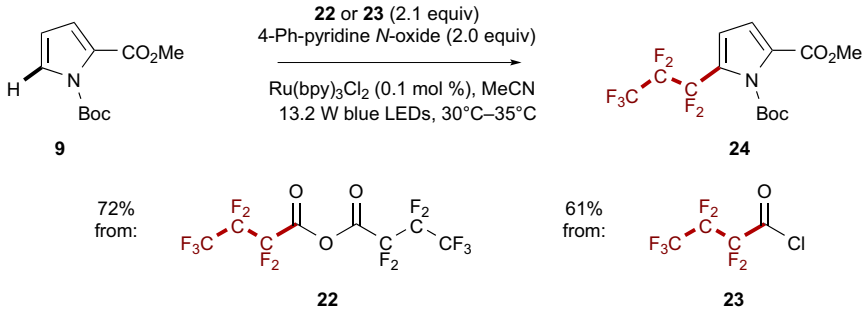

Scheme 4. Heptafluoropropylation of (Hetero)arenes with Acid Anhydrides and Chlorides
All reactions were performed on a 0.8 mmol scale at 0.4 M concentration. Isolated yields are reported in all cases. See also Figures S20 and S21.

λ_{max} values depending on the quantities of TFAA used. Upon the addition of larger amounts (2–8 equiv), the absorbance of the solution stabilized at 367 nm, and subtle changes in absorbance shape were likely due to solvent effects from large excesses of TFAA. These results suggest that the acylation of **1** is a process in equilibrium, which can be forced toward complete acylation through the use of excess TFAA. Although this equilibrium behavior was expected, the large absorbance signals observed in the presence of less TFAA merited closer attention.

To further study this phenomenon, we investigated the possible interaction of the substrate with the fully acylated reagent. The combination of **1**, **2**, and TFAA (1:1:2 ratio; Figure 2A) revealed a strongly absorbing signal in the visible region, and we postulated that this new absorbance could be attributed to an electron donor-acceptor (EDA) interaction.[71] To probe this relationship further, we measured the absorbance profile of the acylated reagent with a number of electron-rich arenes of known ionization potential (I_p), including naphthalene (I_p = 8.12 eV),[72] 1,3,5-trimethoxybenzene (I_p = 7.96 eV),[73] and 2-methoxynaphthalene (I_p = 7.80 eV).[74] EDA complexes have a characteristically linear relationship between their charge-transfer absorbance energy ($h\nu_{CT} \propto \lambda_{max}$) and the ionization potential (I_p) of the constituent donor.[75] The absorbance of the reagent and mesitylene (I_p = 8.39 eV)[76] combination was found to be energetically co-linear with the $h\nu_{CT}$ of the other arenes tested (Figure 2B), providing strong evidence for an EDA interaction.

With significant evidence for the presence of EDA interactions in this reagent system, the large, red-shifted absorbance profiles in the absence of substrate (Figure 1B) may be partially explained by analogy. A large excess of TFAA minimizes the broad absorbance of the reagent mixture in the visible region, whereas fewer equivalents result in the highest magnitude of absorbance. We tentatively propose that these absorbance signals represent an EDA interaction between acylated and non-acylated pyridine *N*-oxide, the latter of which is almost fully consumed upon the addition of 2.0 equiv of TFAA. This is, however, an oversimplified mechanistic picture, given that the shifting values of λ_{max} (and consequently $h\nu_{CT}$) between 0.5 and 1.1 equiv of TFAA imply a more fundamental structural change than the simple equilibrium of two distinct chemical states. It is possible that oligomeric complexation is occurring, in which multiple EDA complexes form macromolecular architectures with altered photophysical properties. Further efforts to elucidate this process are currently underway.

EDA complexes have found a number of elegant applications in organic synthesis; for example, a number of leading examples from Melchiorre detail the ability

Please cite this article in press as: Beatty et al., Photochemical Perfluoroalkylation with Pyridine *N*-Oxides: Mechanistic Insights and Performance on a Kilogram Scale, Chem (2016), http://dx.doi.org/10.1016/j.chempr.2016.08.002

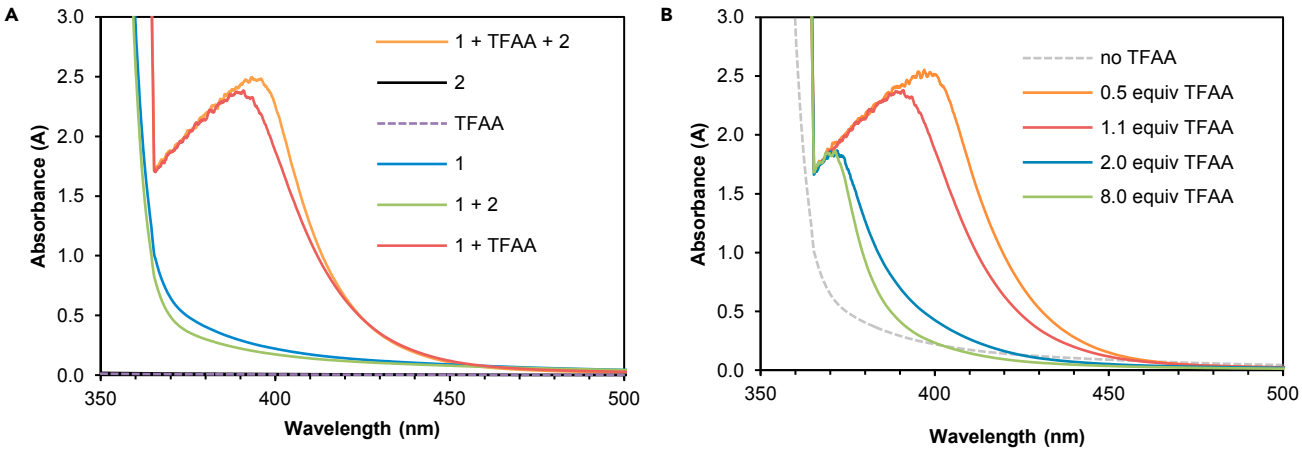

Figure 1. Optical Absorption Spectra of Individual Reaction Components

Measurements were obtained at experimentally relevant concentrations (0.4 M) in MeCN in 1 cm path quartz cuvettes. See also Figure S33.

(A) Varied combinations of reaction components in the absence of $Ru(bpy)_3Cl_2$. Combinations of 4-phenylpyridine *N*-oxide (**1**) and TFAA display strong absorbance in the visible region both in the presence and absence of mesitylene (**2**).

(B) Dramatic changes in absorbance are observed with varied amounts of TFAA in the presence of 1 equiv of **1**.

to utilize these interactions in lieu of a photocatalyst.[77–81] For this work, although a significant background reaction was observable for mesitylene (Table 1, entries 20 and 21), the EDA background reaction was not general and was largely dependent on the substrate ionization potential (Figure 2). For example, benzene (I_p = 9.24 eV)[76] displayed no EDA complex absorbance in the visible spectrum, and only the absorbance of the fully acylated reagent could be observed at reaction concentrations. As a consequence, although the use of photocatalyst provided trifluorotoluene in a 73% yield, the reaction without photocatalyst and with 2.0 equiv of TFAA provided merely 11% yield upon irradiation with blue light (Scheme 5). This background reactivity is likely due to direct absorbance of light by the fully acylated reagent, and we further investigated this possibility through irradiation at longer wavelengths where the reagent does not absorb. Interestingly, when green light (510–520 nm) was used instead of blue light, the background reactivity without catalyst dropped significantly and was undetectable for benzene.

EDA complexes undergo photoinduced electron transfer on irradiation on an extremely fast timescale.[82] Although intramolecular donor-acceptor dyads have been used as photosensitizers,[83] literature precedence suggests that the photoexcited state of the intermolecular EDA complexes in question are extremely short lived, to the point where productive intermolecular collisions with the photoexcited state are not likely to occur. Lorance et al.[84] have studied the rates of back-electron transfer and fragmentation for a series of reduced *N*-methoxypyridinium analogs and report impressively fast rates for each of these processes. Specifically, reduced *N*-methoxy-4-phenylpyridinium demonstrated rates of back-electron transfer and fragmentation of $1.5 \times 10^{12}\ s^{-1}$ and $2.7 \times 10^{11}\ s^{-1}$, respectively. Such processes are faster than the limits of diffusion; therefore, the likelihood of productive intermolecular catalysis without a built-in fragmentation pathway with these complexes is small.

Mechanistically, a complex picture emerges from the data. In the presence of TFAA, **1** is acylated, although this event is an equilibrium that is moderately populated on either

Please cite this article in press as: Beatty et al., Photochemical Perfluoroalkylation with Pyridine *N*-Oxides: Mechanistic Insights and Performance on a Kilogram Scale, Chem (2016), http://dx.doi.org/10.1016/j.chempr.2016.08.002

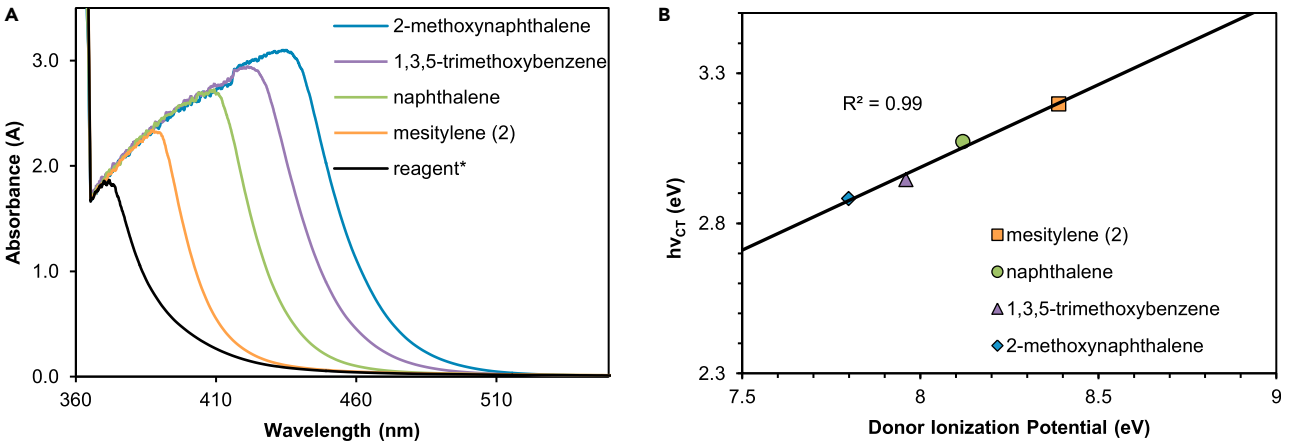

Figure 2. Evidence for the Formation of EDA Complexes

Measurements were obtained at experimentally relevant concentrations (0.4 M) in MeCN in 1 cm path quartz cuvettes.

(A) Optical absorbance spectra of various electron-rich arenes in the presence of 4-phenylpyridine *N*-oxide (1.0 equiv) and TFAA (2 equiv). *Reagent indicates the *N*-oxide/TFAA mixture in the absence of an electron-rich arene in solution.

(B) The charge-transfer energy ($h\nu_{CT}$) of each absorbance trends linearly with each donor arene's ionization potential.

side of the equation unless an excess of TFAA (≥ 1.1 equiv) is used (Scheme 6). This acylated species can readily quench the photoexcited catalyst Ru^{2+}*, and the reduced reagent proceeds to fragment to a carboxyl radical along with 4-phenylpyridine (PhPyr). The carboxyl radical readily extrudes CO_2 to form the CF_3 radical as the key reactive intermediate. In addition to the $Ru(bpy)_3Cl_2$-mediated pathway, the reaction may also proceed through the photoexcitation of EDA complexes in solution, which we propose may arise via complexation of the acylated pyridine *N*-oxide derivative **25** with either an additional equivalent of **1** or with a sufficiently electron-rich arene such as **2**. Photoexcitation of either complex prompts intermolecular electron transfer, which can either be rendered unproductive through back-electron transfer or proceed toward product by prompting the fragmentation of the acylated reagent to form the CF_3 radical. Subsequent addition to an electron-rich pi system results in selective formation of the product after re-aromatization. Re-aromatization may occur through oxidation and deprotonation of the substrate or through the reverse sequence.[85]

A final mechanistic consideration is whether propagative behavior is significantly operative in the reaction. Measurement of the quantum yield under irradiation at 436 nm revealed a quantum yield (Φ) of 0.87, signifying that less than 1 equiv of product is produced by every photon absorbed by the reaction.[86] Although this does not conclusively determine that no propagation occurs in the reaction, it is likely that the re-aromative oxidation to form product is accomplished by the photocatalyst or an oxidized arene such as $\mathbf{1}^{+\cdot}$ or $\mathbf{2}^{+\cdot}$ rather than by another equivalent of **25**.

Application on a Kilogram Scale

At the inception of this project, one of the key goals was to demonstrate a scalable methodology to access trifluoromethylated substrates in up to kilogram quantities. Our original report included a reaction run at 18.3 g scale in a flow system, because it was shown that reaction with 100 g in a batch did not surpass 35% conversion (3.3 mmol hr^{-1}). Upon further investigation, including determination of the quantum yield to be <1,[87] we surmised that a high photon flux was required to achieve high

Please cite this article in press as: Beatty et al., Photochemical Perfluoroalkylation with Pyridine *N*-Oxides: Mechanistic Insights and Performance on a Kilogram Scale, Chem (2016), http://dx.doi.org/10.1016/j.chempr.2016.08.002

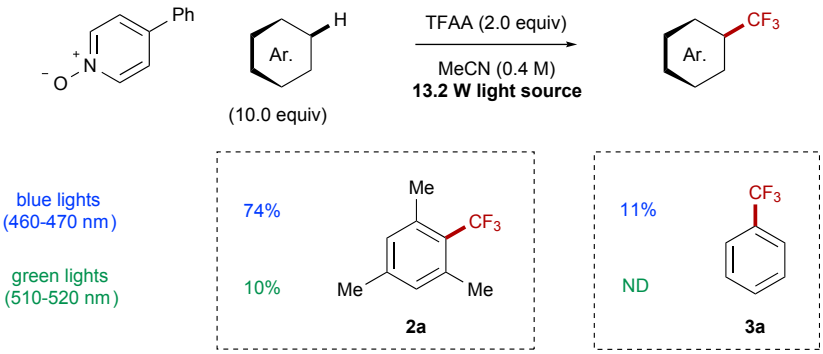

Scheme 5. Effects of Wavelength on Reaction Progress

The observed EDA-promoted background reaction is highly substrate specific. See also Figure S25.

conversions with reasonable reaction times in flow. Currently available commercial flow systems are capable of providing this increased flux; however, limited reactor volumes limit productivity, and a prohibitive economic penalty is associated with scaling out.[88–90] The original design of a continuous flow reactor for UV photochemistry by Berry, Booker-Milburn, and coworkers.[91] has proven general for visible-light irradiation, and there have been several recent examples.[92–94] This method appears to be the most promising avenue for conducting visible-light reactions at a preparative scale on complex substrates, as shown by a series of pioneering examples by Merck, most notably for the synthesis of elbasvir.[95] Following this general template, we constructed our reactor within the design principles of low cost, easy construction from commercially available parts, and that it should fit within a standard walk-in fume hood.[96] The reactor consisted of blue LED lights contained within a glass beaker wrapped with a single layer of perfluoroalkoxy (PFA) tubing (1.6 mm inner diameter) around the outside, giving a volume of approximately 150 mL (Figure 3A, see also Figures S1 and S2). This assembly was housed within a steel casing with both cavities fully filled with water to provide both cooling of the lights and control of the reaction temperature. Although LED lights are generally considered to have low energy consumption, they can still generate significant heat. In our experience on a larger scale, the use of water provides a more efficient and controllable cooling method than air, which is commonly used on a small scale. Finally, we utilized peristaltic pumps because of their relative low cost and proven reliability over extended operating times.

We chose to demonstrate the viability of this reactor by using Boc-pyrrole substrate **9** and conditions employing pyridine *N*-oxide, because all the reagents could be obtained at the quantities required for a kilogram scale (Figure 3B). Using 0.1 mol % $Ru(bpy)_3Cl_2$ and 2.0 equiv of the pyridine *N*-oxide/TFAA adduct, a residence time of 30 min at 45°C was optimal to provide a balance of productivity and conversion, leading to internal assay yields of 60%–65% with <10% of the starting material remaining. These conditions were operated continuously[97] for 48 hr to process 1.2 kg of pyrrole **9**, and assay yields remained constant between 60% and 65%, representing a consumption of **9** of 25 g hr^{-1} (109 mmol hr^{-1}; Figure 4). After workup and isolation, 0.95 kg of pyrrole **9a** (81% purity and 50% yield) was obtained, providing a final productivity of 87.2 mmol hr^{-1}, which greatly surpassed our previous demonstrations in both batch (4.2 mmol hr^{-1}) and flow (14.2 mmol hr^{-1}). Furthermore, the useful pyrrole building block **26** could be obtained in >98% purity as a crystalline solid after an unoptimized Boc deprotection in 77% yield (Figure 3C).[98] The demonstration of productivity close to 0.5 kg per day[99] clearly

Please cite this article in press as: Beatty et al., Photochemical Perfluoroalkylation with Pyridine *N*-Oxides: Mechanistic Insights and Performance on a Kilogram Scale, Chem (2016), http://dx.doi.org/10.1016/j.chempr.2016.08.002

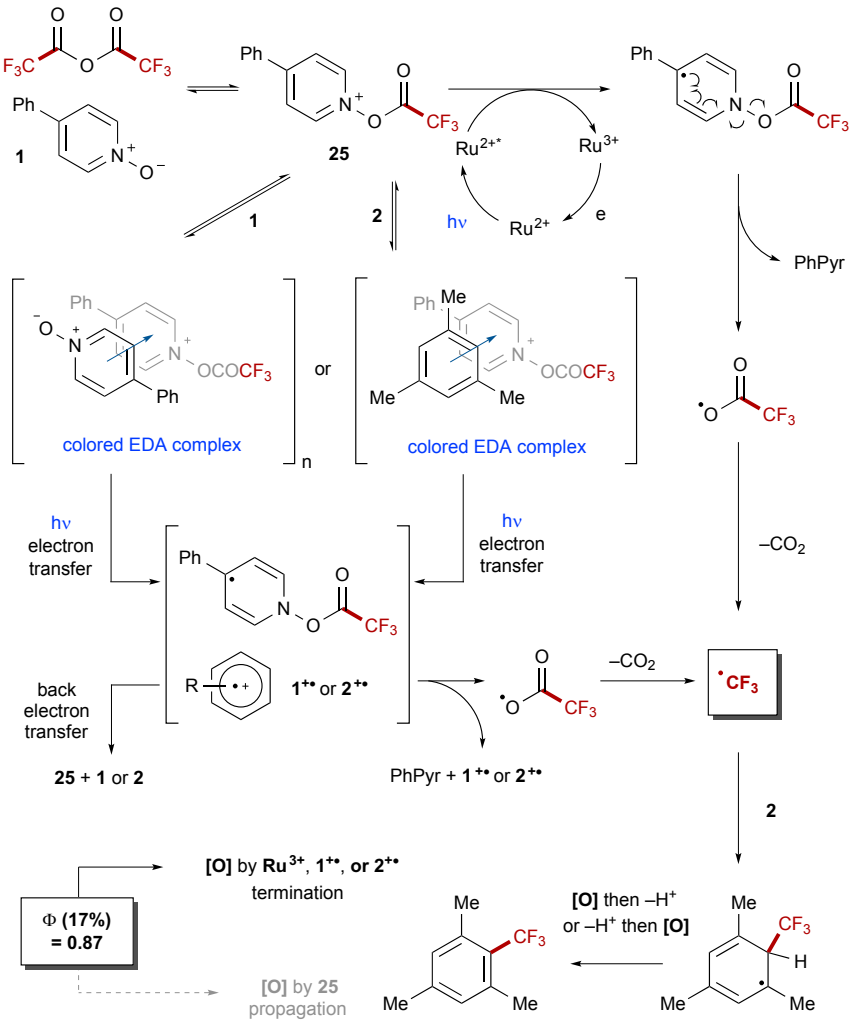

Scheme 6. Mechanistic Proposal

With the formation of EDA complexes in solution, two distinct mechanistic opportunities present themselves for photochemical reaction progress. PhPyr = 4-phenylpyridine. See also Figures S38–S41.

defines this as a proof of concept for the scale-up of visible-light photochemical reactions in flow using simple equipment. The limiting factor of this reactor's construction was the requirement for high photon flux and the necessity that the lights be available commercially. Preliminary studies have indicated that a reactor with increased internal reflectance provides a decreased residence time (30–20 min). Furthermore, a customizable light source of higher photon flux may allow an increased inner diameter (leading to an increased reactor volume), further boosting productivity.[100] Finally, because of the relatively low cost of this reactor, scaling out to meet higher production requirements could be economically viable.

Conclusion

The utility of pyridine *N*-oxides as safe, practical, and inexpensive reagents for the scalable decarboxylation of TFAA under mild reaction conditions has been demonstrated. The nature of the pyridine moiety has been shown to exert a profound influence on the reaction mechanism, given that further conjugation and electrophilicity of the pyridinium

Please cite this article in press as: Beatty et al., Photochemical Perfluoroalkylation with Pyridine *N*-Oxides: Mechanistic Insights and Performance on a Kilogram Scale, Chem (2016), http://dx.doi.org/10.1016/j.chempr.2016.08.002

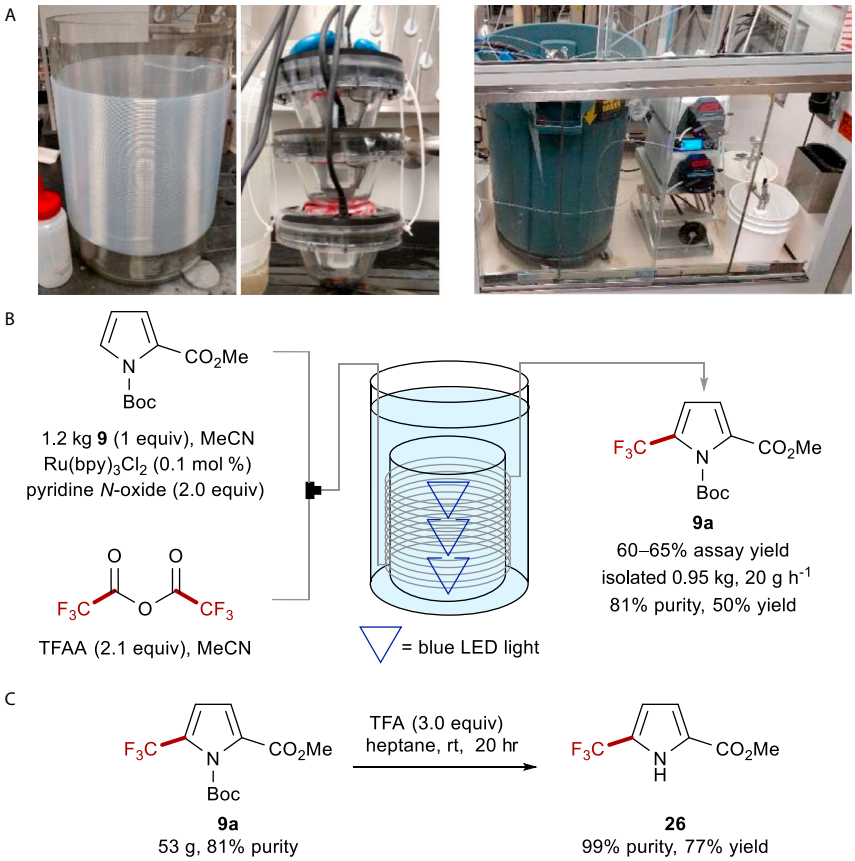

Figure 3. Kilogram-Scale Trifluoromethylation in Flow

Pyrrole **9** was subjected to optimized trifluoromethylation conditions on a kilogram scale.

(A) Using a customized flow reactor, 1.2 kg of pyrrole **9** was processed within 48 hr to provide the desired product in a 60%–65% assay yield. The reactor was immersed in water and cooled with a glycol chiller to maintain a steady temperature profile at room temperature. See also Figures S25–S29.

(B) The reactor was constructed from PFA tubing with an internal volume of 150 mL (left). The three blue LEDs (middle) were placed in the middle of the reactor, and the setup was submerged in the cooling bath and covered during the run (right). See also Figures S1 and S2.

(C) The crude reaction product could be recrystallized to 99% purity after an unoptimized Boc deprotection. See also Figures S31 and S32.

ring system promotes the formation of photoactive EDA complexes. This mechanistic insight has the potential to eliminate the need for transition-metal complexes in this methodology, and further research into this possibility is underway.

EXPERIMENTAL PROCEDURES

General Trifluoromethylation Procedure

To a 2 dram vial equipped with a stir bar was added 4-phenylpyridine *N*-oxide (0.8–3.2 mmol, 1.0–4.0 equiv) and substrate (0.80 mmol) followed by 500 μL of a 1.2 mg/mL solution of $Ru(bpy)_3Cl_2 \cdot 6H_2O$ (0.6 mg, 0.1 mol %) in MeCN. The combined materials were then diluted with dry MeCN (1.5 mL, total volume 2 mL MeCN) and stirred briefly to form a heterogeneous solution; the *N*-oxide was only partially dissolved when it was used in higher equivalents. The reaction was sparged with nitrogen gas for 30 s with a glass pipette, and then trifluoroacetic anhydride (0.88–3.28 mmol, 1.1–4.1 equiv) was added under a stream of nitrogen before the vial was quickly sealed with a rubber-lined screw-on cap. The trifluoroacetic anhydride solubilized any remaining solid *N*-oxide within seconds to minutes. Three 4.4 W LED light strips were turned on, and the reactions

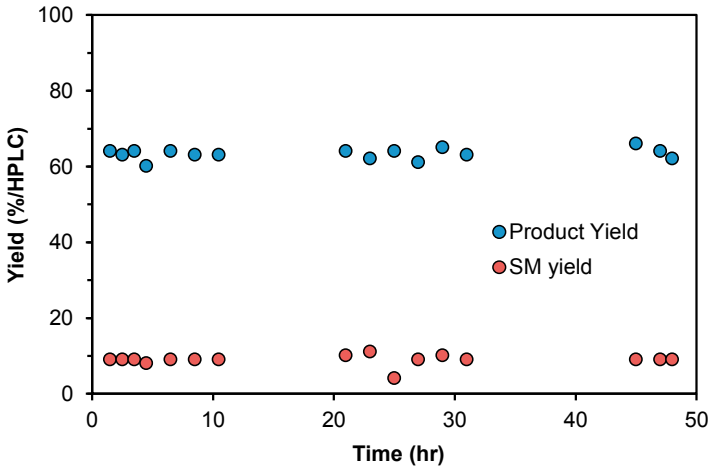

Figure 4. Reaction Profile over Time
The reaction was monitored by high-performance liquid chromatography assay over the 48 hr of continuous processing.

were allowed to proceed for 3–12 hr before removal of the light source (see Figure S3 for the geometry of the LED setup). Upon completion of the reaction, trifluorotoluene (98 μL, 0.80 mmol) was added as a stoichiometric internal standard. A sample of the reaction was removed and diluted with $CDCl_3$ for nuclear magnetic resonance (NMR) analysis, and the trifluorotoluene signal was referenced to δ = −63.72. Workup conditions were substrate dependent.

9a: 1-(*tert*-Butyl) 2-Methyl 5-(Trifluoromethyl)-1*H*-pyrrole-1,2-dicarboxylate

After the general procedure, using 4-phenylpyridine *N*-oxide (273.9 mg, 1.6 mmol, 2.0 equiv) and TFAA (237 μL, 1.68 mmol, 2.1 equiv), the reaction was run for 3 hr. ^{19}F NMR analysis of the crude reaction mixture versus the injected trifluorotoluene standard revealed the title compound in a 63% yield. The reaction was partitioned with 1 N HCl and diluted with dichloromethane. The organic phase was separated, washed with saturated $NaHCO_3$ and brine, and dried over sodium sulfate before filtering and concentrating. The crude reaction mixture was purified on silica gel with 10%–30% dichloromethane in hexanes to yield the title compound as a clear oil.

Yield: 0.140 g (60%); ^1H NMR (700 MHz, $CDCl_3$): δ = 6.80 (d, *J* = 3.8 Hz, 1H), 6.61 (d, *J* = 3.8 Hz, 1H), 3.87 (s, 3H), 1.61 (s, 9H); ^{19}F NMR (470 MHz, $CDCl_3$): δ = −59.66; ^{13}C NMR (175 MHz, $CDCl_3$): δ = 160.2, 147.2, 127.8, 125.6 (q, JC-F = 125.6 Hz), 119.9 (q, JC-F = 267 Hz), 116.1, 112.8 (q, JC-F = 3.6 Hz), 86.9, 52.1, 27.1; high-resolution mass spectrometry (EI+) *m/z*: $[M - Boc + H]^+$ calculated 193.0351, found 193.0351. IR (neat): ν = 2,989, 1,777, 1,728, 1,558, 1,373, 1,247, 1,123.

ACCESSION NUMBERS

The structure of pyrrolidine **17** in this article has been deposited in the Cambridge Crystallographic Data Center under accession number CCDC: 1485256.

SUPPLEMENTAL INFORMATION

Q6 Supplemental Information includes Supplemental Experimental Procedures, 41 figures, and 1 data file and can be found with this article online at http://dx.doi.org/10.1016/j.chempr.2016.08.002.

Please cite this article in press as: Beatty et al., Photochemical Perfluoroalkylation with Pyridine *N*-Oxides: Mechanistic Insights and Performance on a Kilogram Scale, Chem (2016), http://dx.doi.org/10.1016/j.chempr.2016.08.002

AUTHOR CONTRIBUTIONS

J.W.B., J.J.D., R.M., and R.C.M. performed the experiments; J.W.B., J.J.D., K.P.C., and C.R.J.S. designed the experiments and analyzed the data. J.W.B., J.J.D., K.P.C., and C.R.J.S. wrote the manuscript.

ACKNOWLEDGMENTS

We thank Martin Johnson and Jennifer McClary Groh for general discussion about the construction of the flow reactor and calculation of the heat output of the light. We thank John Howell for preparation of pyrrole **9**. We thank Adam McFarland and Jonas Buser for NMR assistance and Dr. Jeff Kampf for X-ray crystallographic analysis. We acknowledge the financial support for this research from the NIH Q7 NIGMS (R01-GM096129), the Camille Dreyfus Teacher Scholar Award Program, Eli Lilly and Co., the University of Michigan, and a Lilly Innovation Fellowship Award to J.J.D. from Eli Lilly and Co.

Received: June 16, 2016
Revised: August 3, 2016
Accepted: August 3, 2016
Published: September 8, 2016

REFERENCES AND NOTES

1. Müller, K., Faeh, C., and Diedrich, F. (2016). Fluorine in pharmaceuticals: looking beyond intuition. Science *317*, 1881–1886.

2. Jeschke, P. (2004). The unique role of fluorine in the design of active ingredients for modern crop protection. ChemBioChem *5*, 570–589.

3. Hagman, W.K. (2008). The many roles for fluorine in medicinal chemistry. J. Med. Chem. *51*, 4359–4368.

4. Wang, J.W., Sánchez-Rosellóo, M., Aceña, J.L., del Pozo, C., Sorochinsky, A.E., Fustero, S., Soloshonok, V.A., and Liu, H. (2014). Fluorine in pharmaceutical industry: fluorine-containing drugs introduced to the market in the last decade (2001-2011). Chem. Rev. *114*, 2432–2506.

5. Siegemund, G., Schwertfeger, W., Feiring, A., Smart, B., Behr, F., Vogel, H., and McKusick, B. (2000). Fluorine compounds, organic. In Ullmann's Encyclopedia of Industrial Chemistry, B. Elvers, ed. (Wiley). http://dx.doi.org/10.1002/14356007.a11_349.pub2.

6. Tomoshenko, O.A., and Grushin, V.V. (2011). Aromatic trifluoromethylation with metal complexes. Chem. Rev. *111*, 4475–4521.

7. Alonso, C., de Marigorta, E.M., Rubiales, G., and Palacios, F. (2015). Carbon trifluoromethylation reactions of hydrocarbon derivatives and heteroarenes. Chem. Rev. *115*, 1847–1935.

8. Prakash, G.K.S., and Mandal, M. (2001). Nucleophilic trifluoromethylation tamed. J. Fluorine Chem. *112*, 123–131.

9. Langlois, B.R., Billard, T., and Roussel, S. (2005). Nucleophilic trifluoromethylation: some recent reagents and their stereoselective aspects. J. Fluorine Chem. *126*, 173–179.

10. Rubiales, G., Alonso, C., de Marigorta, E.M., and Palacios, F. (2014). Nucleophilic trifluoromethylation of carbonyl compounds and derivatives. ARKIVOC *ii*, 362–405.

11. Liu, X., Xu, C., Wang, M., and Liu, Q. (2015). Trifluoromethyltrimethylsilane: nucleophilic trifluoromethylation and beyond. Chem. Rev. *115*, 683–730.

12. Prakash, G.K.S., and Hu, J. (2007). Selective fluoroalkylations with fluorinated sulfones, sulfoxides, and sulfides. Acc. Chem. Res. *40*, 921–930.

13. Prakash, G.K.S., Krishnamurti, R., and Olah, G.A. (1989). Synthetic methods and reactions. 141. Fluoride-induced trifluoromethylation of carbonyl compounds with trifluoromethyltrimethylsilane (TMS-CF3). A trifluoromethide equivalent. J. Am. Chem. Soc. *111*, 393–395.

14. Prakash, G.K.S., Wang, Y., Mogi, R., Hu, J., Mathew, T., and Olah, G.A. (2010). Nucleophilic perfluoroalkylation of imines and carbonyls: perfluoroalkyl sulfones as efficient perfluoroalkyl-transfer motifs. Org. Lett. *12*, 2932–2935.

15. Prakash, G.K.S., Zhang, Z., Wang, F., Munoz, S., and Olah, G.A. (2013). Nucleophilic trifluoromethylation of carbonyl compounds: trifluoroacetaldehyde hydrate as a trifluoromethyl source. J. Org. Chem. *78*, 3300–3305.

16. Charpentier, J., Früh, N., and Togni, A. (2015). Electrophilic trifluoromethylation by use of hypervalent iodine reagents. Chem. Rev. *115*, 650–682.

17. Shibata, N., Matsnev, A., and Cahard, D. (2010). Shelf-stable electrophilic trifluoromethylating reagents: a brief historical perspective. Beilstein J. Org. Chem. *6*, 65.

18. Umemoto, T., Adachi, K., and Ishihara, S. (2007). CF3 oxonium salts, *O*-(Trifluoromethyl) dibenzofuranium salts: in situ synthesis, properties, and application as a real CF3+ species reagent. J. Org. Chem. *72*, 6905–6917.

19. Kieltsch, I., Eisenberger, P., and Togni, A. (2007). Mild electrophilic trifluoromethylation of carbon- and sulfur-centered nucleophiles by a hypervalent iodine(III)-CF3 reagent. Angew. Chem. Int. Ed. Engl. *46*, 754–757.

20. Allen, A.E., and MacMillan, D.W.C. (2010). The productive merger of iodonium salts and organocatalysis: a non-photolytic approach to the enantioselective α-trifluoromethylation of aldehydes. J. Am. Chem. Soc. *132*, 4986–4987.

21. Koike, T., and Akita, M. (2014). Trifluoromethylation by visible-light-driven photoredox catalysis. Top. Catal. *57*, 967–974.

22. Barata-Vallejo, S., and Postigo, A. (2013). Metal-mediated radical perfluoroalkylation of organic compounds. Coord. Chem. Rev. *257*, 3051–3069.

23. Studer, A. (2012). A "renaissance" in radical trifluoromethylation. Angew. Chem. Int. Ed. Engl. *51*, 8950–8958.

24. McClinton, M.A., and McClinton, D.A. (1992). Trifluoromethylations and related reactions in organic chemistry. Tetrahedron *48*, 6555–6666.

25. Zeng, T., Xuan, J., Chen, J., Lu, L., and Xiao, W. (2014). Visible light photoredox catalysis in trifluoromethylation reactions. Imag. Sci. Photochem. *32*, 415–432.

26. Nagib, D.A., and MacMillan, D.W.C. (2011). Trifluoromethylation of arenes and heteroarenes by means of photoredox catalysis. Nature *480*, 224–228.

27. Pham, P.V., Nagib, D.A., and MacMillan, D.W.C. (2011). Photoredox catalysis: a mild, operationally simple approach to the synthesis of α-trifluoromethyl carbonyl compounds. Angew. Chem. Int. Ed. Engl. *50*, 6119–6122.

28. Nagib, D.A., Scott, M.E., and MacMillan, D.W.C. (2009). Enantioselective α-trifluoromethylation of aldehydes vis photoredox organocatalysis. J. Am. Chem. Soc. *131*, 10875–10877.

29. Ji, Y., Bruecki, T., Baxter, R.D., Fujiwara, Y., Seiple, I.B., Su, S., Blackmond, D.G., and Baran, P.S. (2011). Innate C–H trifluoromethylation of heterocycles. Proc. Natl. Acad. Sci. USA *108*, 14411–14415.

30. Fujiwara, Y., Dixon, J.A., O'Hara, F., Daa Funder, D., Dixon, D.D., Rodriguez, R.A., Baxter, R.D., Herlé, B., Sach, N., Collins, M.R., et al. (2012). Practical and innate carbon–hydrogen functionalization of heterocycles. Nature *492*, 95–99.

31. Li, Y., and Studer, A. (2012). Transition-metal-free trifluoromethylaminoxylation of alkenes. Angew. Chem. Int. Ed. Engl. *51*, 8221–8224.

32. Zhang, B., Mück-Lichtenfeld, C., Daniliuc, C.G., and Studer, A. (2013). 6-Trifluoromethyl-phenanthiridines through radical trifluoromethylation of isonitriles. Angew. Chem. Int. Ed. Engl. *52*, 10792–10795.

33. Yasu, Y., Koike, T., and Akita, M. (2012). Three-component oxytrifluoromethylation of alkenes: highly efficient and regioselective difunctionalization of C=C bonds mediated by photoredox catalysis. Angew. Chem. Int. Ed. Engl. *51*, 9567–9571.

34. Wilger, D.J., Gesmundo, N.J., and Nicewicz, D.A. (2013). Catalytic hydrotrifluoromethylation of styrenes and unactivated aliphatic alkenes via an organic photoredox system. Chem. Sci. *4*, 3160–3165.

35. Deng, Q., Chen, J., Wei, Q., Zhao, Q., Lu, L., and Xiao, W. (2015). Visible-light-induced photocatalytic oxytrifluoromethylation of *N*-allylamides for the synthesis of CF3-containing oxazolines and benzoxazines. Chem. Commun. *51*, 3537–3540.

36. Mizuta, S., Verhoog, S., Engle, K.M., Khotavivattana, T., O'Duill, M., Wheelhouse, K., Rassias, G., Médebielle, M., and Gouverneur, V. (2013). Catalytic hydrotrifluoromethylation of unactivated alkenes. J. Am. Chem. Soc. *135*, 2505–2508.

37. Cho, E.J., Senecal, T.D., Kinzel, T., Zhang, Y., Watson, D.A., and Buchwald, S.L. (2010). The palladium-catalyzed trifluoromethylation of aryl chlorides. Science *328*, 1679–1681.

38. Morimoto, H., Tsubogo, T., Litvinas, N.D., and Hartwig, J.F. (2011). A broadly applicable copper reagent for trifluoromethylations and perfluoroalkylations of aryl iodides and bromides. Angew. Chem. Int. Ed. Engl. *50*, 3793–3798.

39. Mazloomi, Z., Bansode, A., Benavente, P., Lishchynskyi, A., Urakawa, A., and Grushin, V.V. (2014). Continuous process for production of CuCF3 via direct cupration of fluoroform. Org. Process. Res. Dev. *18*, 1020–1026.

40. Lishchynskyi, A., Novikov, M.A., Martin, E., Escudero-Adán, E.C., Novák, P., and Grushin, V.V. (2013). Trifluoromethylation of Aryl and heteroaryl halides with fluoroform-derived CuCF3: scope, limitations, and mechanistic features. J. Org. Chem. *78*, 11126–11146.

41. Huiban, M., Tredwell, M., Mizuta, S., Wan, Z., Zhang, X., Collier, T.L., Gouverneur, V., and Passchier, J. (2013). A broadly applicable [18F] trifluoromethylation of aryl and heteroaryl iodides for PET imaging. Nat. Chem. *5*, 941–944.

42. Li, X., Zhao, J., Zhang, L., Hu, M., Wang, L., and Hu, J. (2015). Copper-mediated trifluoromethylation using phenyl trifluoromethyl sulfoxide. Org. Lett. *17*, 298–301.

43. Morstein, J., Hou, H., Cheng, C., and Hartwig, J.F. (2016). Trifluoromethylation of arylsilanes with [(phen)CuCF3]. Angew. Chem. Int. Ed. Engl. http://dx.doi.org/10.1002/anie.201601163.

44. Zanbardi, A., Novikov, M.A., Martin, E., Benet-Buchholz, J., and Grushin, V.V. (2011). Direct cupration of fluoroform. J. Am. Chem. Soc. *133*, 20901–20913.

45. Novák, P., Lishchynskyi, A., and Grushin, V.V. (2012). Fluoroform-derived CuCF3 for low-cost, simple, efficient, and safe trifluoromethylation of aryl boronic acids in air. Angew. Chem. Int. Ed. Engl. *51*, 7767–7770.

46. Depecker, C., Marzouk, H., Trevin, S., and Devynck, J. (1999). Trifluoromethylation of aromatic compounds via Kolbe electrolysis in pure organic solvent. Study on laboratory and pilot scale. New J. Chem. *23*, 739–742.

47. Matsui, K., Tobita, E., Ando, M., and Kondo, K. (1981). A convenient trifluoromethylation of aromatic halides with sodium trifluoroacetate. Chem. Lett. *10*, 1719–1720.

48. Chen, M., and Buchwald, S.L. (2013). Rapid and efficient trifluoromethylation of aromatic and heteroaromatic compounds using potassium trifluoroacetate enabled by a flow system. Angew. Chem. Int. Ed. Engl. *52*, 11628–11631.

49. Tanabe, Y., Matsuo, N., and Ohno, N. (1988). Direct perfluoroalkylation including trifluoromethylation of aromatics with perfluoro carboxylic acids mediated by xenon difluoride. J. Org. Chem. *53*, 4582–4585.

50. Shi, G., Shao, C., Pan, S., Yu, J., and Zhang, Y. (2015). Silver-catalyzed C–H trifluoromethylation of arenes using trifluoroacetic acid as the trifluoromethylating reagent. Org. Lett. *17*, 38–41.

51. Lai, C., and Mallouk, T.E. (1993). A new approach to the photochemical trifluoromethylation of aromatic compounds. J. Chem. Soc. Chem. Commun. 1359–1361.

52. Sawada, H., and Nakayama, M. (1990). Trifluoromethylation of aromatic compounds with bis(trifluoroacetyl) peroxide. J. Fluorine Chem. *46*, 423–431.

53. For a more recent example of this chemistry, see Zhong, S., Hafner, A., Hussal, C., Nieger, M., and Bräse, S. (2015). Metal-free radical perfluoroalkylation of (Hetero)arenes. RSC Adv. *5*, 6255–6258.

54. Zuo, Z., Cong, H., Li, W., Choi, J., Fu, G.C., and MacMillan, D.W.C. (2016). Enantioselective decarboxylative arylation of α-amino acids via the merger of photoredox and nickel catalysis. J. Am. Chem. Soc. *138*, 1832–1835.

55. Nawrat, C.C., Jamison, C.R., Slutskyy, Y., MacMillan, D.W.C., and Overman, L.E. (2015). Oxalates as activating groups for alcohols in visible light photoredox catalysis: formation of quaternary centers by redox-neutral fragment coupling. J. Am. Chem. Soc. *137*, 11270–11273.

56. Chu, L., Lipshultz, J.M., and MacMillan, D.W.C. (2015). Merging photoredox and nickel catalysis: the direct synthesis of ketones by the decarboxylative arylation of α-oxo acids. Angew. Chem. Int. Ed. Engl. *54*, 7929–7933.

57. Ventre, S., Petronijevic, F.P., and MacMillan, D.W.C. (2015). Decarboxylative fluorination of aliphatic carboxylic acids via photoredox catalysis. J. Am. Chem. Soc. *137*, 5654–5657.

58. Noble, A., McCarver, S.J., and MacMillan, D.W.C. (2015). Merging photoredox and nickel catalysis: decarboxylative cross-coupling of carboxylic acids with vinyl halides. J. Am. Chem. Soc. *137*, 624–627.

59. Zuo, Z., and MacMillan, D.W.C. (2014). Decarboxylative arylation of α-amino acids via photoredox catalysis: a one-step conversion of biomass to drug pharmacophore. J. Am. Chem. Soc. *136*, 5257–5260.

60. Zuo, Z., Ahneman, D.T., Chu, L., Terrett, J.A., Doyle, A.G., and MacMillan, D.W.C. (2014). Merging photoredox with nickel catalysis: coupling of α-carboxyl sp3-carbons with aryl halides. Science *345*, 437–440.

61. Cassani, C., Bergonzini, G., and Wallentin, C.-J. (2014). Photocatalytic decarboxylative reduction of carboxylic acids and its application in asymmetric synthesis. Org. Lett. *16*, 4228–4231.

62. Griffin, J.D., Zeller, M.A., and Nicewicz, D.A. (2015). Hydrodecarboxylation of carboxylic and malonic acid derivatives via organic photoredox catalysis: substrate scope and mechanistic insight. J. Am. Chem. Soc. *137*, 11340–11348.

63. Huang, H., Jia, K., and Chen, Y. (2015). Hypervalent iodine reagents enable chemoselective deboronative/decarboxylative alkenylation by photoredox catalysis. Angew. Chem. Int. Ed. Engl. *54*, 1881–1884.

64. Beatty, J.W., Douglas, J.J., Cole, K.P., and Stephenson, C.R.J. (2015). A scalable and operationally simple trifluoromethylation. Nat. Commun. *6*, 7919.

65. Boekelheide, V., and Linn, W.J. (1954). Rearrangements of *N*-oxides. A novel synthesis of pyridyl carbinols and aldehydes. J. Am. Chem. Soc. *76*, 1286–1291.

66. Attempts to trifluoromethylate aryltrifluoroborate salts were unsuccessful

because of the reactivity of TFAA with fluoride anions. Off-gassing was observed, which is attributed to the formation of CF_3COF (bp= –59°C). This phenomenon has been previously proposed: Roscales, S., and Csákÿ, A.G. (2014). Metal-free ring-opening of epoxides with potassium trifluoroborates. Chem. Commun. *50*, 454.

67. Kondratov, I.S., Dolovanyuk, V.G., Tolmachova, N.A., Gerus, I.I., Bergander, K., Frölich, R., and Haufe, G. (2012). Reactions of β-alkoxyvinyl polyfluoroalkyl ketones with ethyl isocyanoacetate and its use for the synthesis of new polyfluoroalkyl pyrroles and pyrrolidines. Org. Biomol. Chem. *10*, 8778–8785.

68. Dolbier, W.R. (1996). Structure, reactivity, and chemistry of fluoroalkyl radicals. Chem. Rev. *96*, 1557–1584.

69. Tarrant, P. (1984). Fluorocarbon iodides—versatile reagents. J. Fluorine Chem. *25*, 69–74.

70. Haszeldine, R.N. (1951). The reactions of metallic salts of acids with halogens. Part I. The reaction of metal trifluoroacetates with iodine, bromine, and chlorine. J. Chem. Soc. 584–587.

71. Lima, C.G.S., Lima, T.D.M., Duarte, M., Jurberg, I.D., and Paixão, M.W. (2016). Organic synthesis enabled by light-irradiation of EDA complexes: theoretical background and synthetic applications. ACS Catal. *6*, 1389–1407.

72. Yoon, K.B., and Kochi, J.K. (1991). Stepwise assembly of charge-transfer complexes within zeolite supercages as visual probes for shape selectivity. J. Phys. Chem. *95*, 3780–3790.

73. Verhoeven, J.W., Dirkx, I.P., and de Boer, T.J. (1969). Studies of inter- and intra-molecular donor-acceptor interactions—II: intermolecular charge transfer involving substituted pyridinium ions. Tetrahedron *25*, 3395–3405.

74. Nagy, O.B., Dupire, S., and Nagy, J.B. (1975). New ionization potentials from charge-transfer spectra. Tetrahedron *31*, 2453–2456.

75. Lee, K.W., and Kochi, J.K. (1992). Charge-transfer structures of aromatic EDA complexes with *n*-heteroatom-substituted pyridinium cations. J. Chem. Soc. Perkin Trans. *2*, 1011–1017.

76. Miller, L.L., Nordblom, G.D., and Mayeda, E.A. (1972). Simple, comprehensive correlation of organic oxidation and ionization potentials. J. Org. Chem. *37*, 916–918.

77. Arceo, E., Jurberg, I.D., Álvarez-Fernández, A., and Melchiorre, P. (2013). Photochemical activity of a key donor-acceptor complex can drive stereoselective catalytic α-alkylation of aldehydes. Nat. Chem. *5*, 750–756.

78. Woźniak, Ł., Murphy, J.J., and Melchiorre, P. (2015). Photo-organocatalytic enantioselective perfluoroalkylation of β-ketoesters. J. Am. Chem. Soc. *137*, 5678–5681.

79. Kanukuri, S.R., Bahamonde, A., Chatterjee, I., Jurberg, I.D., Escudero-Adán, E.C., and Melchiorre, P. (2015). X-ray characterization of an electron donor-acceptor complex that drives the photochemical alkylation of indoles. Angew. Chem. Int. Ed. Engl. *54*, 1485–1489.

80. Arceo, E., Bahamonde, A., Bergonzini, G., and Melchiorre, P. (2014). Enantioselective direct α-alkylation of cyclic ketones by means of photo-organocatalysis. Chem. Sci. *5*, 2438–2442.

81. Nappi, M., Bergonzini, G., and Melchiorre, P. (2014). Metal-free photochemical aromatic perfluoroalkylation of α-cyano arylacetates. Angew. Chem. Int. Ed. Engl. *53*, 4921–4925.

82. Hilinski, E.F., Masnovi, J.M., Amatore, C., Kochi, J.K., and Rentzepis, P.M. (1983). Charge-transfer excitation of electron donor-acceptor complexes. Direct observation of ion pairs by time-resolved picosecond spectroscopy. J. Am. Chem. Soc. *105*, 6167–6168.

83. Luo, J., and Zhang, J. (2016). Donor-acceptor fluorophores for visible-light-promoted organic synthesis: photoredox/Ni dual catalytic C(sp3)–C(sp2) cross-coupling. ACS Catal. *6*, 873–877.

84. Lorance, E.D., Kramer, W.H., and Gould, I.R. (2004). Barrierless electron transfer bond fragmentation reactions. J. Am. Chem. Soc. *126*, 14071–14078.

85. Dewanji, A., Murarka, S., Curran, D.P., and Studer, A. (2013). Phenyl hydrazine as initiator for direct arene C–H arylation via base promoted homolytic aromatic substitution. Org. Lett. *15*, 6102–6105.

86. Cismesia, M.A., and Yoon, T.P. (2015). Characterizing chain processes in visible light photoredox catalysis. Chem. Sci. *6*, 5426–5434.

87. As previously noted, the reaction also becomes dark, thus further limiting light penetration.

88. The concept of scaling out photochemical reactions has been effectively demonstrated Su, Y., Kuijpers, K., Hessel, V., and Noël, T. (2016). A convenient numbering-up strategy for the scale-up of gas-liquid photoredox catalysis in flow. React. Chem. Eng. *1*, 73–81.

89. Reis, N.M., and Puma, G.L. (2015). A novel microfluidic approach for extremely fast and efficient photochemical transformations in fluoropolymer microcapillary films. Chem. Commun. *51*, 8414–8417.

90. Elvira, K.S., Wootton, R.C.R., Reis, N.M., Mackley, M.R., and deMello, A.J. (2013). Through-wall mass transport as a modality for safe generation of singlet oxygen in continuous flows. ACS Sustain. Chem. Eng. *1*, 209–213.

91. Hook, B.D.A., Dohle, W., Hirst, P.R., Pickworth, M., Berry, M., and Booker-Milburn, K.I. (2005). A practical flow reactor for continuous organic photochemistry. J. Org. Chem. *70*, 7558–7564.

92. Su, Y., Straathof, N.J.W., Hessel, V., and Noël, T. (2014). Photochemical transformations accelerated in continuous-flow reactors: basic concepts and applications. Chem. Eur. J. *20*, 10562–10589.

93. Cambié, D., Bottecchia, C., Straathof, N.J.W., Hessel, V., and Noël, T. (2016). Applications of continuous-flow photochemistry in organic synthesis, material science, and water treatment. Chem. Rev. http://dx.doi.org/10.1021/acs.chemrev.5b00707.

94. Garlets, Z.J., Nguyen, J.D., and Stephenson, C.R.J. (2014). The development of visible-light photoredox catalysis in flow. Isr. J. Chem. *54*, 351–360.

95. Yayla, H.G., Peng, F., Mangion, I.K., McLaughlin, M.M., Campeau, L.-C., Davies, I.W., DiRocco, D.A., and Knowles, R.R. (2016). Discovery and mechanistic study of a photocatalytic indoline dehydrogenation for the synthesis of elbasvir. Chem. Sci. *7*, 2066–2073.

96. See the Supplemental Information for full details of the reactor design.

97. Pumps were temporarily stopped for <1 min while the feed bottles were refilled.

98. We appreciate that direct trifluoromethylations to form pyrrole **25** have been reported; however, it remains unclear whether those processes could be operated at a kilogram scale. See Baar, M., and Blechert, S. (2015). Graphitic carbon nitride polymer as a recyclable photoredox catalyst for fluoroalkylation of arenes. Chem. Eur. J. *21*, 526–530.

99. We use 24 hr to define a day, but it should be appreciated that in many cases, other restrictions may prevent full 24 hr operation on a large (e.g., plant) manufacturing scale.

100. Many visible-light-mediated reactions have higher quantum yields, i.e., ≫1 where photon flux may not be the limiting factor. See Luo and Zhang.[83]

Chem, Volume *1*

Supplemental Information

Photochemical Perfluoroalkylation with Pyridine *N*-Oxides: Mechanistic Insights and Performance on a Kilogram Scale

Joel W. Beatty, James J. Douglas, Richard Miller, Rory C. McAtee, Kevin P. Cole, and Corey R.J. Stephenson

A

B

C

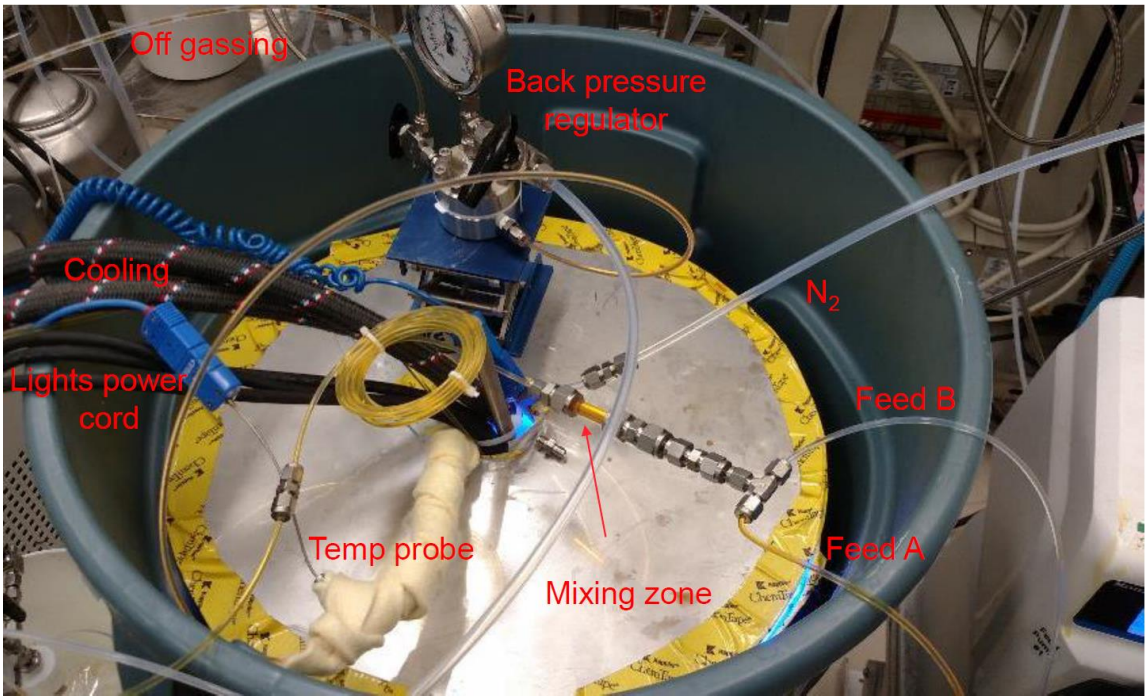

D

Figure S1. Pictures detailing reactor setup, Related to Figure 3.
(A) Glass reactor and tubing.
(B) Aquadock light source and holding stand.
(C) Assembly of reactor, lights, stainless steel housing, and outer secondary container.
(D) Detail of reactor construction from top down view.

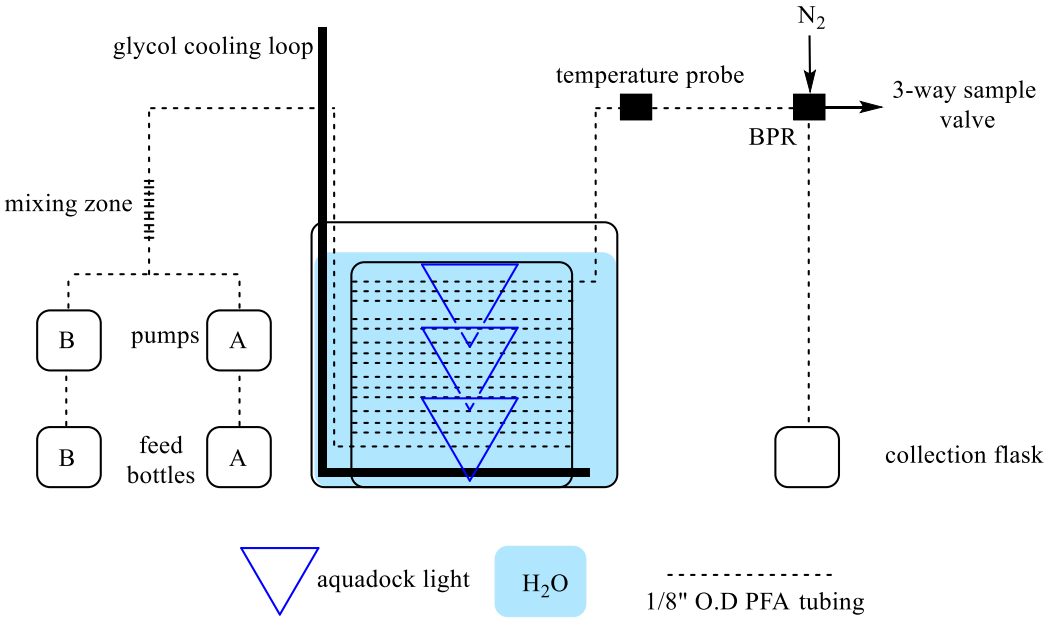

* secondary container, nitrogen line, and internal temperature probe omitted for clarity

Figure S2. Schematic representation of the flow reactor, Related to Figure 3.

Supplemental Experimental Procedures

General Information: All chemicals were used as received. Reactions were monitored by TLC and visualized with a dual short wave/long wave UV lamp. Column flash chromatography was performed using 230-400 mesh silica gel or via automated column chromatography. Preparative TLC purifications were run on silica plates of 1000 µm thickness. NMR spectra were recorded on Varian MR400, Varian Inova 500, Varian Vnmrs 500, or Varian Vnmrs 700 spectrometers. Chemical shifts for ^{1}H NMR were reported as δ, parts per million, relative to the signal of $CHCl_3$ at 7.26 ppm. Chemical shifts for ^{13}C NMR were reported as δ, parts per million, relative to the center line signal of the $CDCl_3$ triplet at 77.0 ppm. Chemical shifts for ^{19}F NMR were reported as δ, parts per million, relative to the signal of a trifluorotoluene internal standard at -63.72 ppm. *N*-oxide screening experiments were quantitatively analyzed by ^{19}F NMR with a relaxation delay of 1s, while later optimization experiments (entries 13 through 23) and all other internal standard yields were quantified by ^{19}F NMR with a 5s relaxation delay. The abbreviations s, br. s, d, dd, br. d, ddd, t, q, br. q, qi, m, and br. m stand for the resonance multiplicity singlet, broad singlet, doublet, doublet of doublets, broad doublet, doublet of doublet of doublets, triplet, quartet, broad quartet, quintet, multiplet and broad multiplet, respectively. IR spectra were recorded on a Perkin-Elmer Spectrum BX FT-IR spectrometer fitted with an ATR accessory. Mass Spectra were recorded at the Mass Spectrometry Facility at the Department of Chemistry of the University of Michigan in Ann Arbor, MI on an Agilent Q-TOF HPCL-MS with ESI high resolution mass spectrometer. Fluorescence, actinometry, and quantum yield measurements were performed with a Fluoromax-2 fluorimeter equipped with a 150W Xe arc lamp. UV-VIS measurements were obtained on a Shimadzu UV-1601 UV-VIS Spectrometer. LED lights and the requisite power box and cables were purchased from Creative Lighting Solutions (http://www.creativelightings.com) with the following item codes: CL-FRS5050-12WP-12V (4.4W blue LED light strip), CL-PS94670-25W (25 W power supply), CL-PC6FT-PCW (power cord), CL-TERMBL-5P (terminal block).

Unless stated otherwise, all reactions were run on a 0.8mmol scale in a 2 dram vial equipped with stir bar and septum. The light apparatuses used to irradiate the reactions were constructed from test tube racks and wrapped with three 4W LED strips. Reactions were run only in slots marked by an X in the picture below so as to keep a moderate distance from the light source (~2.5 cm). At this distance the temperature of the reactions did not exceed 35 ˚C (**Figure S3**).

Figure S3: Experimental light array.

Optimization and Control Experiments: All optimization experiments were performed on a 0.8 mmol scale at 0.4 M concentration (2 ml of solvent) unless stated otherwise, with the equivalents or reagents used, atmosphere, catalyst loadings found in Table 1 of the manuscript.

Entries 1-16: To a 2 dram vial equipped with a stir bar was added the *N*-oxide derivative (0.4–1.6 mmol, 0.5–2.0 equiv.), $Ru(bpy)_3Cl_2•6H_2O$ (6.0 mg, 1.0 mol%), and substrate (0.80 mmol). The combined materials were then dissolved in dry MeCN (2.0 ml) and stirred briefly (~1 minute). Trifluoroacetic anhydride (120 µl, 190 mg, 0.88 mmol, 1.1 equiv.) was then added to the resulting solution. The vial was equipped with a screw-on cap. Three 4.4 W LED light strips were turned on and the reactions allowed to proceed for 12 hours before removal of the light source. Trifluorotoluene (98 µl, 0.80 mmol) was added as a stoichiometric internal standard. A sample of the reaction was removed and diluted with $CDCl_3$ for NMR analysis. The trifluorotoluene signal was referenced to δ -63.72. Product peaks in the crude ^{19}F NMR were integrated with 1,3,5-trimethyl-2-(trifluoromethyl)benzene observed at δ -54.70 (s, 3F) and 1,3,5-trimethyl-2,4-bis(trifluoromethyl)benzene observed at δ -53.89 (s, 6F).

Entries 17-23: Procedurally identical to entries 1-16, with key differences. For reactions with 0.1 mol% catalyst (**entries 19, 20, 23, 24**), 500 µl of a solution 1.2 mg/ml $Ru(bpy)_3Cl_2•6H_2O$ in dry MeCN (0.6 mg, 0.1 mol%) was added in lieu of 500 µl of solvent. Reactions were degassed (**entries 17-24**) upon dissolution of catalyst, *N*-oxide, and mesitylene in dry MeCN by sparging of the solution with nitrogen for 30 seconds, followed by the addition of TFAA (not degassed) under a stream of nitrogen. The reactions were quickly sealed with a rubber-lined screw on cap, and wrapped with parafilm. Light exclusion (**entry 23**) was achieved by wrapping the reaction in foil (before addition of TFAA) while placing the vessel in front of the light source so as to match the temperature profile of the other reactions. Before analysis of the light-exclusion experiment, methanol (500 µl) was added via syringe and the reaction was allowed to stir for 5 minutes before exposure to light during analysis.

Preparation of Compounds 2a-20, 23: General Perfluoroalkylation Procedure: To a 2 dram vial equipped with a stir bar was added 4-phenylpyridine *N*-oxide (0.8–3.2 mmol, 1.0–4.0 equiv.) and substrate (0.80 mmol) followed by 500 ul of a 1.2 mg/ml solution of $Ru(bpy)_3Cl_2•6H_2O$ (0.6 mg, 0.1 mol%). The combined materials were then diluted with dry MeCN (1.5 ml, total volume 2 ml MeCN) and stirred briefly to form a heterogeneous solution, with the *N*-oxide only partially dissolved when used in higher equivalents. The reaction was sparged with nitrogen gas for 30 seconds with a glass pipette, followed by the addition of the fluorinated acylating reagent (0.88–3.28 mmol, 1.1–4.1 equiv.) under a stream of nitrogen before quickly sealing the vial with a rubber-lined screw-on cap. The trifluoroacetic anhydride solubilizes any remaining solid *N*-oxide within seconds to minutes. Three 4.4 W LED light strips were turned on and the reactions were allowed to proceed for 3–12 hours before removal of the light source (see Supplemental Information for geometry of LED setup). Upon reaction completion, trifluorotoluene (98 µl, 0.80 mmol) was added as a stoichiometric internal standard. A sample of the reaction was removed and diluted with $CDCl_3$ for NMR analysis, with the trifluorotoluene signal referenced to δ -63.72. Workup conditions were substrate-dependent.

1,3,5-trimethyl-2-(trifluoromethyl)benzene[1] (2a) and 1,3,5-trimethyl-2,4-bis(trifluoromethyl)benzene[2] (2b)

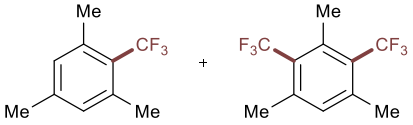

Following the general procedure, using 4-phenylpyridine *N*-oxide (273.9 mg, 1.6 mmol, 2.0 equiv.) and TFAA (237 µl, 1.68 mmol, 2.1 equiv.), the reaction was run for 12 hours. ^{19}F NMR analysis of the crude reaction mixture vs. the injected trifluorotoluene standard revealed the volatile title compounds 1,3,5-trimethyl-2-(trifluoromethyl)benzene [^{19}F NMR (470 MHz, $CDCl_3$) δ = -54.70 (s, 3F, 65% yield)] and 1,3,5-trimethyl-2,4-bis(trifluoromethyl)benzene [^{19}F NMR (470 MHz, $CDCl_3$) δ = -53.89 (s, 6F, 14% yield)] in a 4.6:1 ratio.
Yield: 0.632 mmol (79%, 4.6:1 2a:2b); ^{19}F NMR (470 MHz, $CDCl_3$) δ = -54.70 (s, 3F, 2a 65% yield), -53.89 (s, 3F, 2b 14% yield). The isolation and characterization of these compounds has previously been reported.[3]

(trifluoromethyl)benzene (3a)

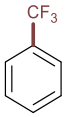

Following the general procedure, using 4-phenylpyridine *N*-oxide (137.0 mg, 0.8 mmol, 1.0 equiv.) as the limiting reagent, TFAA (124 µl, 0.88 mmol, 1.1 equiv.), and benzene (713 µl, 8.0 mmol, 10.0 equiv.), the reaction was run for 12 hours. Upon completion, the reaction was quenched with methanol (500 µl) and removed from the light source. Trifluoroethanol (58 µl, 0.8 mmol) was added as internal standard. Due to the wide availability and volatility of the product, no purification was attempted on this reaction mixture.
Yield: 0.632 mmol (79%); ^{19}F NMR (500 MHz, $CDCl_3$) δ = -63.72 (s, 3F). The proton and fluorine signals of the product were identical to those of a commercial sample.

4-(tert-butyl)-1-methoxy-2-(trifluoromethyl)benzene[4] (4a)

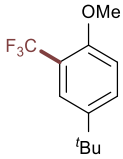

Following the general procedure, using 4-phenylpyridine *N*-oxide (273.9 mg, 1.6 mmol, 2.0 equiv.) and TFAA (237 µl, 1.68 mmol, 2.1 equiv.), the reaction was run for 5 hours. ^{19}F NMR analysis of the crude reaction mixture vs. the injected trifluorotoluene standard revealed the volatile title compound in 59% yield. The reaction was partitioned with 1N HCl and diluted with dichloromethane. The organic phase was separated, washed with sat. $NaHCO_3$, brine, and dried over sodium sulfate before filtering and concentrating. The crude reaction mixture was purified by prep TLC (100% hexanes run up x2) to yield to title compound as a volatile, clear oil (R_f = 0.32, hexanes).
Yield: 0.472 mmol (59%) ^{1}H NMR (400 MHz, $CDCl_3$) δ = 7.56 (d, J = 2.4 Hz, 1H), 7.50 (dd, J = 8.8, 2.4 Hz, 1H), 6.94 (d, J = 8.8 Hz, 1H), 3.88 (s, 3H), 1.31 (s, 9H); ^{19}F NMR (470 MHz, $CDCl_3$) δ = -63.13 (s, 3F); ^{13}C NMR (175 MHz, $CDCl_3$) δ = 155.2 (q, JC-F = 1.4 Hz), 142.9, 129.9, 123.9 (q, JC-F = 272.5 Hz), 123.89 (q, JC-F = 4.8 Hz), 118.0 (q, JC-F = 30.7 Hz), 111.7, 55.9, 34.2, 31.3; HRMS (EI+) m/z: $[M + H]^+$ calculated 232.1075, found 232.1077. IR (neat): ν = 2965, 1620, 1589, 1509, 1325, 1280, 1253, 1119, 1057.

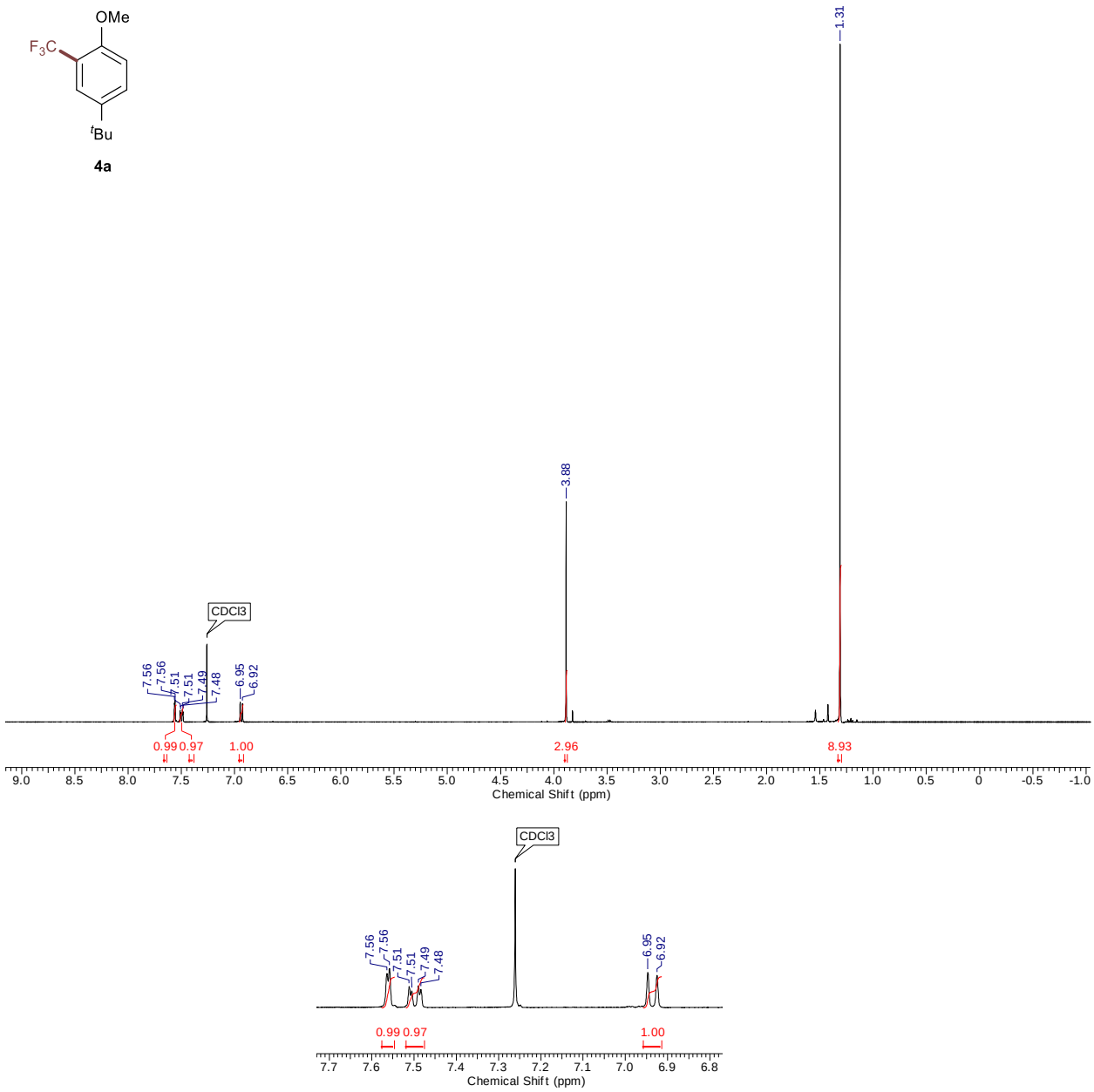

Figure S4. ^{1}H NMR spectrum (700 MHz, $CDCl_3$) of **4a**.

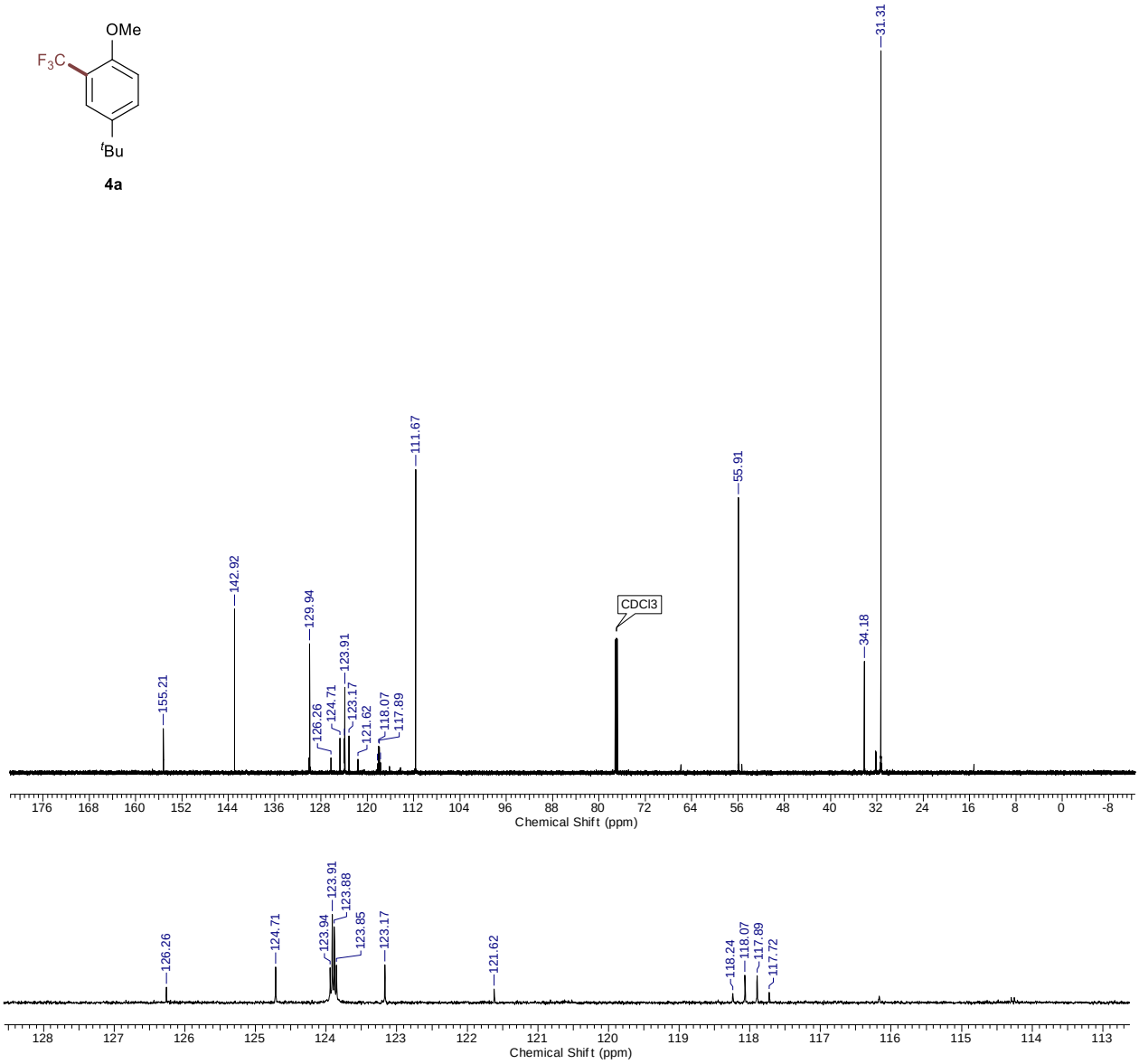

Figure S5. ^{13}C NMR spectrum (175 MHz, $CDCl_3$) of **4a**.

1-methyl-3-(trifluoromethyl)pyridine-2(1H)-one[3,5] (5a)

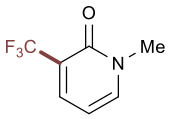

Following the general procedure using 4-phenylpyridine *N*-oxide (137.0 mg, 0.8 mmol, 1.0 equiv.) and TFAA (124 µl, 0.88 mmol, 1.1 equiv.), the reaction was run for 15 hours. ^{19}F NMR analysis of the crude reaction mixture vs. the injected trifluorotoluene standard revealed the title compound in 50% yield. The reaction was partitioned with 1N HCl and diluted with ethyl acetate. The organic phase was separated and washed with sat. $NaHCO_3$, brine, and dried over sodium sulfate before filtering and concentrating. Re-extraction of the combined and basified aqueous phase (basified further with sat. $NaHCO_3$) led to full material recovery, while the initial acidic workup conditions result in a significant loss of material. The crude reaction mixture was purified on silica gel with 0-50% EtOAc in hexanes to yield the title compound as a tan solid.
Yield: 71.8 mg (51%) The characterization of this compound has previously been reported.[3]

methyl 1-methyl-6-oxo-5-(trifluoromethyl)-1,6-dihydropyridine-3-carboxylate[3] (6a)

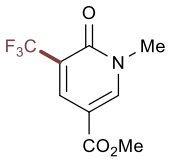

Following the general procedure using 4-phenylpyridine *N*-oxide (273.9 mg, 1.6 mmol, 2.0 equiv.) and TFAA (237 µl, 1.68 mmol, 2.1 equiv.), the reaction was run for 15 hours. ^{19}F NMR analysis of the crude reaction mixture vs. the injected trifluorotoluene standard revealed the title compound in **49% yield**. The reaction mixture was diluted with ethyl acetate and washed with sat. $NaHCO_3$. The aqueous layer was washed twice with ethyl acetate, and the combined organic layers were washed with brine, dried over sodium sulfate, and concentrated. The crude reaction mixture was purified by prep TLC (20% CH_2Cl_2 in EtOAc) to yield the title compound as a tan solid.
Yield: 93.0 mg (49%) The characterization of this compound has been previously reported.[3]

4,6-dimethoxy-5-(trifluoromethyl)pyrimidine (7a)

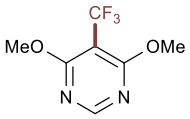

Following the general procedure using 4-phenylpyridine *N*-oxide (237.9 mg, 1.6 mmol, 2.0 equiv.) and TFAA (451 µl, 3.2 mmol, 4.0 equiv.), the reaction was run for 12 hours. ^{19}F NMR analysis of the crude reaction mixture vs. the injected trifluorotoluene standard revealed the title compound in **39% yield**. The reaction mixture was diluted with ethyl acetate and was partitioned with 1N HCl. The organic phase was separated, washed with sat. $NaHCO_3$, brine, and dried over sodium sulfate before filtering and concentrating. The crude reaction mixture was purified by prep TLC (30% EtOAc in hexanes) to yield the title compound as a clear crystalline solid.
Yield: 53.0 mg (32%) The characterization of this compound has previously been reported.[3]

tert-butyl 2-acetyl-5-(trifluoromethyl)-1H-pyrrole-1-carboxylate (8a)

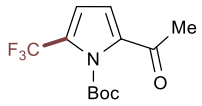

Following the general procedure, using 4-phenylpyridine *N*-oxide (273.9 mg, 1.6 mmol, 2.0 equiv.) and TFAA (237 µl, 1.68 mmol, 2.1 equiv.), the reaction was run for 5 hours. ^{19}F NMR analysis of the crude reaction mixture vs. the injected trifluorotoluene standard revealed the title compound in **70% yield**. The reaction was partitioned with 1N HCl and diluted with dichloromethane. The organic phase was separated, washed with sat. $NaHCO_3$, brine, and dried over sodium sulfate before filtering and concentrating. The crude reaction mixture was purified on silica gel with 50% dichloromethane in hexanes to yield the title compound as a clear oil (R_f = 0.3, 70% dichloromethane in hexanes).
Yield: 157.2 mg (71%); ^{1}H NMR (500 MHz, $CDCl_3$) δ = 6.80 (d, J = 3.6 Hz, 1H), 6.61 (d, J = 3.6 Hz, 1H), 2.48 (s, 3H), 1.61 (s, 9H); ^{19}F NMR (470 MHz, $CDCl_3$) δ = -59.82; ^{13}C NMR (100 MHz, $CDCl_3$) δ = 187.8, 147.8, 135.1 (q, JC-F = 1.8 Hz), 126.5 (q, JC-F = 40.1 Hz), 119.9 (q, JC-F = 268.6 Hz), 116.1, 112.2 (q, JC-F = 3.4 Hz), 86.8, 27.0, 26.7; HRMS (ESI+) m/z: $[M - Boc + H]^+$ calculated 177.0401, found 177.0404. IR (neat): v = 2988, 1775, 1679, 1550, 1372, 1248, 1125;

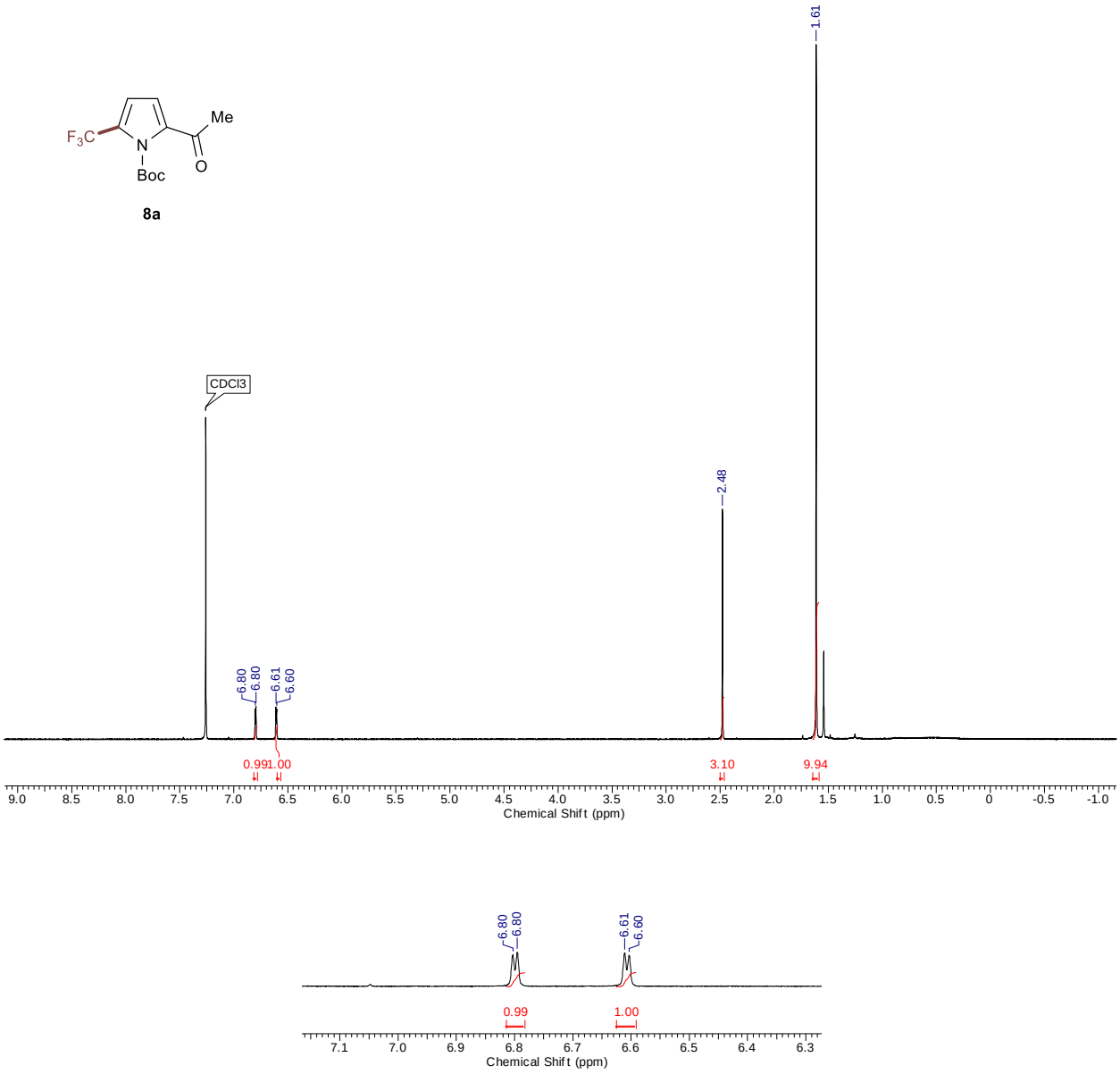

Figure S6 ^{1}H NMR spectrum (500 MHz, $CDCl_3$) of **8a**.

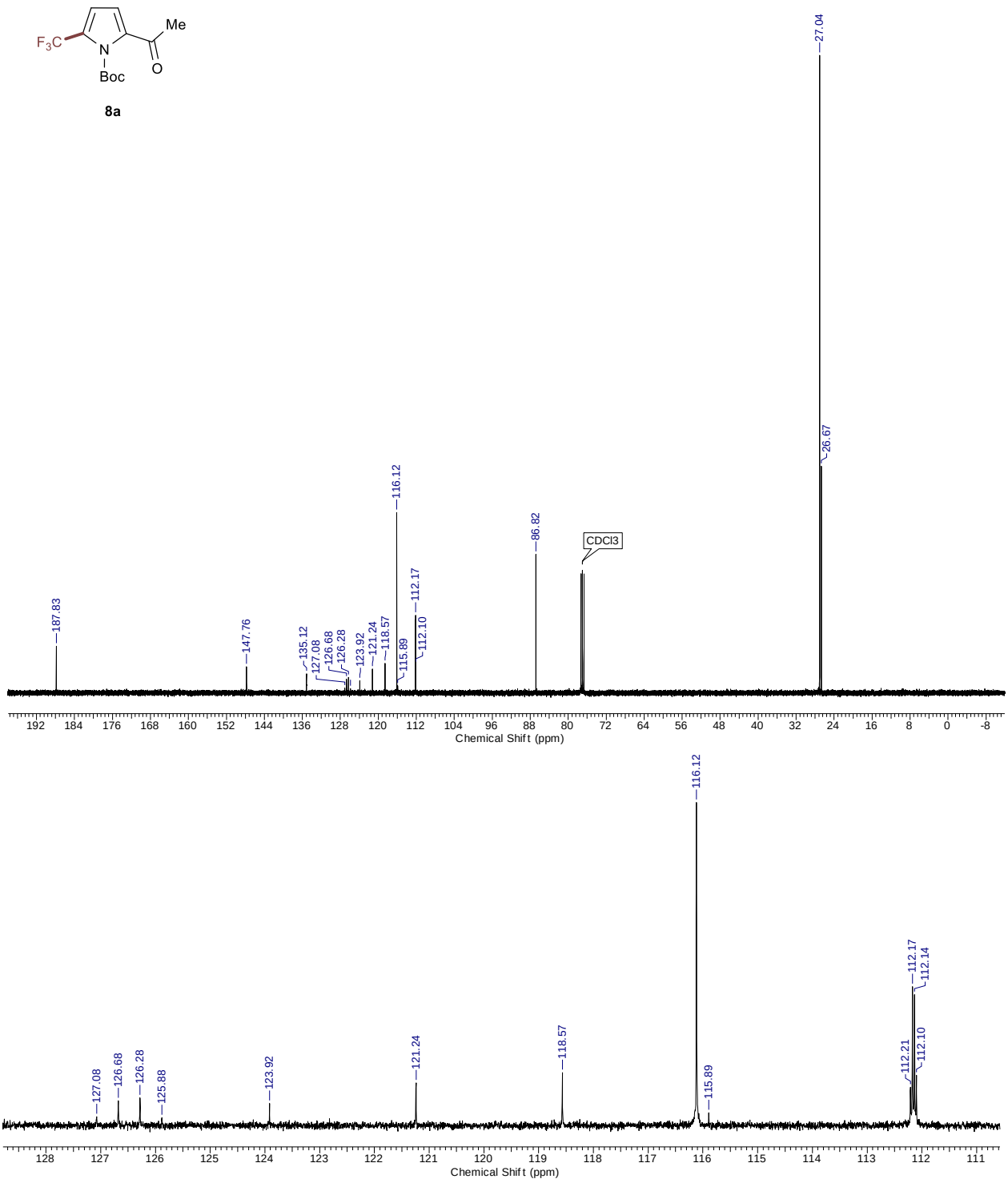

Figure S7. ^{13}C NMR spectrum (100 MHz, $CDCl_3$) of **8a**.

1-(tert-butyl) 2-methyl 5-(trifluoromethyl)-1H-pyrrole-1,2-dicarboxylate (9a)

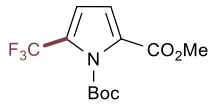

Following the general procedure, using 4-phenylpyridine *N*-oxide (273.9 mg, 1.6 mmol, 2.0 equiv.) and TFAA (237 µl, 1.68 mmol, 2.1 equiv.), the reaction was run for 3 hours. ^{19}F NMR analysis of the crude reaction mixture vs. the injected trifluorotoluene standard revealed the title compound in 63% yield. The reaction was partitioned with 1N HCl and diluted with dichloromethane. The organic phase was separated, washed with sat. $NaHCO_3$, brine, and dried over sodium sulfate before filtering and concentrating. The crude reaction mixture was purified on silica gel with 10%–30% dichloromethane in hexanes to yield the title compound as a clear oil (R_f = 0.14, 40% dichloromethane in hexanes).
Yield: 140.1 mg (60%); ^{1}H NMR (700 MHz, $CDCl_3$) δ = 6.80 (d, J = 3.8 Hz, 1H), 6.61 (d, J = 3.8 Hz, 1H), 3.87 (s, 3H), 1.61 (s, 9H); ^{19}F NMR (470 MHz, $CDCl_3$) δ = -59.66; ^{13}C NMR (175 MHz, $CDCl_3$) δ = 160.2, 147.2, 127.8, 125.6 (q, JC-F = 125.6 Hz), 119.9 (q, JC-F = 267 Hz), 116.1, 112.8 (q, JC-F = 3.6 Hz), 86.9, 52.1, 27.1; HRMS (EI+) m/z: $[M - Boc + H]^+$ calculated 193.0351, found 193.0351. IR (neat): v = 2989, 1777, 1728, 1558, 1373, 1247, 1123.

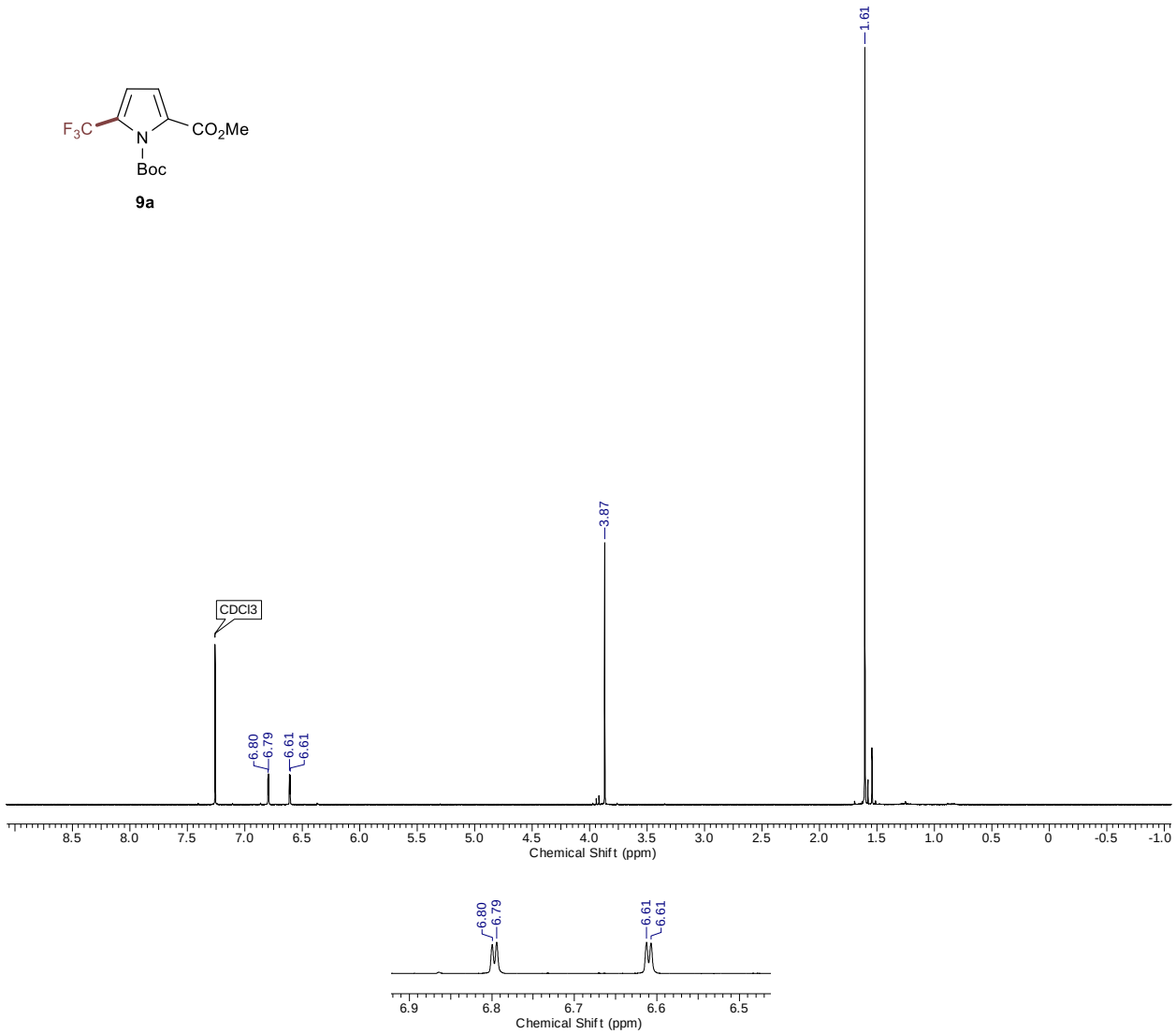

Figure S8. ^{1}H NMR spectrum (700 MHz, $CDCl_3$) of **9a**.

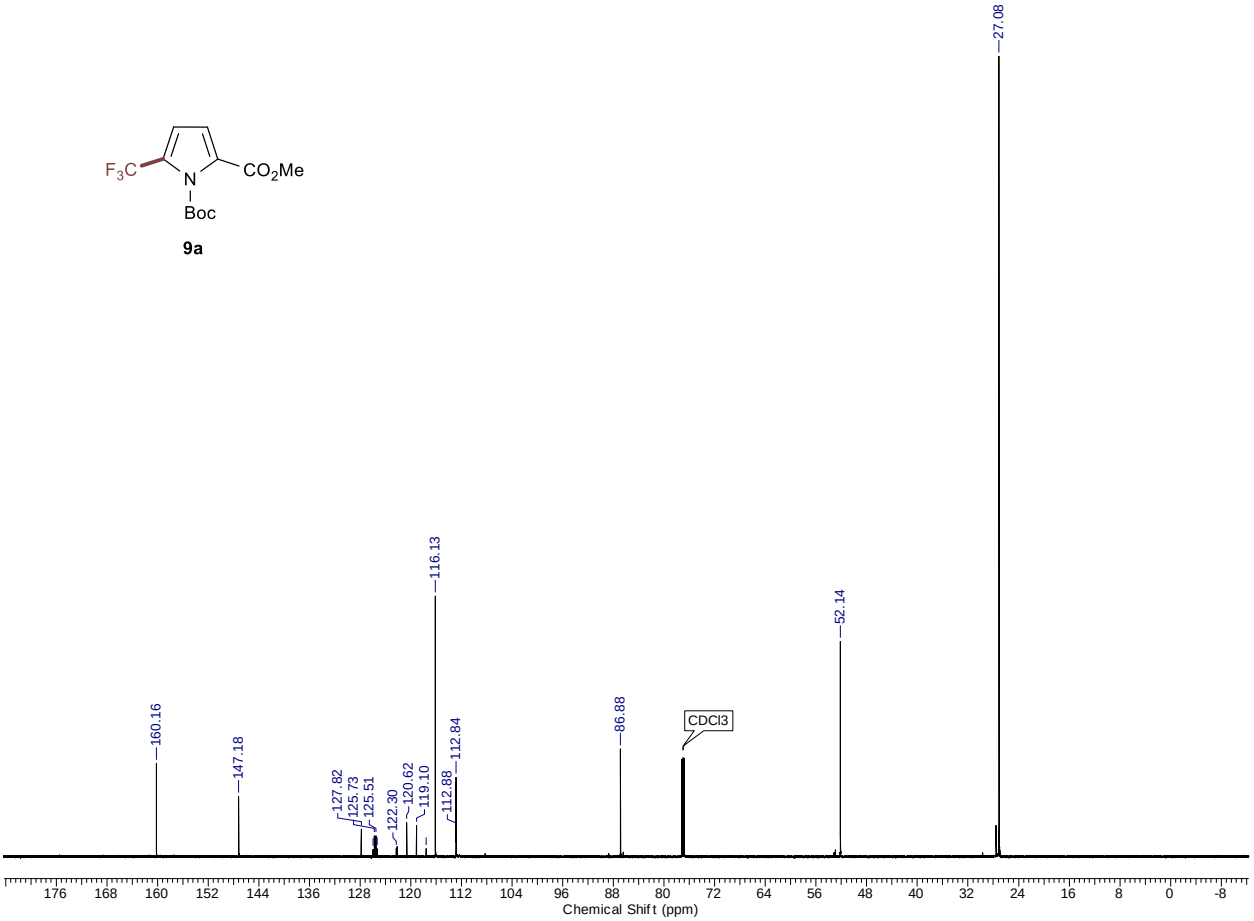

Figure S9. ^{13}C NMR spectrum (175 MHz, $CDCl_3$) of **9a.**

2,2,2-trifluoro-1-(1-phenyl-5-(trifluoromethyl)-1H-pyrrol-2-yl)ethan-1-one (10a)

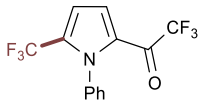

Following the general procedure, using 4-phenylpyridine *N*-oxide (273.9 mg, 1.6 mmol, 2.0 equiv.) and TFAA (237 µl, 1.68 mmol, 2.1 equiv.), the reaction was run for 7 hours. ^{19}F NMR analysis of the crude reaction mixture vs. the injected trifluorotoluene standard revealed the title compound in **59% yield** with 22% remaining starting material. The use of more equivalents of reagent did not result in higher yields of product, but further consumed the starting material. The reaction was partitioned with 1N HCl and diluted with dichloromethane. The organic phase was separated, washed with sat. $NaHCO_3$, brine, and dried over sodium sulfate before filtering and concentrating. The crude reaction mixture was purified by prep TLC (10% ethyl acetate in hexanes) to yield the title compound as a clear oil (R_f = 0.53, 25% dichloromethane in hexanes).
Yield: 143.0 mg (53%). The isolation and characterization of this compound has previously been reported.[3]

(5-(trifluoromethyl)thiophen-2-yl)boronic acid MIDA ester (11a)

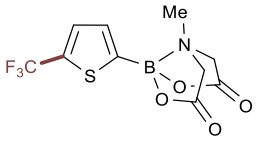

Following the general procedure, using 4-phenylpyridine *N*-oxide (547.8 mg, 3.2 mmol, 4.0 equiv.) and TFAA (463 µl, 3.28 mmol, 4.1 equiv.) with 4 ml total of dry MeCN (0.2M) the reaction was run for 12 hours. ^{19}F NMR analysis of the crude reaction mixture vs. the injected trifluorotoluene standard revealed the title compound in 73% yield. The use of fewer equivalents of reagent at shorter reaction times provided comparable yields of product, but incompletely consumed the starting material, which was inseparable from the product. The reaction was partitioned with 1N HCl and diluted with dichloromethane. The organic phase was separated, washed with brine, and dried over sodium sulfate before filtering and concentrating. The crude reaction mixture was purified on silica gel. Pyridine derivatives were flushed off the column with ~750 ml of 2% methanol in diethyl ether[6] before the product was eluted with 10% MeCN in CH_2Cl_2 as an amorphous, off-white solid (R_f = 0.44, 100% THF).
Yield: 179.7 mg (73%). The isolation and characterization of this compound has previously been reported.[3]

(1-(tert-butoxycarbonyl)-5-(trifluoromethyl)-1H-pyrrol-2-yl)boronic acid MIDA ester (12a)

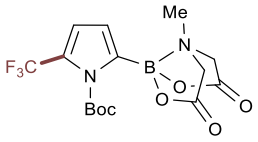

Following the general procedure, using 4-phenylpyridine *N*-oxide (410.9 mg, 2.4 mmol, 3.0 equiv.) and TFAA (350 µl, 2.48 mmol, 3.1 equiv.) with 4 ml total of dry MeCN (0.2M) the reaction was run for 12 hours. It should be noted that for this substrate the reaction mixture gets very dark upon exposure to light, which limits conversion at higher concentrations (0.4M). ^{19}F NMR analysis of the crude reaction mixture vs. the injected trifluorotoluene standard revealed the title compound in 75% yield. The reaction was filtered through silica gel with 50% MeCN in CH_2Cl_2 and concentrated. The crude reaction mixture was purified on silica gel. Pyridine derivatives were flushed off the column with ~750 ml of 2% methanol in diethyl ether before the product was eluted with 10% MeCN in CH_2Cl_2 as an off-white solid (R_f = 0.43, 25% MeCN in CH_2Cl_2). This material was further purified by preparative TLC (25% MeCN in CH_2Cl_2) to yield the title compound as a white solid.
Yield: 190.6 mg (62%); ^{1}H NMR (500 MHz, $CDCl_3$) δ = 6.72 (d, J = 3.6 Hz, 1H), 6.68 (d, J = 3.6 Hz, 1H), 4.18 (d, J = 16.8 Hz, 2H), 3.95 (d, J = 16.8 Hz, 2H), 3.00 (s, 3H), 1.57 (s, 9H); ^{19}F NMR (470 MHz, $CDCl_3$) δ = –58.01; ^{13}C NMR (175 MHz, $CDCl_3$) δ = 169.7, 150.8, 125.5 (q, JC-F = 38.8 Hz), 121.9 (q, JC-F = 265.7 Hz), 121.7, 117.4 (q, JC-F = 4.1 Hz), 87.8, 65.9, 50.5, 27.6; HRMS (EI+) m/z: $[M – Boc + H]^+$ calculated 290.0686, found 290.0687; IR (neat): v = 2999, 1741, 1564, 1454, 1334, 1220, 1126, 1032.

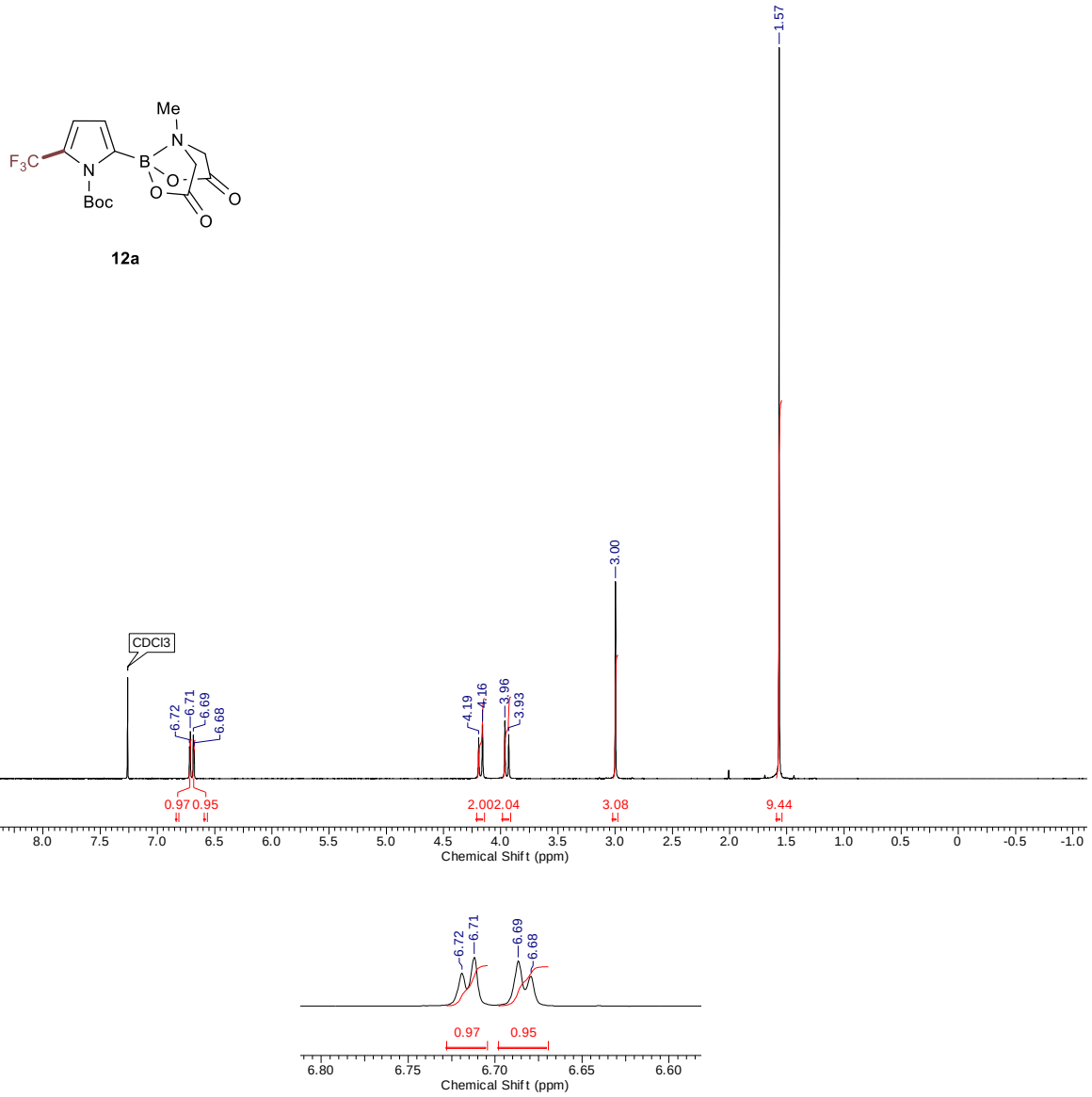

Figure S10. ^{1}H NMR spectrum (500 MHz, $CDCl_3$) of **12a**.

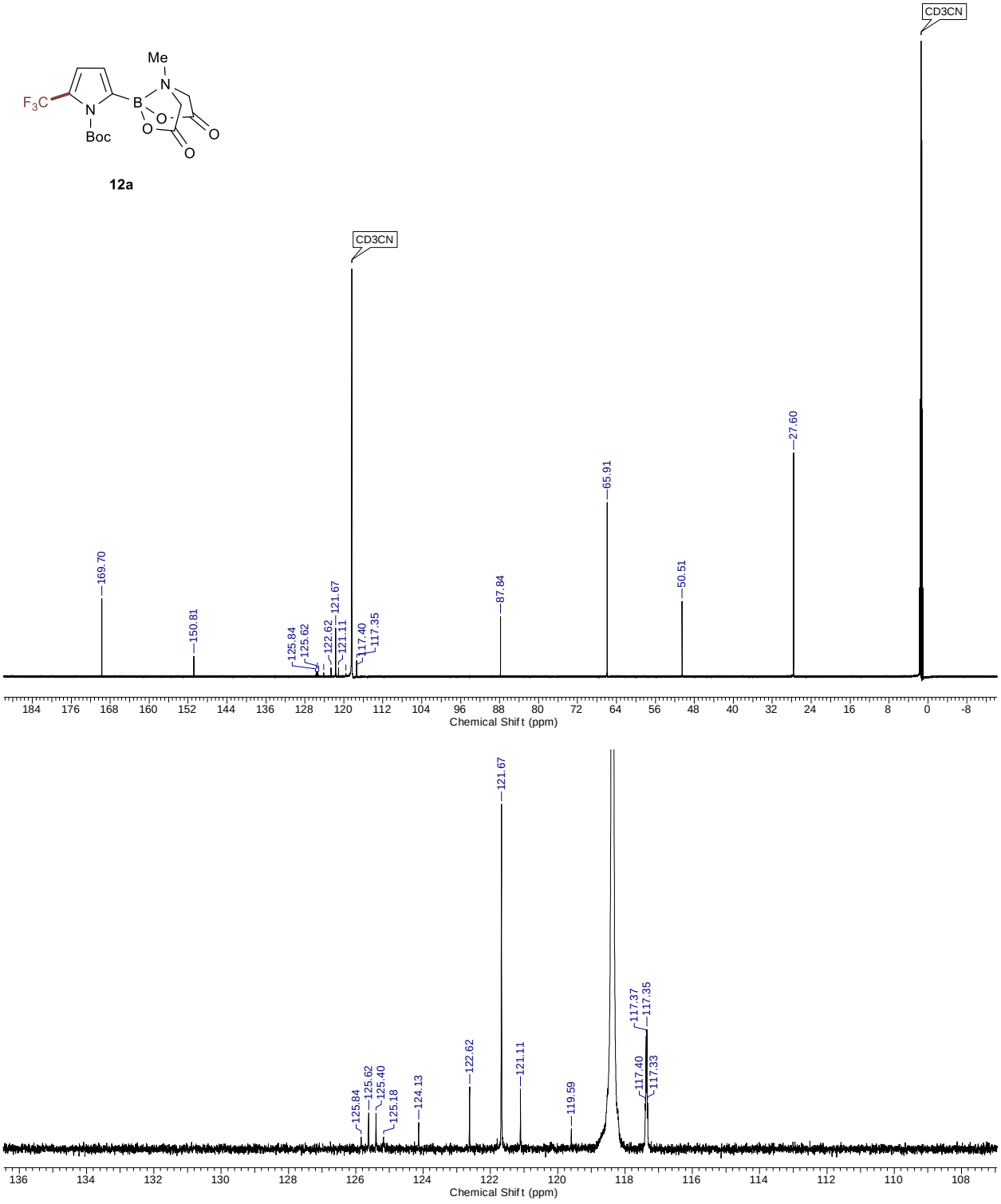

Figure S11. ^{13}C NMR spectrum (175 MHz, CD_3CN) of **12a**.

(5-(trifluoromethyl)furan-2-yl)boronic acid MIDA ester (13a)

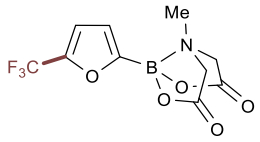

Following the general procedure, using 4-phenylpyridine *N*-oxide (273.9 mg, 1.6 mmol, 2.0 equiv.) and TFAA (237 µl, 1.68 mmol, 2.1 equiv.), the reaction was run for 6 hours. ^{19}F NMR analysis of the crude reaction mixture vs. the injected trifluorotoluene standard revealed the title compound in 60% yield. The reaction was filtered through silica gel with 50% MeCN in CH_2Cl_2 and concentrated. The crude reaction mixture was purified on silica gel. Pyridine derivatives were flushed off the column with ~750 ml of 2% methanol in diethyl ether[6] before the product was eluted with 10% MeCN in CH_2Cl_2 as an amorphous, off-white solid (R_f = 0.46, 20% MeCN/CH_2Cl_2).
Yield: 137.8 mg (59%); ^{1}HNMR (700 MHz, MeCN-*d3*) δ = 6.99 (d, J = 3.2 Hz, 1H), 6.85 (d, J = 3.2 Hz, 1H), 4.12 (d, J = 17.3 Hz, 2H), 3.96 (d, J = 17.3 Hz, 2H), 2.70 (s, 3H); ^{19}F NMR (470 MHz, $CDCl_3$) δ = -64.95; ^{13}C NMR (175 MHz, MeCN-*d3*) δ = 169.3, 145.4 (q, JC-F = 41.8 Hz), 120.9 (q, JC-F = 267.7 Hz), 120.5, 113.8 (q, JC-F = 2.7 Hz), 63.1, 48.6; HRMS (ESI+) m/z: $[M + NH_4]^+$ calculated 309.0864, found 309.0866; IR (neat): v = 2953, 1757, 1605, 1462, 1309, 1279, 1218, 1173, 1125, 1102, 1050, 1009, 936.

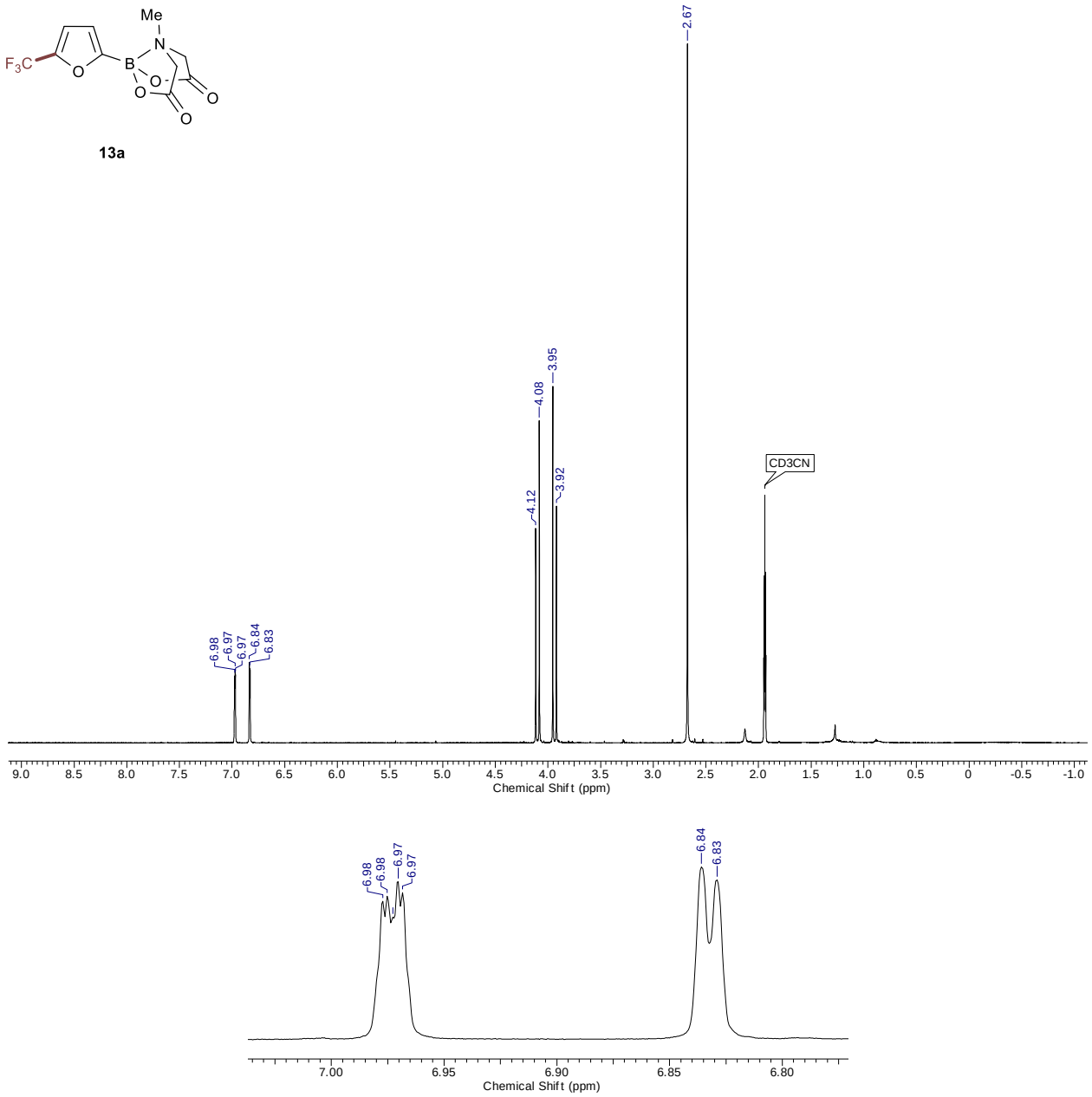

Figure S12. ^{1}H NMR spectrum (500 MHz, $CDCl_3$) of **13a**.

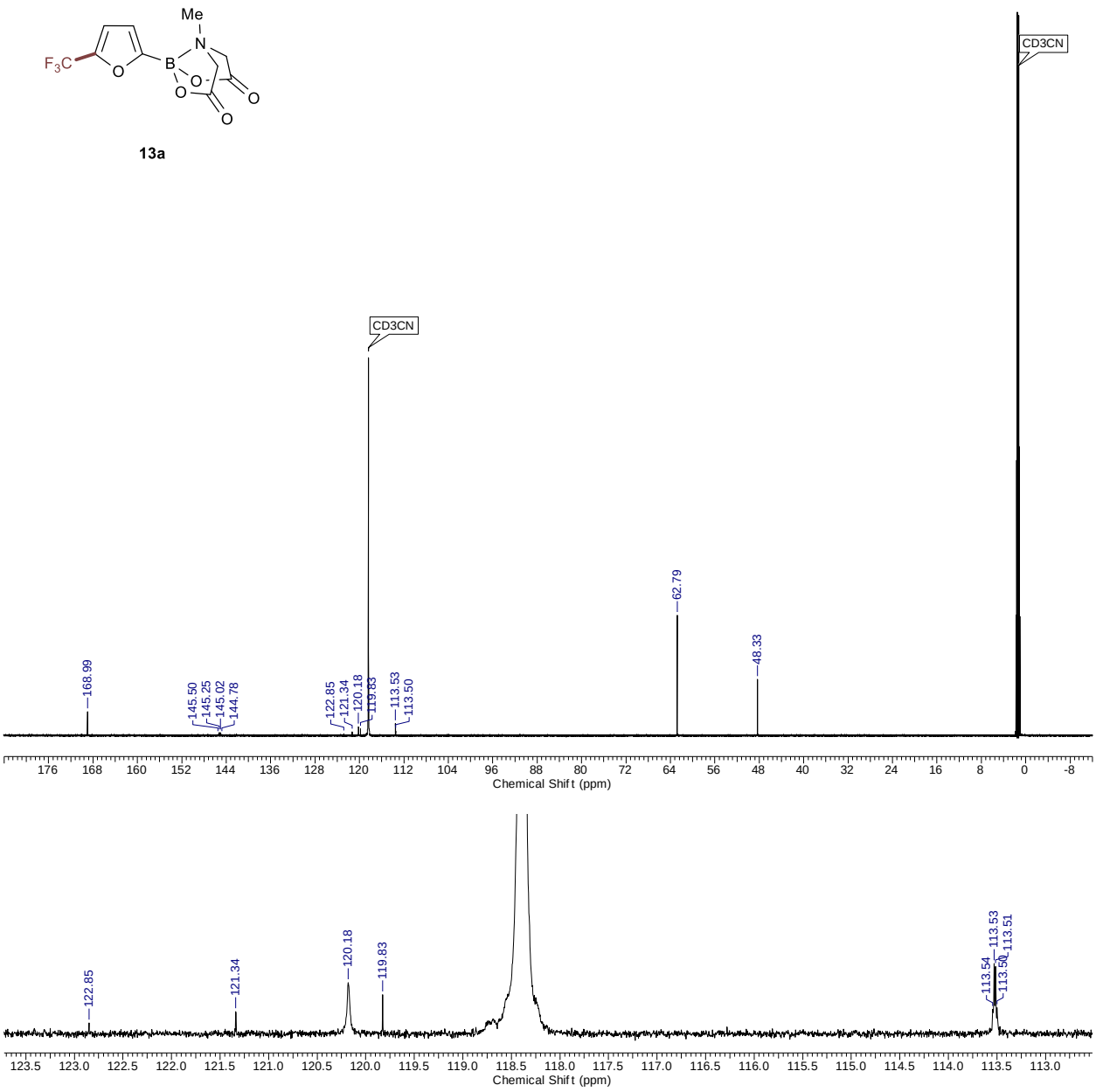

Figure S13. ^{13}C NMR spectrum (175 MHz, CD_3CN) **13a**.

tert-butyl 2-(trifluoromethyl)-1H-pyrrole-1-carboxylate (14a)

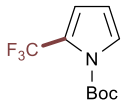

Following the general procedure using 4-phenylpyridine *N*-oxide (137.0 mg, 0.8 mmol, 1.0 equiv.) and TFAA (124 µl, 0.88 mmol, 1.1 equiv.), the reaction was run for 15 hours. ^{19}F NMR analysis of the crude reaction mixture vs. the injected trifluorotoluene standard revealed the volatile title compound tert-butyl 2-(trifluoromethyl)-1H-pyrrole-1-carboxylate [^{19}F NMR (470 MHz, $CDCl_3$) δ = -59.29 (s, 3F, 56% yield)] and tert-butyl 2,5-bis(trifluoromethyl)-1H-pyrrole-1-carboxylate [^{19}F NMR (470 MHz, $CDCl_3$) δ = -59.36 (s, 6F, 9% yield)] in a 6:1ratio.
Yield: 0.520 mmol (65%, 6:1 14a:14b); ^{19}F NMR (470 MHz, $CDCl_3$) δ = -59.29 (s, 3F, 14a 56% yield), -59.36 (s, 6F, 14b 9%). The isolation and characterization of this compound has been previously reported.[3]

tert-butyl 2,5-bis(trifluoromethyl)-1H-pyrrole-1-carboxylate (15a)

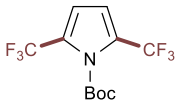

Following the general procedure using 4-phenylpyridine *N*-oxide (410.9 mg, 2.4 mmol, 3.0 equiv.) and TFAA (350 µl, 2.48 mmol, 3.1 equiv.), the reaction was run for 15 hours. ^{19}F NMR analysis of the crude reaction mixture vs. the injected trifluorotoluene standard revealed the volatile title compound tert-butyl 2-(trifluoromethyl)-1H-pyrrole-1-carboxylate [^{19}F NMR (470 MHz, $CDCl_3$) δ = -59.29 (s, 3F, 7% yield)] and tert-butyl 2,5-bis(trifluoromethyl)-1H-pyrrole-1-carboxylate [^{19}F NMR (470 MHz, $CDCl_3$) δ = -59.36 (s, 6F, 56% yield)] in a 8:1ratio.
Yield: 0.504 mmol (63%, 1:8 14a:14b); ^{19}F NMR (470 MHz, $CDCl_3$) δ = -59.29 (s, 3F, 14a 7% yield), -59.36 (s, 6F, 14b 56%). The isolation and characterization of this compound has been previously reported.[3]

1,3-dimethyl-3-(2,2,2-trifluoroethyl)indolin-2-one (16a)

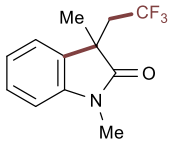

Following the general procedure using 4-phenylpyridine *N*-oxide (273.9 mg, 1.6 mmol, 2.0 equiv.) and TFAA (451 µl, 3.2 mmol, 4.0 equiv.), the reaction was run for 12 hours. ^{19}F NMR analysis of the reaction mixture cannot be accurately accomplished due to peak overlap of theproduct with a minor impurity. The reaction was partitioned with 1N HCl and diluted with ethyl acetate. The organic phase was separated, washed with sat. $NaHCO_3$, brine, and dried over sodium sulfate before filtering and concentrating. The crude reaction mixture was purified by column chromatography (0% to 50% ethyl acetate in hexanes) to yield the title compound.
Yield: 89.5 mg (46%). The isolation and characterization of this compound has been previously reported.[3]

1-(tert-butyl) 2-methyl 5-(perfluoroethyl)-1H-pyrrole-1,2-dicarboxylate (18)

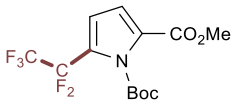

Following the general procedure, using 4-phenylpyridine *N*-oxide (137.0 mg, 0.8 mmol, 1.0 equiv.) and pentafluoropropionic anhydride (174 µl, 0.88 mmol, 1.1 equiv.), the reaction was run for 6 hours. ^{19}F NMR analysis of the crude reaction mixture vs. the injected trifluorotoluene standard revealed the title compound in 80% yield. The reaction was partitioned with 1N HCl and diluted with dichloromethane. The organic phase was separated, washed with sat. $NaHCO_3$, brine, and dried over sodium sulfate before filtering and concentrating. The crude reaction mixture was purified by column chromatography (30% dichloromethane in hexanes) to yield the title compound as a clear oil (R_f = 0.1, 25% dichloromethane in hexanes).

Yield: 198.9 mg (72%); ^{1}H NMR (700 MHz, $CDCl_3$) δ = 6.87 (d, J = 3.8 Hz, 1H), 6.58 (d, J = 3.8 Hz, 1H), 3.87 (s, 3H), 1.61 (s, 9H); ^{19}F NMR (376 MHz, $CDCl_3$) δ = -84.23 (3F), -107.82 (2F); ^{13}C NMR (175 MHz, $CDCl_3$) δ = 159.8, 147.7, 127.3, 123.1 (t, JC-F = 27.2 Hz), 118.5 (qt, JC-F = 287.1, 38.1 Hz), 116.1, 113.6 (app. tq, JC-F = 5.7, 1.9 Hz), 110.3 (tq, JC-F = 252.7, 40.1 Hz), 87.1, 52.1, 27.0; HRMS (EI+) m/z: $[M - Boc + H]^+$ calculated 243.0319, found 243.0314; IR (neat): v = 2991, 1782, 1726, 1546, 1373, 1250, 1207, 1133, 1096, 1034.

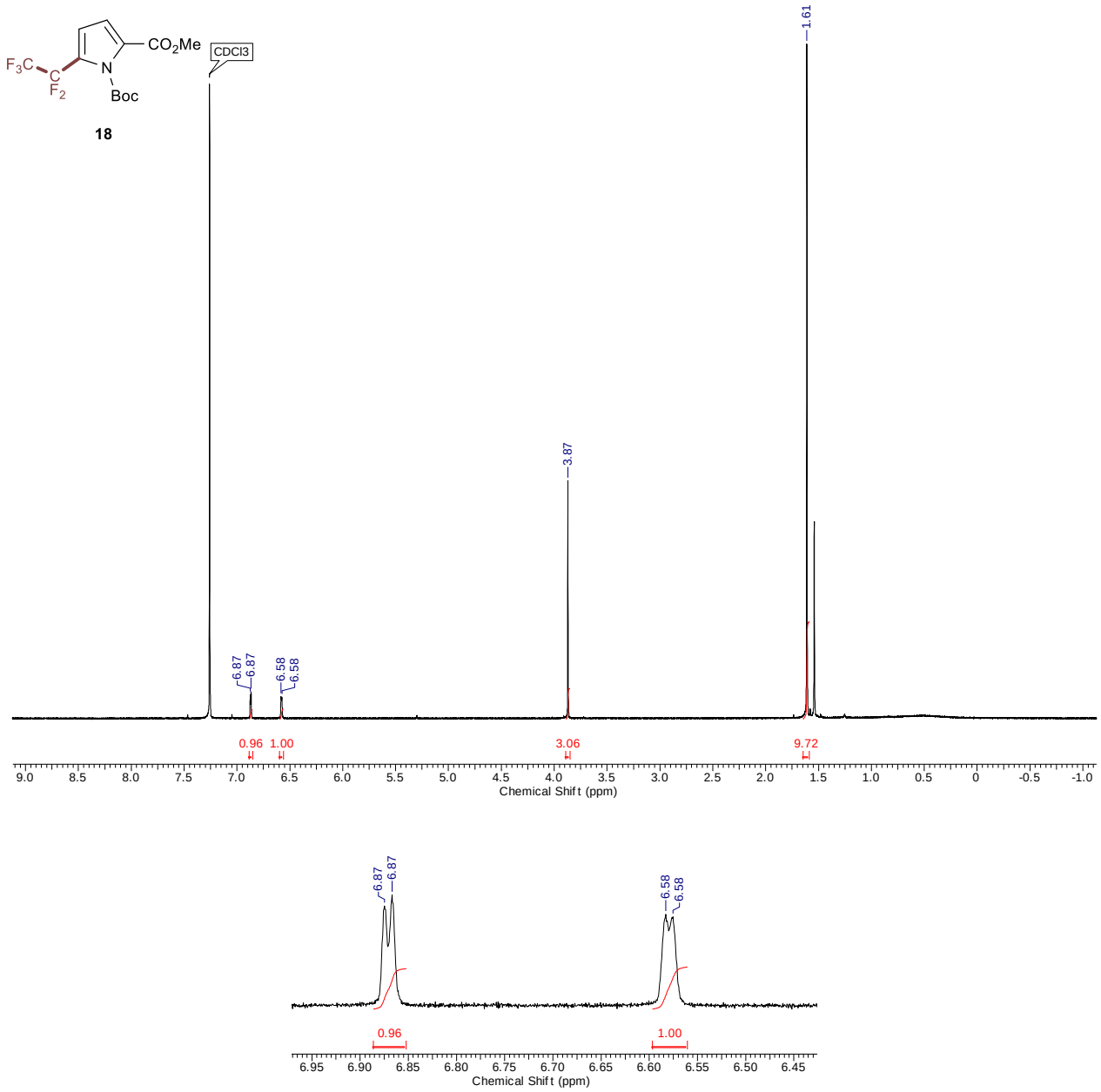

Figure S14. ^{1}H NMR spectrum (500 MHz, $CDCl_3$) of **18**.

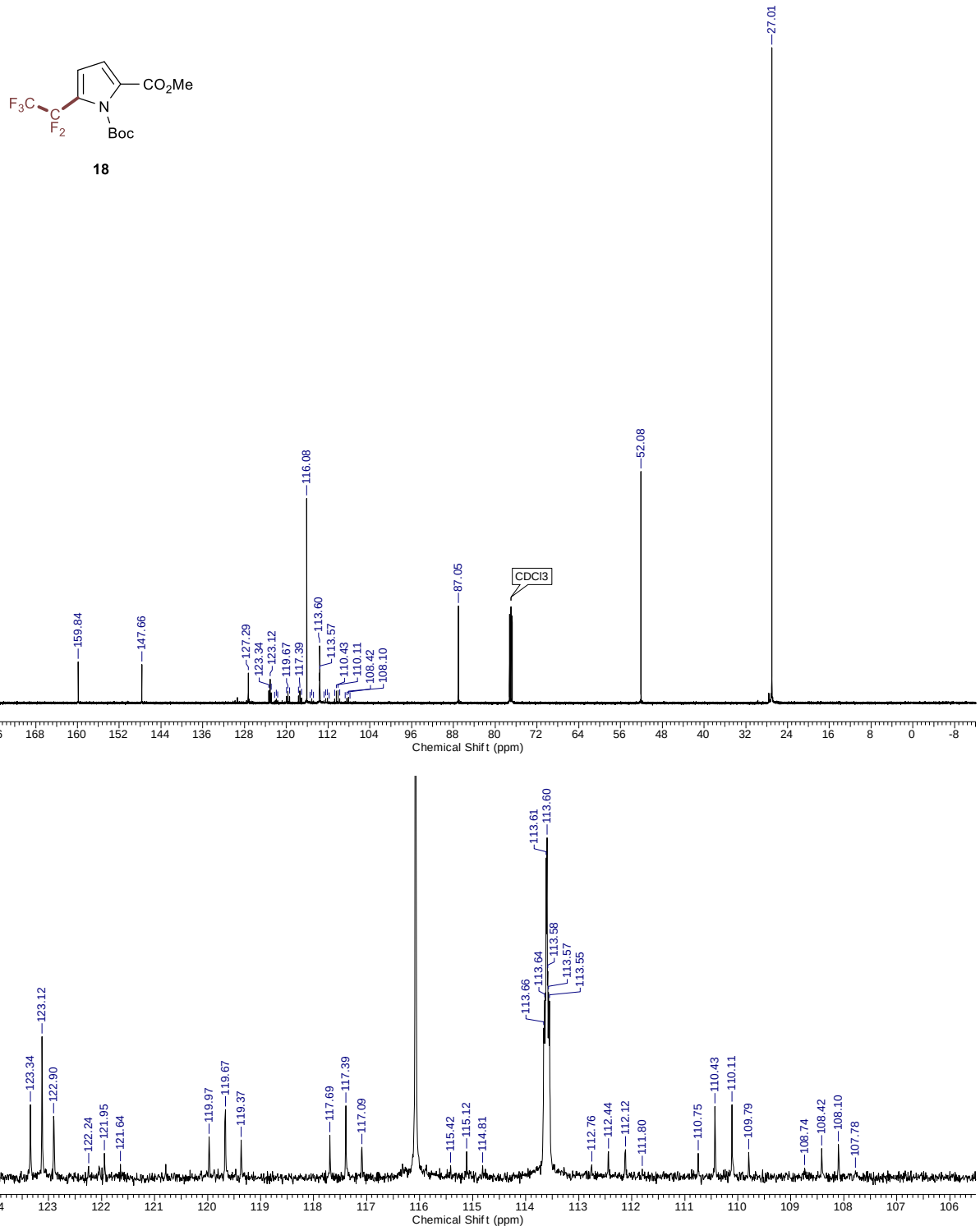

Figure S15. ^{13}C NMR spectrum (175 MHz, $CDCl_3$) of **18**.

(5-(perfluoroethyl)thiophen-2-yl)boronic acid MIDA ester (19)

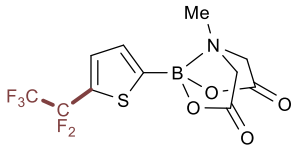

Following the general procedure, using 4-phenylpyridine *N*-oxide (410.9 mg, 2.4 mmol, 3.0 equiv.) and pentafluoropropionic anhydride (517 µl, 2.48 mmol, 3.1 equiv.) with 4 ml total of dry MeCN (0.2M) the reaction was run for 12 hours. ^{19}F NMR analysis of the crude reaction mixture vs. the injected trifluorotoluene standard revealed the title compound in 95% yield. The reaction was partitioned with 1N HCl and diluted with dichloromethane. The organic phase was separated, washed with brine, and dried over sodium sulfate before filtering and concentrating. The crude reaction mixture was purified on silica gel. Pyridine derivatives were flushed off the column with ~750 ml of 2% methanol in diethyl ether[6] before the product was eluted with 10% MeCN in CH_2Cl_2 as an amorphous, off-white solid (R_f = 0.33, 20% MeCN in CH_2Cl_2).

Yield: 260.0 mg (91%); ^{1}H NMR (700 MHz, MeCN-*d3*) δ = 7.62 (d, J = 3.5 Hz, 1H), 7.36 (dt, J = 3.5 Hz, JH-F = 1.9 Hz, 1H), 4.12 (d, J = 17.2 Hz, 2H), 3.96 (d, J = 17.2 Hz, 2H), 2.65 (s, 3H); ^{19}F NMR (376 MHz, MeCN-*d3*) δ = -86.08 (br. s, 3F), -105.14 (s, 2F); ^{13}C NMR (175 MHz, MeCN-*d3*) δ = 168.9, 134.9, 133.0 (t, JC-F = 29.7 Hz), 132.9 (t, JC-F = 5.4 Hz), 119.9 (qt, JC-F = 285.4, 40.9 Hz), 113.7 (tq, JC-F = 251.4, 39.5 Hz), 62.8, 48.7; HRMS (ESI+) m/z: $[M + H]^+$ calculated 358.0338, found 358.0344, $[M + Na]^+$ calculated 380.0159, found 380.0159; IR (neat): ν = 3011, 1760, 1535, 1459, 1337, 1285, 1258, 1196, 1165, 1030, 980.

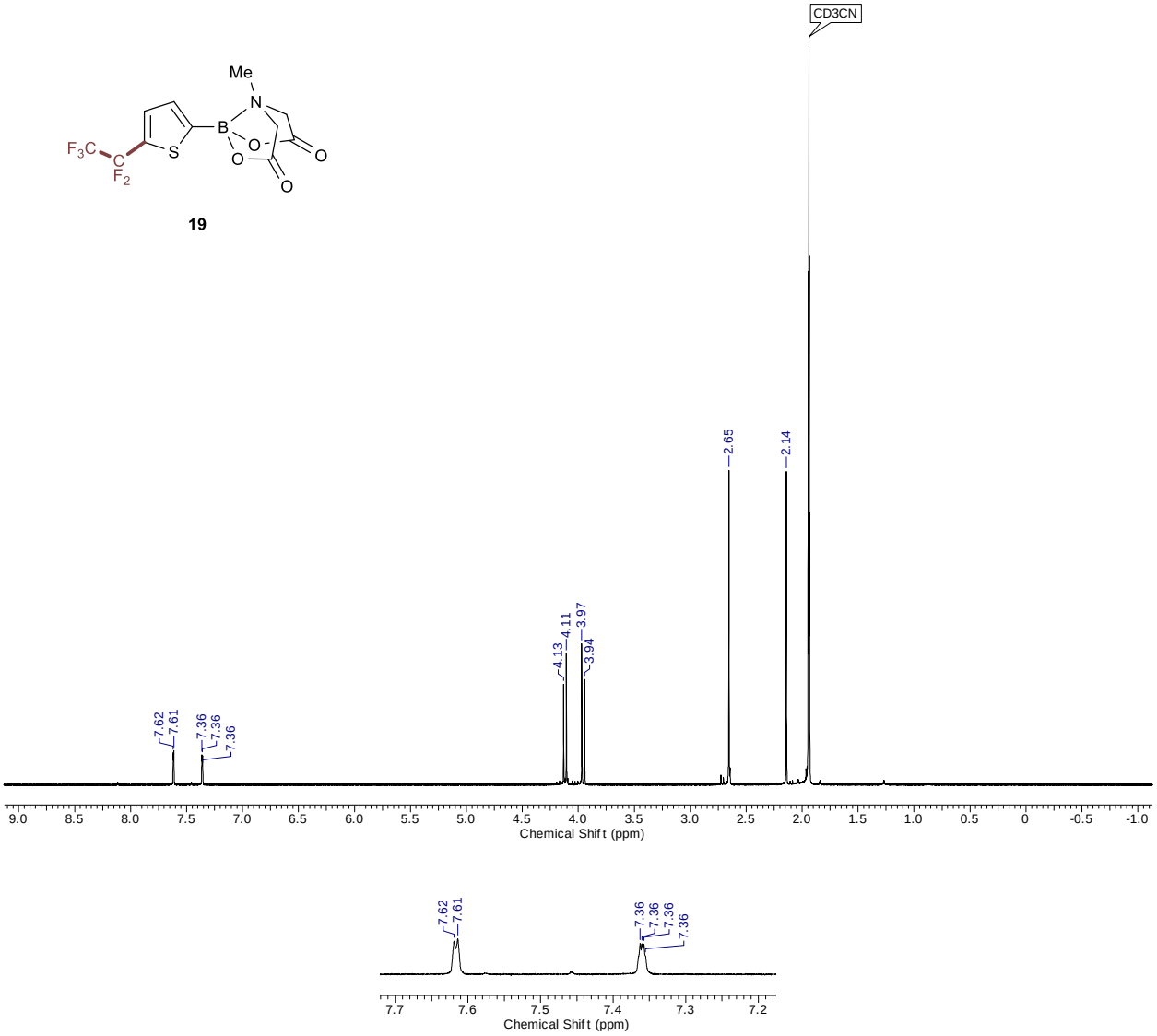

Figure S16. ^{1}H NMR spectrum (700 MHz, CD_3CN) of **19**.

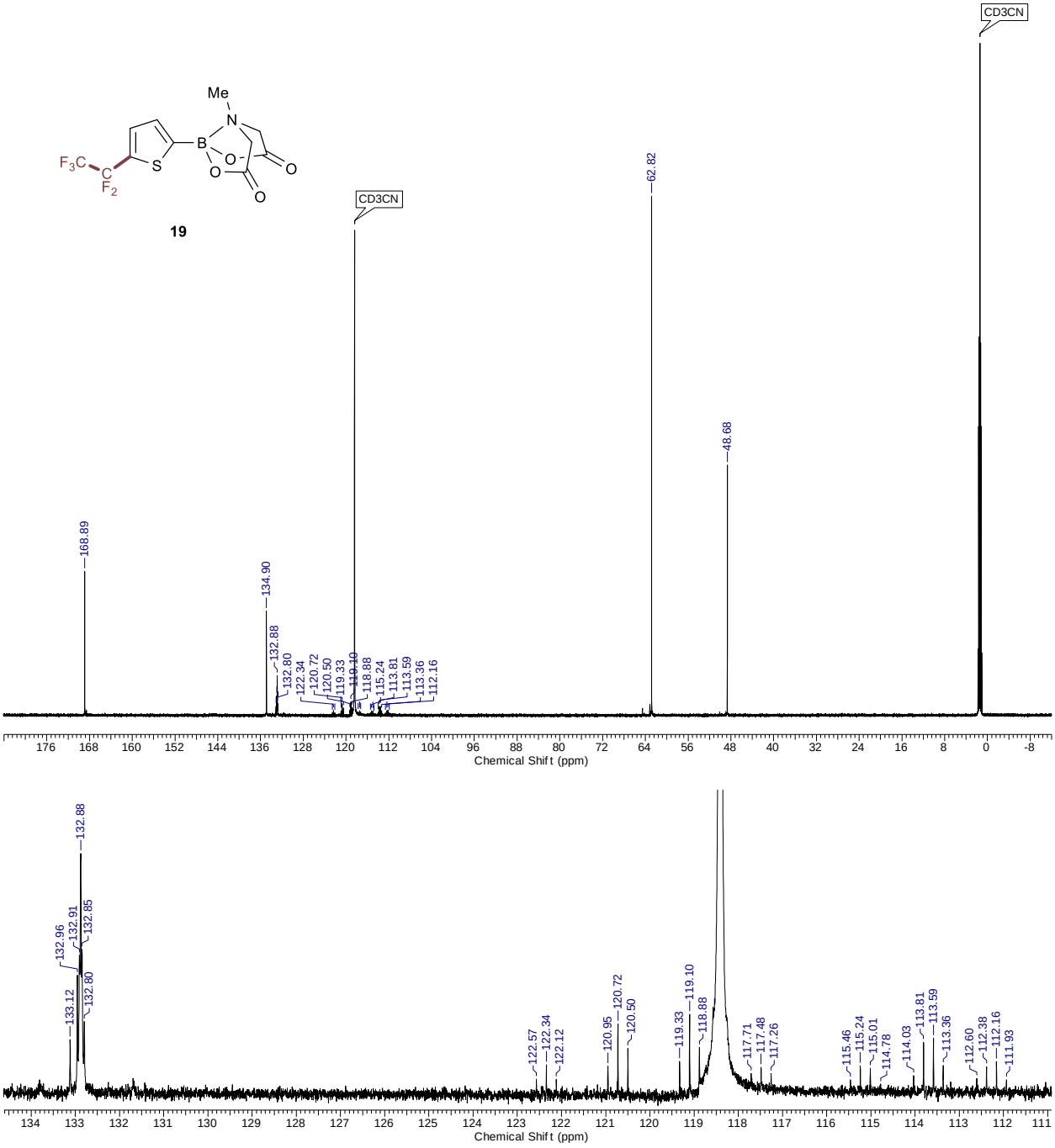

Figure S17. ^{13}C NMR spectrum (175 MHz, CD_3CN) of **19**.

4-(tert-butyl)-1-methoxy-2-(perfluoroethyl)benzene (20)

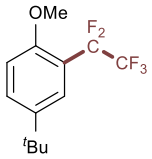

Following the general procedure, using 4-phenylpyridine *N*-oxide (410.9 mg, 2.4 mmol, 3.0 equiv.) and pentafluoropropionic anhydride (489 µl, 2.48 mmol, 3.1 equiv.), the reaction was run for 8 hours. ^{19}F NMR analysis of the crude reaction mixture vs. the injected trifluorotoluene standard revealed the title compound in 81% yield. The reaction was partitioned with 1N HCl and diluted with dichloromethane. The organic phase was separated, washed with sat. $NaHCO_3$, brine, and dried over sodium sulfate before filtering and concentrating. The crude reaction mixture was purified by prep TLC (100% hexanes run up x2) to yield the slightly volatile title compound as a clear oil (R_f = 0.57, 10% dichloromethane in hexanes). Yield: 0.648 mmol (81%); ^{1}H NMR (400 MHz, $CDCl_3$) δ = 7.53-7.49 (m, overlap, 2H), 6.95 (d, J = 8.4 Hz, 1H), 3.85 (s, 3H), 1.31 (s, 9H); ^{19}F NMR (376 MHz, $CDCl_3$) δ = -84.89 (3F), -112.60 (2F); ^{13}C NMR (175 MHz, $CDCl_3$) δ = 156.0 (t, JC-F = 2.7 Hz), 143.2, 130.2, 125.6 (t, JC-F = 8.5 Hz), 119.5 (qt, JC-F = 287.5, 39.5 Hz), 115.9 (t, JC-F = 115.9 Hz), 113.9 (tq, JC-F = 254.8, 41.6 Hz), 112.2, 56.0, 34.2, 31.3; HRMS (EI+) m/z: $[M]^+$ 282.1043, found 282.1042; IR (neat): v = 2961, 1617, 1510, 1464, 1268, 1194, 1074, 1030, 991.

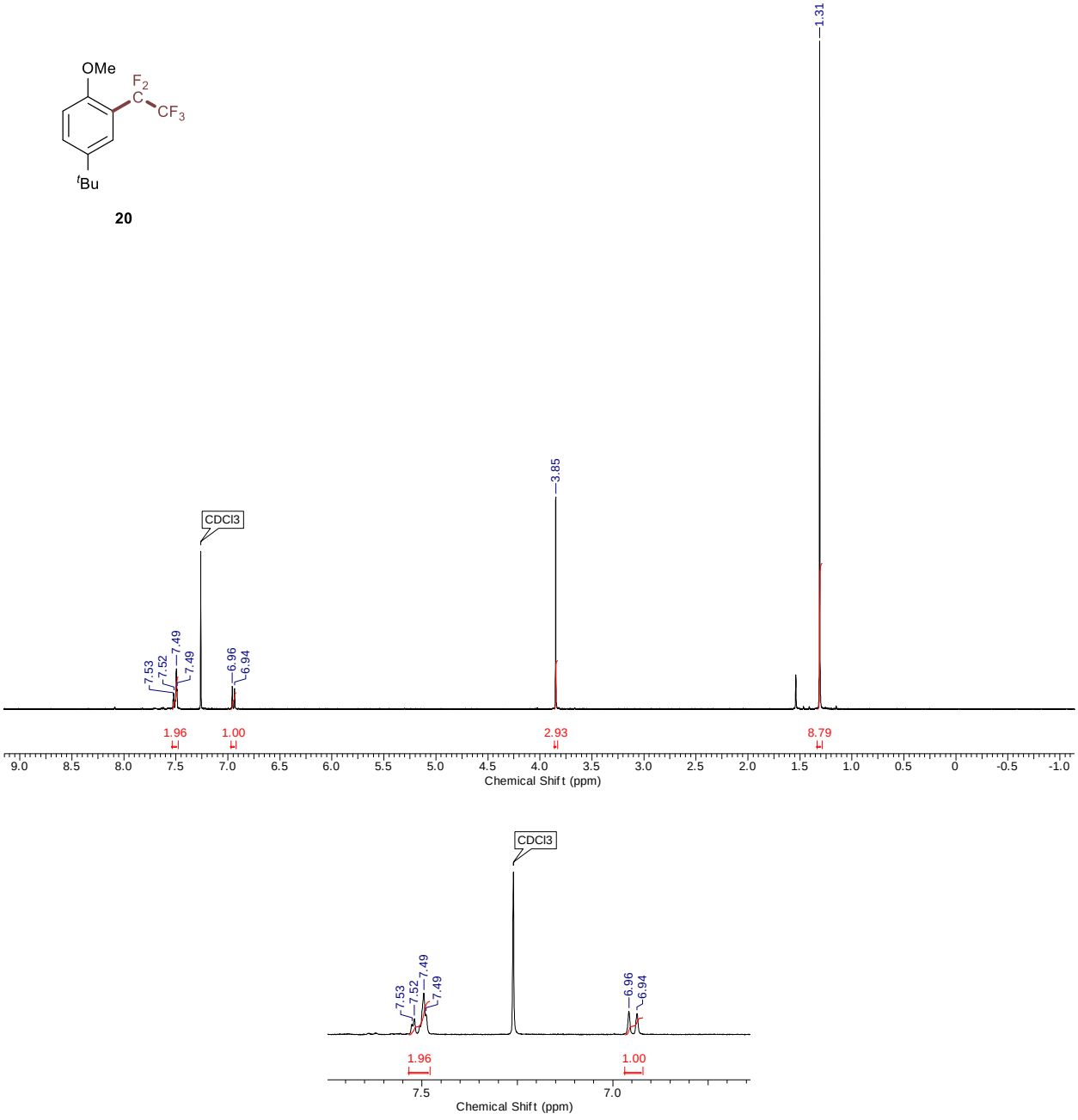

Figure S18. ^{1}H NMR spectrum (500 MHz, $CDCl_3$) of **20**.

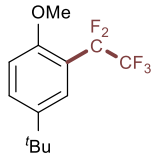

20

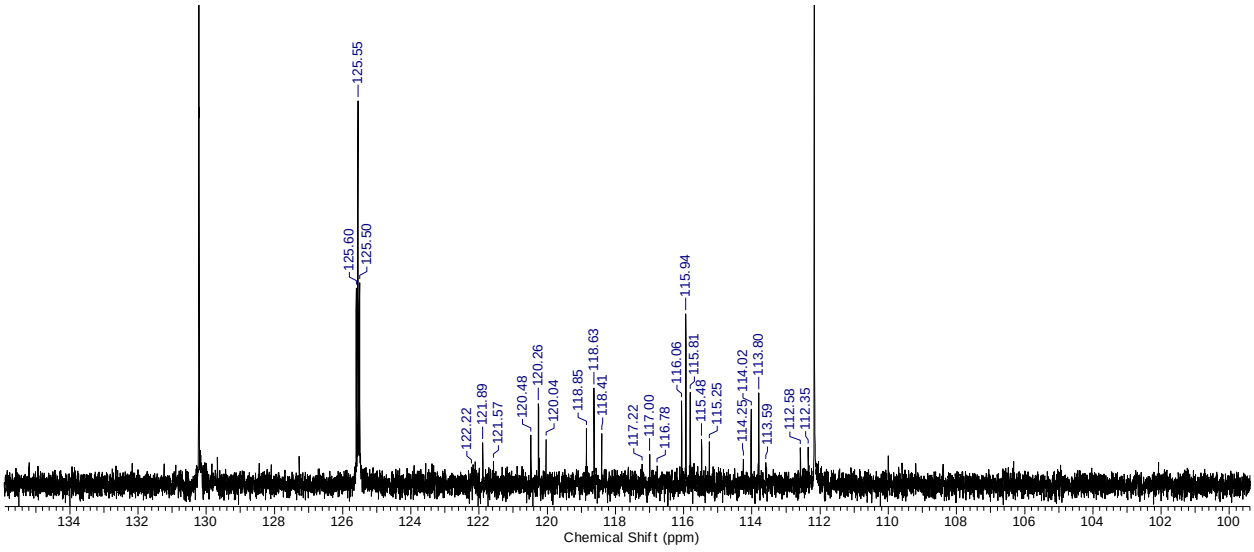

Figure S19. ^{13}C NMR spectrum (175 MHz, $CDCl_3$) of **20**.

(perfluoroethyl)benzene (21)

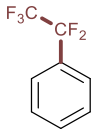

Following the general procedure, using 4-phenylpyridine *N*-oxide (137.0 mg, 0.8 mmol, 1.0 equiv.) as the limiting reagent, pentafluoropropionic anhydride (174 µl, 0.88 mmol, 1.1 equiv.), and benzene (713 µl, 8.0 mmol, 10.0 equiv.), the reaction was run for 12 hours. Upon completion, the reaction was quenched with methanol (500 µl) and removed from the light source. ^{19}F NMR analysis of the crude reaction mixture vs. the injected trifluorotoluene standard revealed the title compound in 76% yield. Due to the volatility of the product, no purification was attempted on this reaction mixture. The fluorine signals of the product were consistent to those reported in the literature: in one report,[7] values are listed vs. trifluorotoluene (referenced to δ 0.0) with positive values to high field, and are reproduced here with trifluorotoluene referenced to δ -63.72: ^{19}F NMR (no solvent reported, 60 MHz): δ -119.3 (m, 2F), -88.9 (t, J_{FF} = 1.7 Hz, 3F); Another report[8] reports the shifts in toluene-*d8* (δ -84, -113), while yet another[9] reports the shifts in benzene-*d6* (δ -84.86, -114.75).
Yield: 0.608 mmol (76%); ^{19}F NMR ($CDCl_3$, 470 MHz): δ -85.78 (s, 3F), -115.95 (s, 2F).

1-(tert-butyl) 2-methyl 5-(perfluoropropyl)-1H-pyrrole-1,2-dicarboxylate (24)

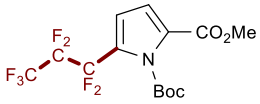

With heptafluorobutyric anhydride: Following the general procedure, using 4-phenylpyridine *N*-oxide (273.9 mg, 1.6 mmol, 2.0 equiv.) and heptafluorobutyric anhydride (412 µl, 1.68 mmol, 2.1 equiv.), the reaction was run for 4 hours. ^{19}FNMR analysis of the crude reaction mixture vs. the injected trifluorotoluene standard revealed the title compound in 78% yield. The reaction was partitioned with 1N HCl and diluted with dichloromethane. The organic phase was separated, washed with sat. $NaHCO_3$, brine, and dried over sodium sulfate before filtering and concentrating. The crude reaction mixture was purified by column chromatography (10-30% dichloromethane in hexanes) to yield the title compound as a clear oil (R_f = 0.31, 50% CH_2Cl_2 in hexanes).
Yield: 225.9 mg (72%); ^{1}H NMR (400 MHz, $CDCl_3$) δ = 6.89 (dt, J = 4.0, 1.2 Hz, 1H), 6.59 (d, J = 4.0 Hz, 1H), 3.87 (s, 3H), 1.60 (s, 9H); ^{19}F NMR (376 Hz, $CDCl_3$) δ = -81.01 (t, J_{FF} = 9.5 Hz, 3F), -105.91 (ap. sxt, tq, J_{FF} = 9.5, 8.9 Hz, 2F), -125.84 (t, J_{FF} = 8.9 Hz, 2F); ^{13}C NMR (175 MHz, $CDCl_3$) δ = 159.9, 147.7, 127.2, 123.1 (t, JC-F = 29.3 Hz), 117.9 (qt, JC-F = 287.5, 34.7), 116.1, 114.1 (t, JC-F = 5.4 Hz), 112.5 (tt, JC-F = 254.8, 32.7 Hz). 108.4 (ttq, JC-F = 265.0, 38.1, 38.1 Hz), 87.1, 52.1, 27.0 Hz; HRMS (EI+) m/z: $[M - Boc + H]^+$ calculated 293.0287, found 293.0291; IR (neat): v = 2984, 1784, 1727, 1546, 1437, 1373, 1248, 1202, 1154, 111, 1088, 838, 741.

With heptafluorobutyryl chloride: Following the general procedure, using 4-phenylpyridine *N*-oxide (273.9 mg, 1.6 mmol, 2.0 equiv.) and heptafluorobutyryl chloride (251 µl, 1.68 mmol, 2.1 equiv.), the reaction was run for 4 hours. ^{19}FNMR analysis of the crude reaction mixture vs. the injected trifluorotoluene standard revealed the title compound in 67% yield. The reaction was partitioned with 1N HCl and diluted with dichloromethane. The organic phase was separated, washed with sat. $NaHCO_3$, brine, and dried over sodium sulfate before filtering and concentrating. The crude reaction mixture was purified by column chromatography (10-30% dichloromethane in hexanes) to yield the title compound as a clear oil.
Yield: 193.2 mg (61%); Full characterization is above.

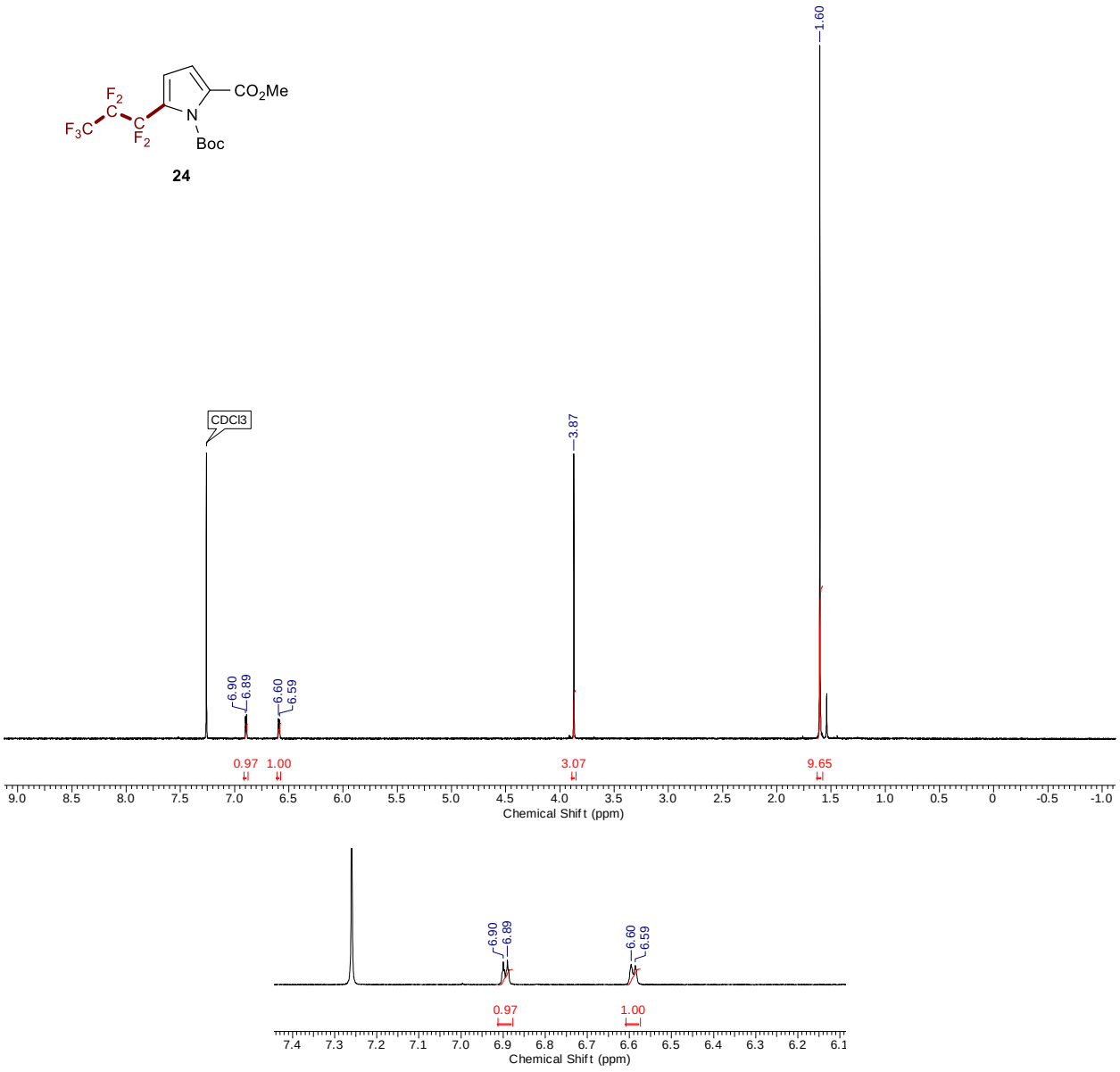

Figure S20. ^{1}H NMR spectrum (400 MHz, $CDCl_3$) of **24**.

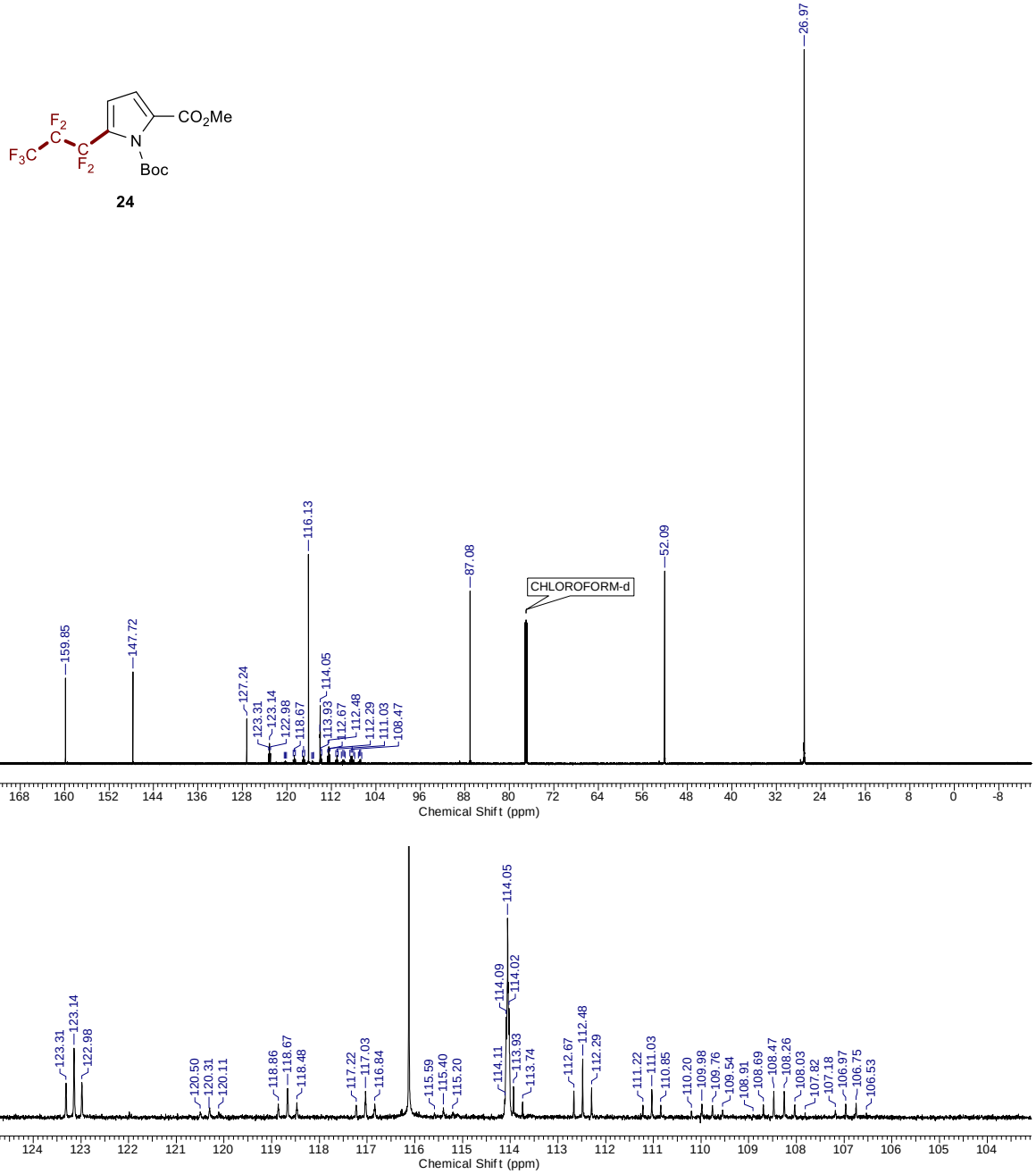

Figure S21. ^{13}C NMR spectrum (175 MHz, $CDCl_3$) of **24**.

***cis*-1-(tert-butyl) 2-methyl 5-(trifluoromethyl)pyrrolidine-1,2-dicarboxylate (17)**

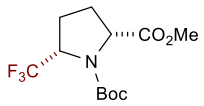

To a 10mL RBF equipped with a stir bar was added palladium on activated carbon (17 mg, 10 wt %, 0.016 mmol, 0.10 equiv). The flask was evacuated and backfilled with N_2 three times. Methanol (3 mL) was then added to the flask followed by pyrrole **9a** (46 mg, 0.16 mmol, 1 equiv). The heterogeneous mixture was stirred for 10 min under a H_2 atmosphere (gas balloon), filtered over silica, and concentrated under reduced pressure to give pure pyrrolidine **17** as white solid (R_f = 0.15, 10% ethyl acetate in hexanes). The solid could be re-crystallized in a minimum (1 mL) 1:1 pentane/Et_2O mixture to give colorless crystals.

Yield: 45.2 mg (97%); ^{1}H NMR (400 MHz, DMSO at 60 °C) δ = 4.61 (p, J = 8.2 Hz, 1H), 4.44 (t, J = 8.7 Hz, 1H), 3.78 (s, 3H), 2.45 (dd, J = 11.4, 8.2 Hz, 1H), 2.32 (dt, J = 12.5, 8.4 Hz, 1H), 2.13 (dd, J = 7.6, 5.6 Hz, 1H), 2.08 (m, 1H), 1.51 (s, 9H); ^{19}F NMR (376 MHz, $CDCl_3$) δ = -74.73 (3F); ^{13}C NMR (175 MHz, $CDCl_3$) δ = 172.0, 153.8, 125.3 (q, JC-F = 283.9 Hz), 81.4, 60.4 (d, JC-F = 96.0), 58.4 (m), 52.0, 28.3 (d, JC-F = 109.2), 27.9, 25.8 (d, JC-F = 111.6); HRMS (EI+) m/z: $[M - Boc + H]^+$ calculated 198.0736, found 198.0737; IR (neat): v = 2978, 1760, 1708, 1438, 1364, 1284, 1156, 1118, 1053.

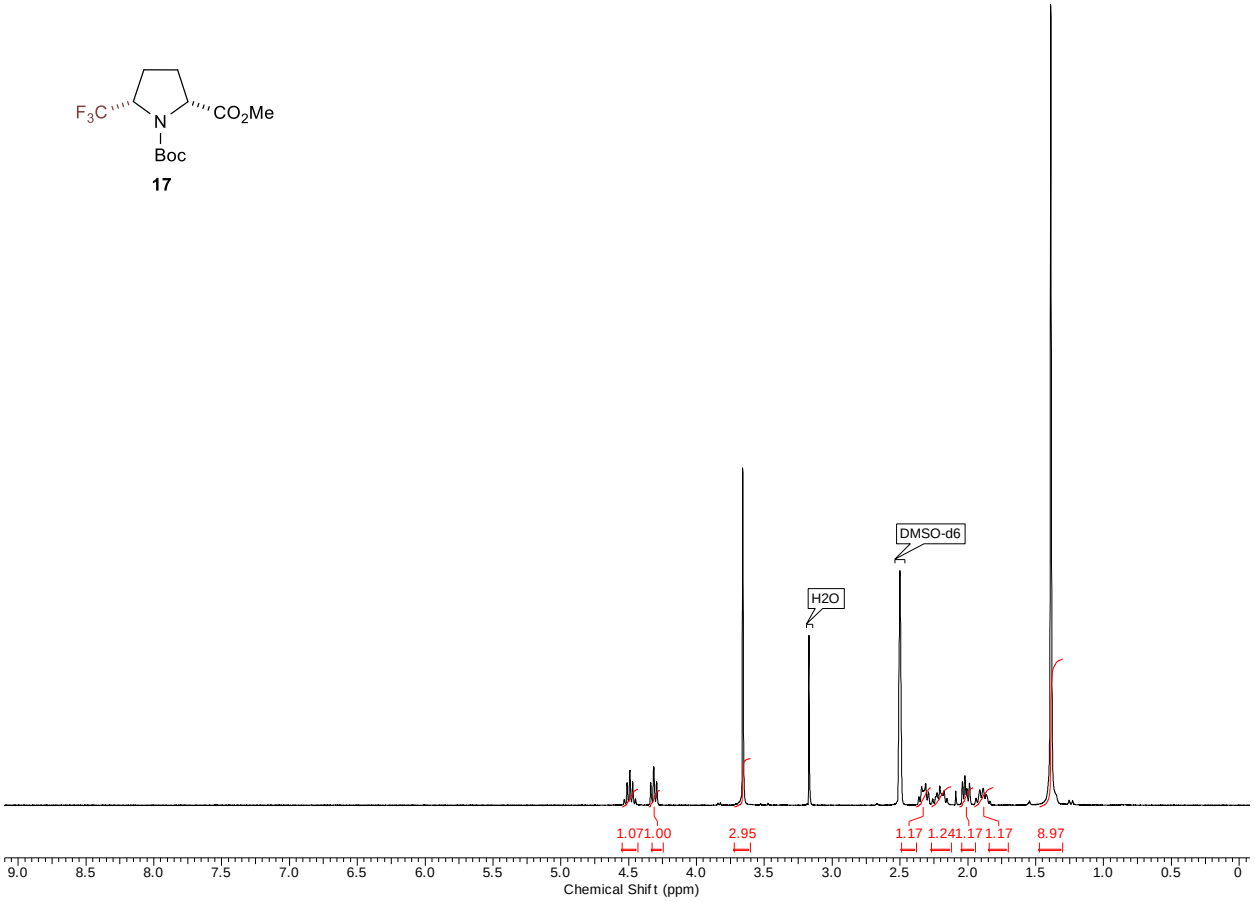

Figure S22. ^{1}H NMR spectrum (400 MHz, $CDCl_3$) of **17**.

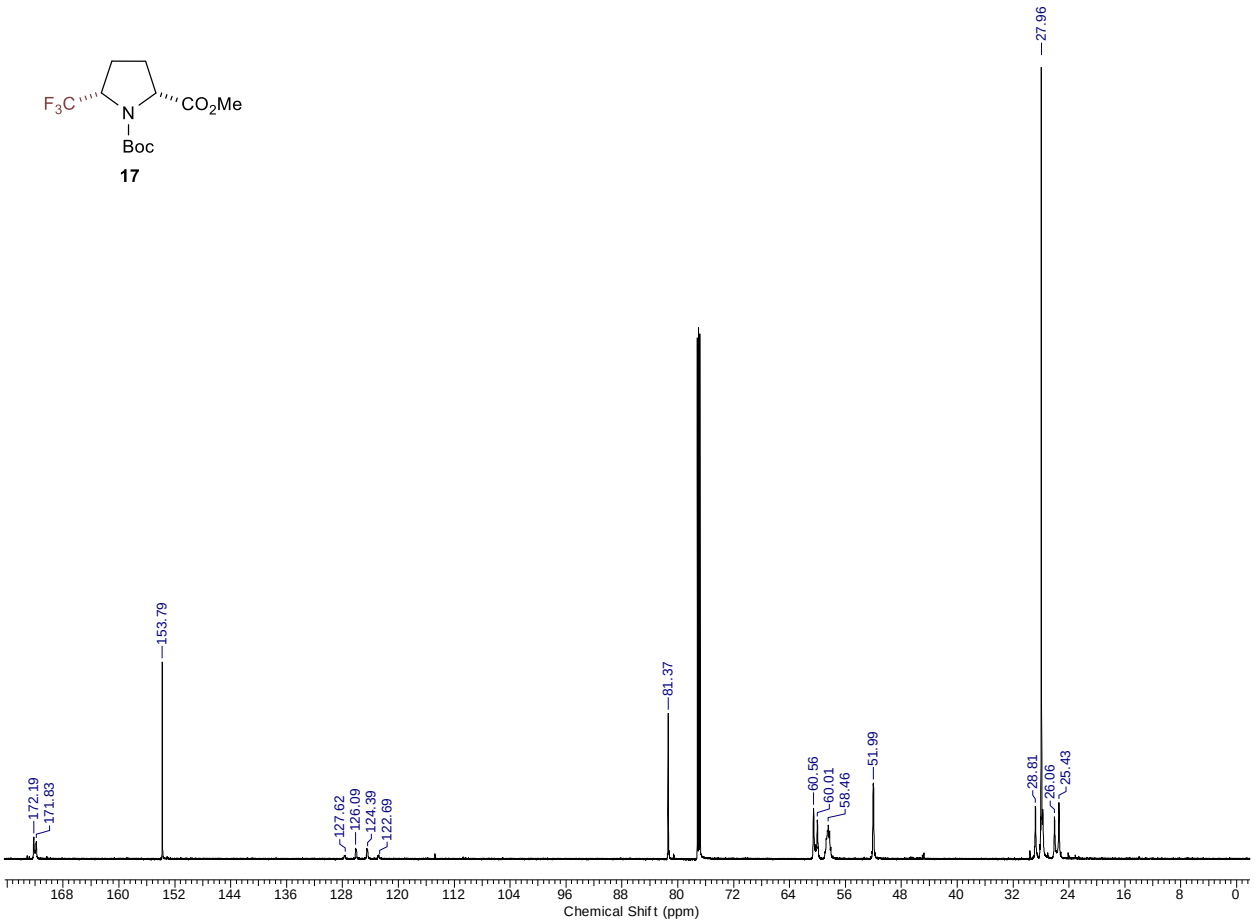

Figure S23. ^{13}C NMR spectrum (175 MHz, $CDCl_3$) of **17**.

Crystallographic data for *cis*-1-(tert-butyl) 2-methyl 5-(trifluoromethyl)pyrrolidine-1,2-dicarboxylate (17)

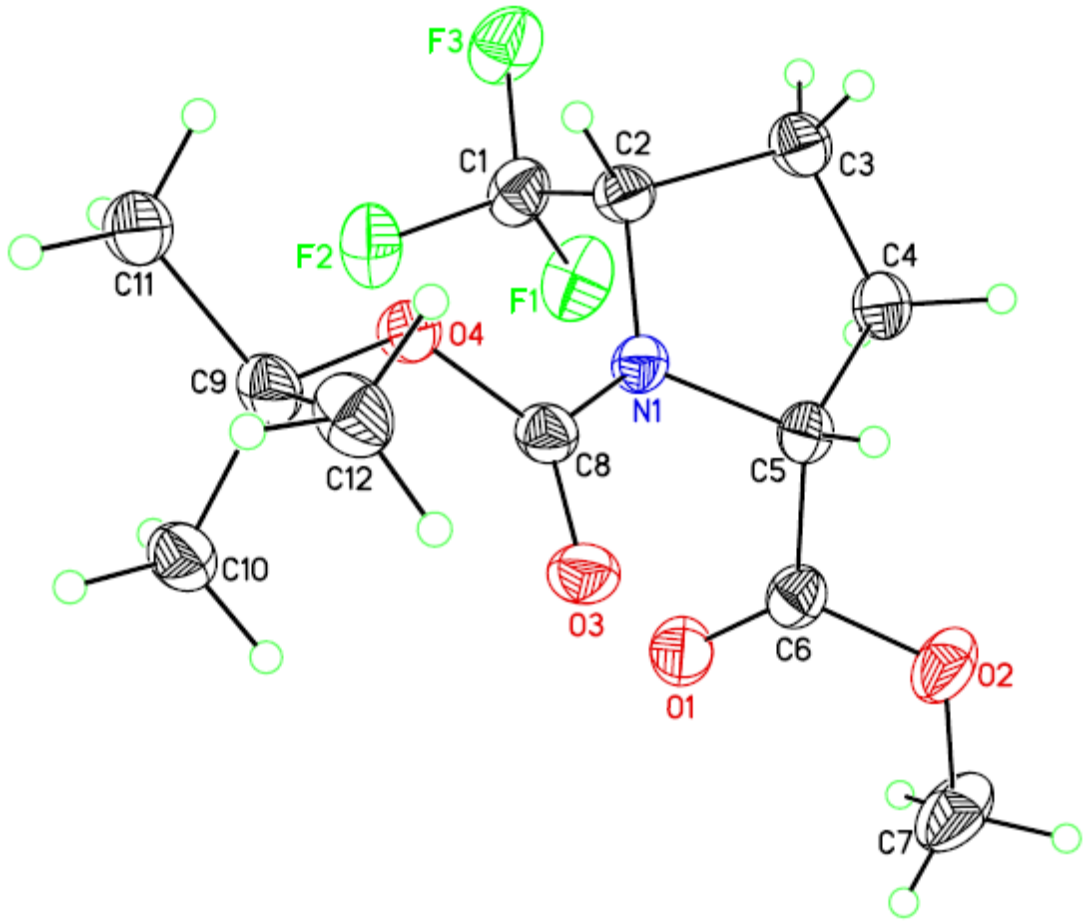

Figure S24. Structural figure of compound **17**, with 50% probability ellipsoids.

Structure Determination

Colorless plates of **17** were grown from a diethyl ether/pentane solution of the compound at 22 deg. C. A crystal of dimensions 0.10 x 0.07 x 0.02 mm was mounted on a Rigaku AFC10K Saturn 944+ CCD-based X-ray diffractometer equipped with a low temperature device and Micromax-007HF Cu-target micro-focus rotating anode (λ = 1.54187 A) operated at 1.2 kW power (40 kV, 30 mA). The X-ray intensities were measured at 85(1) K with the detector placed at a distance 42.00 mm from the crystal. A total of 2028 images were collected with an oscillation width of 1.0˚ in ω. The exposure times were 1 sec. for the low angle images, 8 sec. for high angle. Rigaku d*trek images were exported to CrysAlisPro for processing and corrected for absorption. The integration of the data yielded a total of 21112 reflections to a maximum 2θ value of 139.34˚ of which 2668 were independent and 2483 were greater than 2σ(I). The final cell constants (Table 1) were based on the xyz centroids 10158 reflections above 10σ(I). Analysis of the data showed negligible decay during data collection. The structure was solved and refined with the Bruker SHELXTL (version 2014/6) software package, using the space group P2(1)/c with Z = 4 for the formula $C_{12}H_{18}NO_4F_3$. All non-hydrogen atoms were refined anisotropically with the hydrogen atoms placed in idealized positions. Full matrix least-squares refinement based on F^2 converged at R1 = 0.0395

and wR2 = 0.1035 [based on I > 2σ(I)], R1 = 0.0420 and wR2 = 0.1070 for all data. Acknowledgement is made for funding from NSF grant CHE-0840456 for X-ray instrumentation.

Sheldrick, G.M. SHELXTL, v. 2014/6; Bruker Analytical X-ray, Madison, WI, 2014.

CrystalClear Expert 2.0 r16, Rigaku Americas and Rigaku Corporation (2014), Rigaku Americas, 9009, TX, USA 77381-5209, Rigaku Tokyo, 196-8666, Japan.

CrysAlisPro 1.171.38.41 (Rigaku Oxford Diffraction, 2015).

Background EDA Reaction Controls:

For each substrate type, control reactions without catalyst were performed to determine the degree of contribution of the EDA mechanism to the overall transformation. These were specifically designed to probe substrate-specific effects, and consequently a ratio of 2:1 TFAA:4-Ph-pyridine *N*-oxide was employed for these reactions, despite the fact that optimized conditions in the manuscript utilize a 1.1:1 ratio. This is to eliminate the contribution of the putative complexation between acylated and non-acylated *N*-oxide, which also results in productive chemistry. The reactions below were performed on 0.2 mmol scale (0.4 M in MeCN, 0.5 ml MeCN), with 2 equivalents of 4-Ph-PNO and 4 equivalents of TFAA.

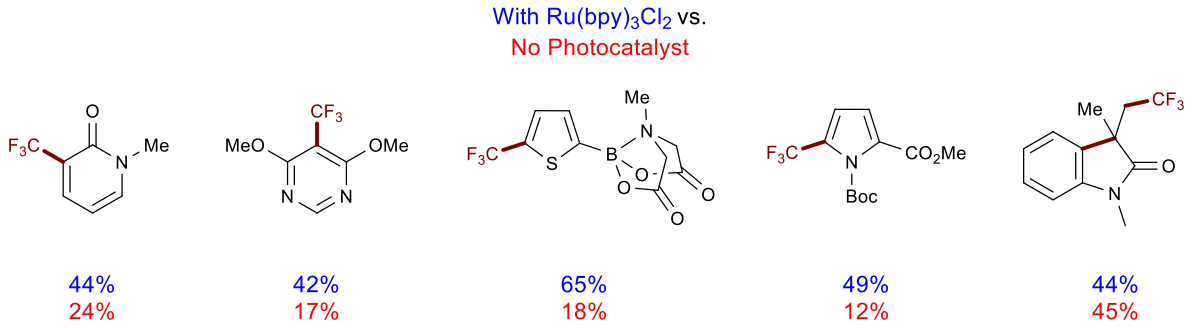

Figure S25. Control reactions with and without photocatalyst.

Flow reactor design

Reactor: The main reactor is 250 ft of 1/8" O.D 0.0625" I.D PFA (theoretical volume 150.8 mL) tubing *(Sain-Gobain vendor catalog # TSFE14-0125-031/250FT Catalog number NC0942238 purchased from Cole Palmer)* wrapped around a glass beaker (12" O.D 18" high). The ends are fixed with transparent duct tape and the total height of the coiled tubing is 11 " orientated 3.5 " from the bottom and 3.5" from the top (Figure S1A).
Inside the Pyrex beaker is a clamp stand with 3 AquaDock Blue MegaWatt LED lights *(http://aquadocklights.com/buy/)* facing downwards inserted onto the clamp stand pole. There are spacing weights between the lights to match the height of the lights to that of the tubing and to counter the buoyancy of the lights. They are further fixed together with cable ties (Figure S1B). The AquaDock lights are designed to be operated fully submerged in water and should not be illuminated unless so.

Reactor housing:
The glass beaker is placed inside a stainless steel housing tube with a 16" O.D and a 20" height (Figure S1C). The housing is constructed from regular stainless steel and has only a moderate level of

reflectiveness. Preliminary unreported results indicate that the use of a steel housing with increased reflectance may lead to higher photon flux within the reactor and allow shorter residence times. There is a coil of 10 ft, ¼" O.D stainless steel tubing in the bottom of the reactor housing around the pyrex beaker that is connected to glycol cooling fluid outlet −7 °C, metered via a peristaltic pump. Both the internal pyrex reactor and cavity between the reactor and stainless steel housing is filled with deionized water above the height of the pyrex reactor. A nitrogen feed line is placed into the bottom of the cavity between the pyrex glass reactor and the stainless steel housing to provide fluid turbulence. There was no appreciable temperature difference between the top and bottom of the water once the water had reached a constant temperature (after approximately 3 h). Cooling was required to maintain a water temperature of 45 °C ± 3 °C as the lights were calculated to contribute 0.84 kW/h of heat. A stainless steel lid 20" in diameter with a 2" diameter hole is placed on the top of the reactor housing. Through the hole is placed the reactor tubing inlet and outlet, the power cables for the lights, the cooling fluid and return hose, the nitrogen feed line, and a temperature probe to monitor the water temperature inside the pyrex reactor (Figure S1D). The stainless steel reactor housing is placed within a secondary container (purchased from home depot Model # FG863292GRAY) placed upon a moving dolly (purchased from home depot Model # FG264020BLA)

Feed streams:

The reaction components are separated into two feed streams A and B. Feeds were prepared in batches containing 300 g of pyrrole **9** due to the limitation in volume of the 2.0 L feed bottles.

Both feed streams are pumped from individual pressure bottles fitted with stainless Swagelok fittings comprising a pressure gauge and a check valve, a nitrogen inlet and an outflow. The feed bottles are placed on balances. The outflow is connected to a Masterflex® peristaltic pump (Item# HV-07522-20) fitted with an easy load head (Item# HV-77200-60) with a L/S 16 Gore Sta-Pure tube (Cole-Palmer Part # 96212-16). Two ft of 1/8" PFA tubing connects the outlet of the pump to a stainless steel Swagelok T piece uniting the two individual feed streams. The outlet of the T piece is connected to 1" of 3/8" PFA tubing that acts as a mixing zone for the two feeds. This 3/8" PFA tubing ids connected to the inlet of the reactor by 12 ft of 1/8" PFA tubing. The inlet for the liquid flow begins at the bottom of the reactor and flows upwards around the pyrex beaker to the outlet (Fig S1D details of reactor from top down view). The outlet of the reactor is connected via a stainless steel Swagelok union to 2 feet of 1/8" PFA tubing that terminates at a stainless steel Swagelok T piece. One entry to the T piece contains a thermocouple heat probe connected to monitor the outlet temperature of the reaction solution. The outlet of the T piece is connected via 2 feet of 1/8" PFA tubing to a Equilibar® diaphragm back pressure regulator (BPR) (Serial number EB1U1F1-HC276) set to 20 psi. Significant off gassing is observed downstream of the BPR (Fig S1D details of reactor from top down view). At the outlet of the BPR is placed a Swagelok 3-way valve to allow sampling of the reaction solution. 3 ft of 1/8" PFA tubing connects one outlet of the 3-way valve to a 4L collection bottle (headspace swept with nitrogen) placed on a balance. A schematic of the setup is depicted in Figure S2.

Large scale reaction:

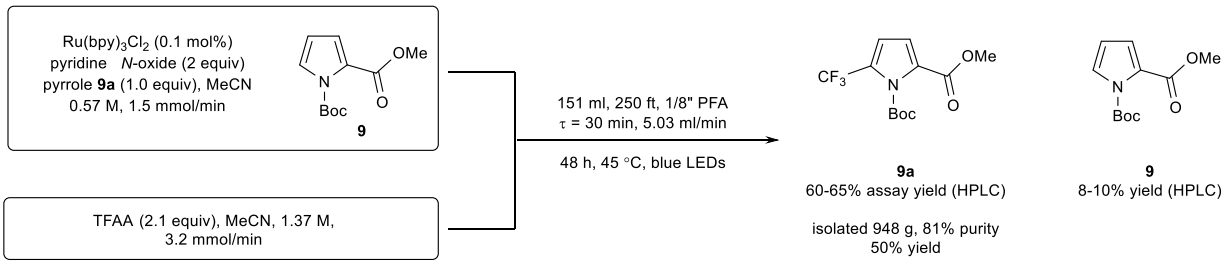

Figure S26. Kilogram scale trifluoromethylation in flow.

Synthesis of methyl-1-boc-pyrrole-2-carboxylate (9):
To a 3 Neck 3L RBF with an overhead stirrer, temp probe and a pressure equalized dropping funnel with a nitrogen inlet was added; methyl 1H-pyrrole-2-carboxylate (100 g, 1.00 equiv, 775 mmol), 4-dimethylaminopyridine (4.83 g, 0.05 equiv, 39.5 mmol), ethyl acetate (775 mL), and triethylamine (120 mL, 1.11 equiv, 861 mmol, 87.1 g) and the homogenous solution was stirred as the temperature decreased to about 13 °C upon dissolution. A solution of di-tert-butyl-dicarbonate (186 g, 1.10 equiv, 853 mmol) in ethyl acetate (775 mL) was added over 1.25 h with a temperature rise to 20 °C. The homogenous solution was stirred for 1 h before the addition of 1 N HCl (400 mL) and further stirring for 5 minutes. The biphasic solution was transferred to a 4 L separatory funnel, the lower layer removed and the remaining orangic layer washed with 1 N HCl (400 mL) followed by sat NaCl (400 mL). The organic solution was concentrated under reduced pressure to give methyl-1-boc-pyrrole-2-carboxylate **9** as a colorless oil with data consistent with that reported in the literature.[10]
Yield: 176 g, (98%, 98% purity by NMR)

Feed preparation:
Feed stream A: To a solution of $Ru(bpy)_3Cl_2.6H_20$ (0.98 g, 1.31 mmol, 0.001 equiv) dissolved in deoxygenated MeCN (2000 mL) (*note: a small quantity of black solid remained insoluble in the MeCN*), was added methyl-1-boc-pyrrole-2-carboxylate **9** (300 g, 1.31 mol, 1.0 equiv). Pyridine-*N*-oxide (248 g, 2.61 mol, 2.0 equiv) was dissolved separately in in deoxygenated MeCN (200 mL) (note: there is a significant endotherm upon pyridine-*N*-oxide dissolution, a water bath was used to hasten full dissolution). The pyridine–*N*-oxide solution was added to the solution of $Ru(bpy)_3Cl_2$ and pyrrole **9**, and the combined solution sparged with nitrogen with 2 minutes.
Total volume 2300 mL, density 0.855 g/ml, 0.568 M wrt to pyrrole X. Pump set to 2.67 mL/min providing 1.53 mmol/min.

Feed stream B: Trifluoroactic anhydride (576 g, 2.74 mol, 2.1 equiv) was dissolved in deoxygenated MeCN (1640 mL) (*note: it takes significant agitation to reach a homogenous solution)* and the combined solution was sparged with nitrogen for 2 minutes.
Total volume 2000 mL, density 0.917 g/ml, 1.37 M wrt to trifluoroacetic anhydride. Pump set to 2.34 mL/min providing 3.21 mmol/min.

Reaction and isolation

2 L of feed stream A was transferred to a 2 L pressure bottle and used with feed stream B (prepared directly in a 2 L pressure bottle). The reaction was started with the reactor filled with MeCN and the total contents of the reaction collected. The contents of the feed stream pressure bottles were refilled as required during the run at which point the pumps were temporarily stopped. Samples were taken at 1 h intervals until the 4.5 h mark, then sampling was conducted every 2 h. The *in situ* HPLC assay yield remained 60-66% over the course of the run with 4-11% starting material remaining. A representative HPLC trace of the crude reaction is below. *Feed streams were prepared as above a total of 4 times during a 48 h run giving the total quantities of reactants as:* Methyl-1-boc-pyrrole-2-carboxylate **9** (1.20 Kg, 5.22 mol, 1.0 equiv), pyridine-*N*-oxide (992 g, 10.4 mol, 2.0 equiv), $Ru(bpy)_3Cl_2.6H_20$ (3.92 g, 5.22 mmol, 0.001 equiv), trifluoroactic anhydride (1.73 Kg, 11.0 mol, 2.1 equiv) and MeCN (15.4 L). Once the

4L collection bottle approached capacity it was switched and the contents concentrated to approximately 1 L under reduced pressure to give a viscous black solution. This solution was transferred to a 5 L vessel to conduct the work up. To the black solution was added heptane (1.0 L, 1 vol) and 1 N HCl (1.0 L, 1 vol) and the contents stirred vigorously for 5 min before separation. The aqueous phase was extracted a further 2 times with heptane (2 × 1.0 L), the organic heptane portion combined and washed with saturated Na_2CO_3 (1.0 L) upon which the heptane changed from a light yellow to light pink in color. The heptane was then washed with saturated NaCl (1.0 L). This solution was retained under an atmosphere of nitrogen prior to the combination of all solutions after work up and concentration in a rotary evaporator at reduced pressure. Concentration of the combined heptane solutions in a rotary evaporator at reduced pressure following work up gave a 1-(tert-butyl) 2-methyl 5-(trifluoromethyl)-1H-pyrrole-1,2-dicarboxylate **9a** as dark red/black oil (948 g, 81% strength by HPLC, 50% yield *adjusted for purity*) with data in accordance with that reported. The major impurities present were identified as unreacted starting material **9** 7%, 1-tert-butyl 2-methyl 3-(trifluoromethyl)-1H-pyrrole-1,2-dicarboxylate 1%, 1-tert-butyl 2-methyl 3,5-bis(trifluoromethyl)-1H-pyrrole-1,2-dicarboxylate 0.8%.

The pumps were calibrated prior to the reaction using MeCN. Catch and weigh samples reported 105-110% observed mass flow rate vs the predicted during the course of the reaction. For more accurate flow rates pumps should be calibrated with the reaction solutions which in our case had densities that deviated from that of the calibration solvent.

The overall mass balance for the entire run was calculated at 95.2% = (total recorded mass input/total recorded mass output) = (15139 g/14416 g) = 95.2%. Reaction HPLC traces before and after workup are shown below, as well as ^{1}H NMR and ^{19}F NMR spectra of the crude reaction following workup to demonstrate purity.

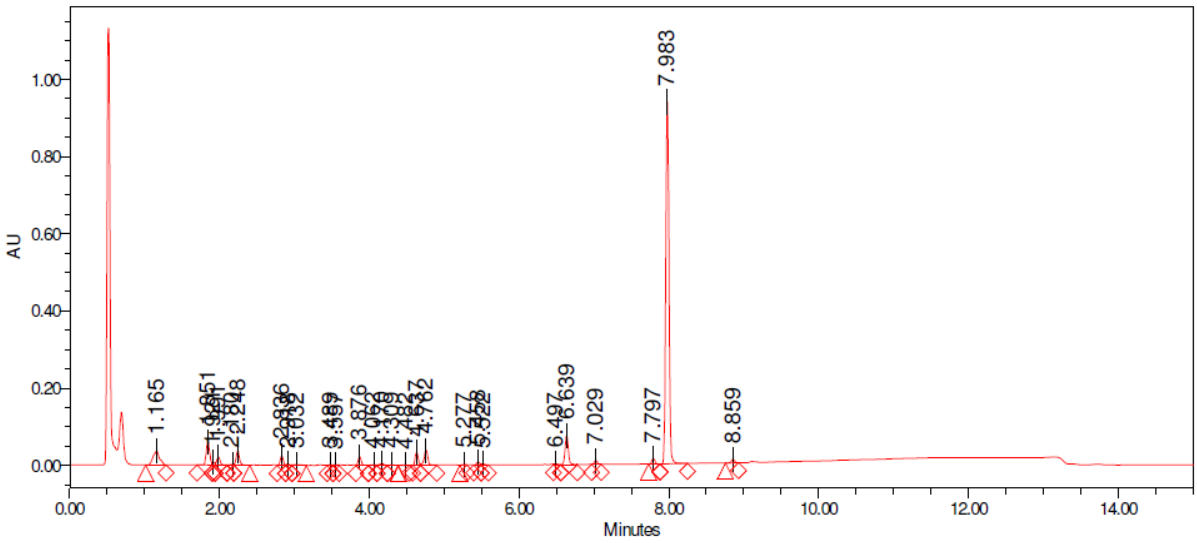

Figure S27. HPLC chromatogram showing representative reaction sample at steady state.

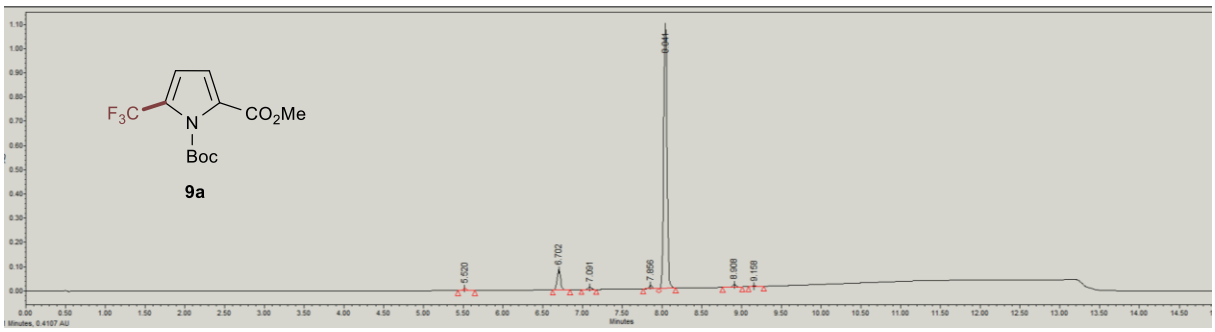

Retention Time (min)	Area (µV*sec)	% Area	Height (µV)	Int Type	Amount	Units	Dissolved Amount	Dissolved Percent	Peak Type	Peak Codes	ActivityFactor	ActivityResult	AdjArea	AdjAreaPct
5.520	26978	0.76	9358	bb					Unknown	C06			26978	0.760995
6.702	247181	6.97	83142	bb					Unknown	C06			247181	6.972350
7.091	30036	0.85	10358	bb					Unknown	C06			30036	0.847228
7.856	40453	1.14	13937	bv					Unknown	C06			40453	1.141088
8.041	3160760	89.16	1083712	vb					Unknown	C06			3160760	89.157059
8.908	29748	0.84	10330	bb					Unknown	C06			29748	0.839117
9.158	10003	0.28	2390	bb					Unknown	C06			10003	0.282162

Figure S28. HPLC chromatogram showing the crude material following work up.

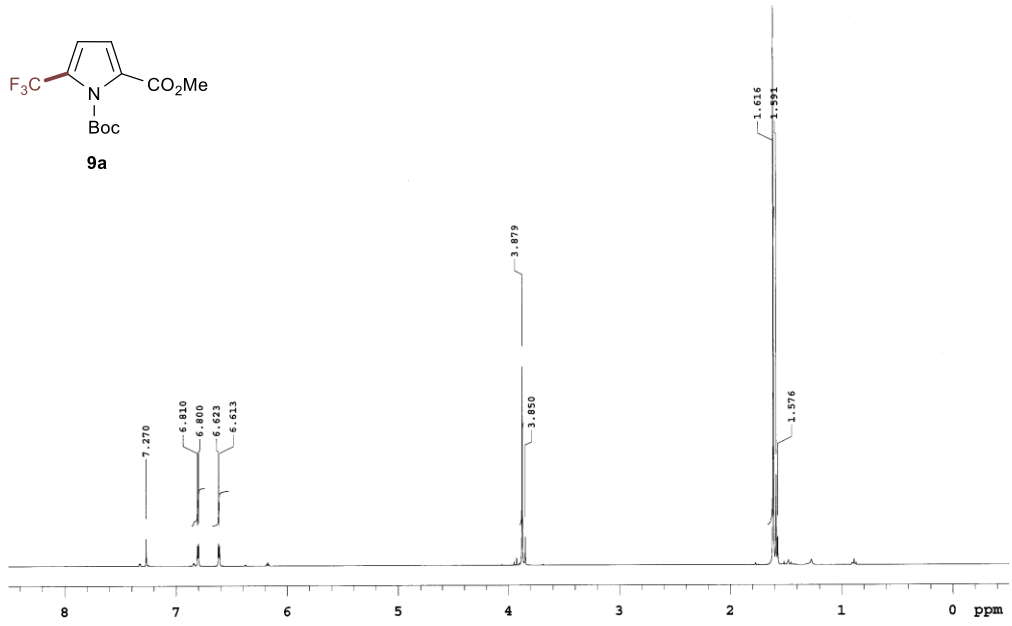

Figure S29. ^{1}H NMR showing the crude material **9a** following workup.

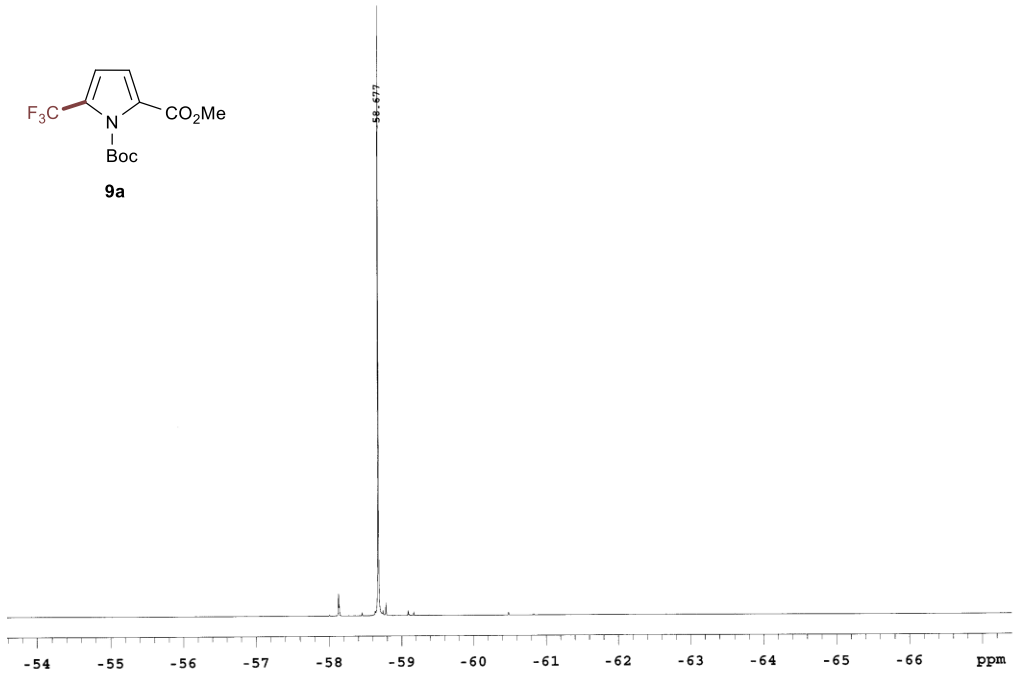

Figure S30. ^{19}F NMR showing the crude material **9a** following workup

Boc de-protection: Synthesis of methyl 5-(trifluoromethyl)-1H-pyrrole-2-carboxylate (26):

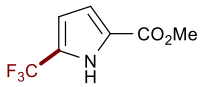

This is an un-optimized process. To a one neck 200 mL flask under an atmosphere of nitrogen was added crude 1-(tert-butyl) 2-methyl 5-(trifluoromethyl)-1H-pyrrole-1,2-dicarboxylate (52.8 g, 140 mmol, 1.0 equiv, 81% purity) and heptane (50 mL) to give a bright red solution. Trifluoroacetic acid (16.0 mL, 24.13 g, 212 mmol, 1.51 equiv) was added and the solution stirred for 14 h. Trifluoroacetic acid (16.0 mL, 24.13 g, 212 mmol, 1.51 equiv) was added and the solution stirred for a further 6 h before concentration under reduced pressure. The light pink solid was redissolved in 25 mL of heptane at 60 °C and slowly cooled to rt over 4 h and stirred for a further 10 h. The slurry was filtered, the filtrate cooled to 0 °C to induce further precipitation then filtered. The combine solids were dried in a vacuum oven at 40 C for 2 to give methyl 5-(trifluoromethyl)-1H-pyrrole-2-carboxylate **26** as a light pink solid.
Yield: 20.9 g (77%, 99% purity); ^{1}H NMR (400 MHz, CD_3CN) δ = 10.04 (s, 1H), 6.14–6.15 (m, 1H), 5.95–5.96 (m, 1H), 3.13 (s, 1H); ^{19}F NMR (376 MHz, CD_3CN) δ = -60.6 (s). This data is in accordance with that previously reported.[11]

HPLC chromatogram of 26

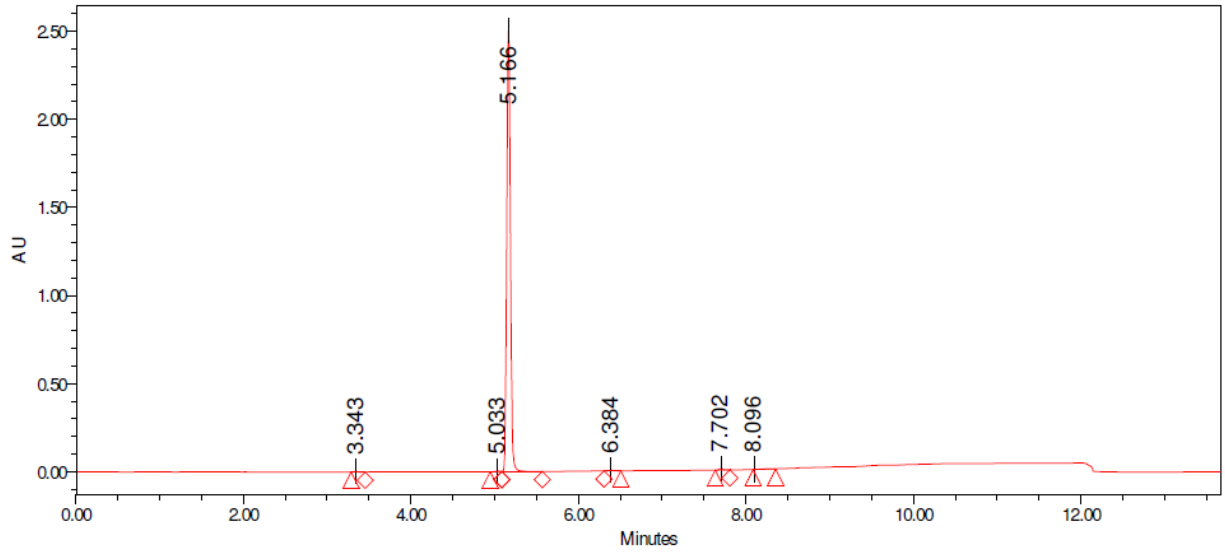

Figure S31. HPLC chromatogram of **26**.

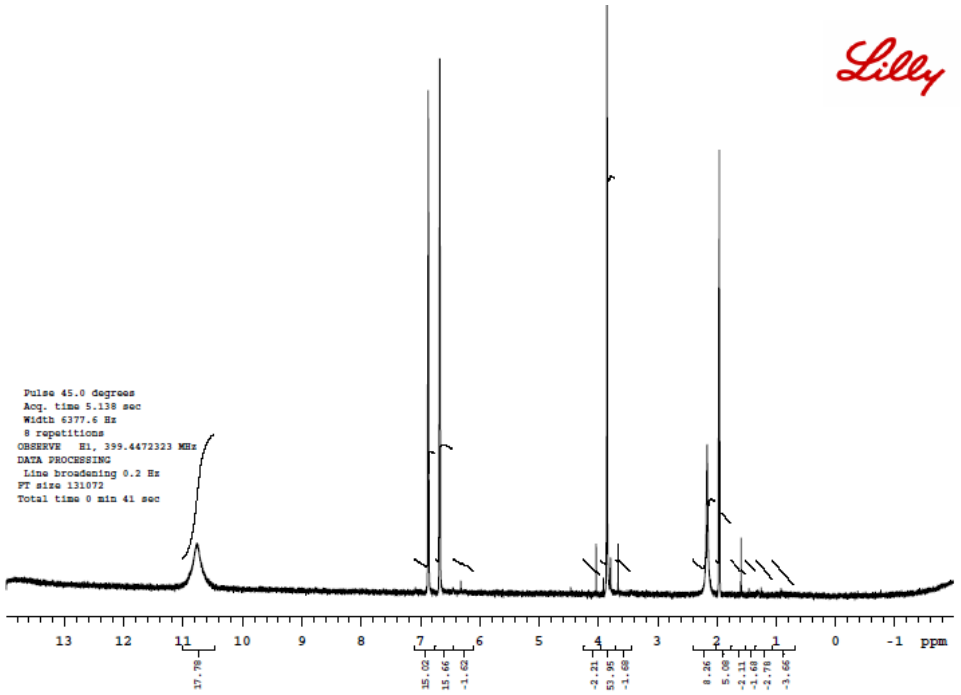

Figure S32. ^{1}H NMR of **26**.

UV-Vis Studies:
All UV-VIS measurements were performed on a Shimadzu UV-1601 UV-VIS Spectrometer. Samples were prepared using dry MeCN as the solvent. Measurements were taken in 1cm path length quartz cuvettes at room temperature and were not degassed. Evaluation of the various component contributions to the EDA absorbance at 0.4M is performed in the manuscript; these effects were seen at lower concentrations as well (orange curve, below), however, there is a threshold at which the EDA shoulder peak is unobservable. Optical absorbance spectra of a mixture of 4-phenylpyridine *N*-oxide, mesitylene, and TFAA in relevant stoichiometry (1.0 : 1.0 : 1.1) over a range of concentrations in dry MeCN.

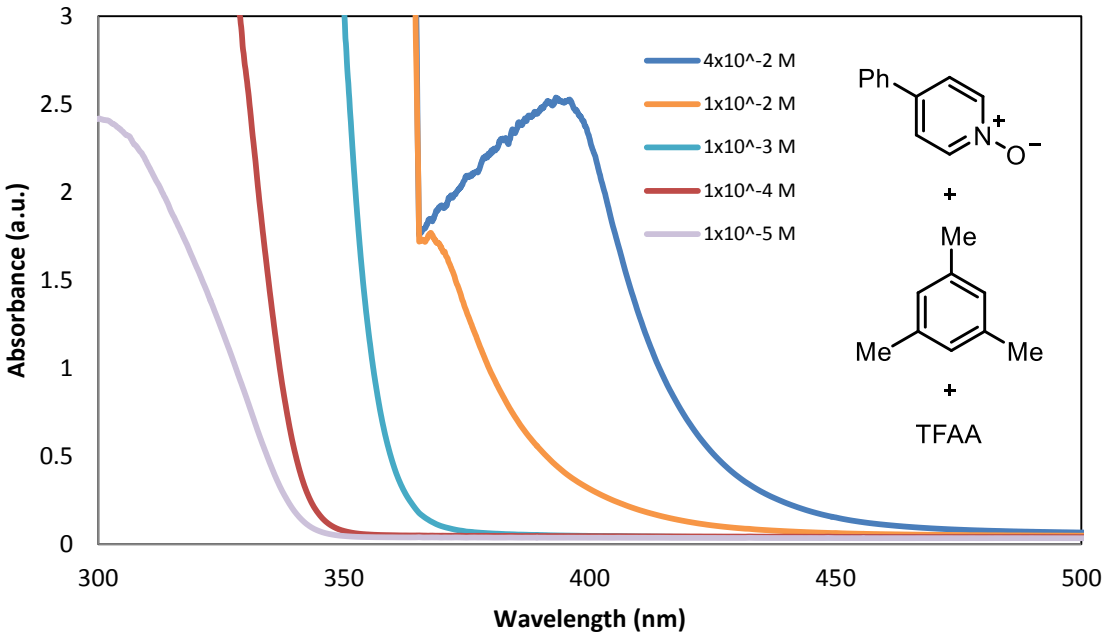

Figure S33. Optical absorbance spectra of the reaction solution at varied concentrations.

Electrochemical Measurements
The measurement of reduction potentials for the acylonium salts reported in this manuscript cannot be accurately performed through cyclic voltammetry analysis. The observed signal using cyclic voltammetry has variations in shape and peak potential from run to run, and the peak shape in particular is dependent upon sweep rate. Literature precedent in this area for alkylated pyridine *N*-oxides suggests that these molecules can undergo extremely fast ("barrierless") fragmentation upon single-electron reduction (k_{obs} on the order of 1.8×10^{12} s^{-1} for 1-methoxy-4-phenylpyridinium and 4.1×10^{12} s^{-1} for 1-methoxypyridinium).[12] Furthermore, another paper concerning similar structures reports that "[r]eduction potentials of *N*-methoxypyridinium salts are not readily accessible through conventional electrochemical techniques because of the relatively fast reductive cleavage of these compounds."[13]

Differential pulse voltammetry (DPV) was performed to obtain the reduction potentials of the various pyridine *N*-oxide/anhydride combinations, and reproducible potentials were obtained through these methods. Measurements were performed with a model CHI660C multi-potentiostat from CH Instruments. Measurements were performed with a glassy carbon working electrode, Pt auxiliary electrode, Ag/AgCl reference electrode, Bu_4NPF_6 electrolyte (0.1 M in MeCN), and analyte (pyridine-N-oxide:TFAA, 1:1, 0.01 M) with the following settings: Incr E (V) = 0.001, Amplitude (V) = 0.005, Pulse Width (sec) = 0.05, Sampling Width (sec) = 0.01, Pulse Period (sec) = 0.5.

All voltammograms are reported/displayed *after* conversion to voltage vs. SCE, where:

$$\mathbf{V_{SCE} = V_{AgCl} - 0.05\ V}$$

Onset potentials are estimated based on the intersection of the baseline and onset slope (shown).

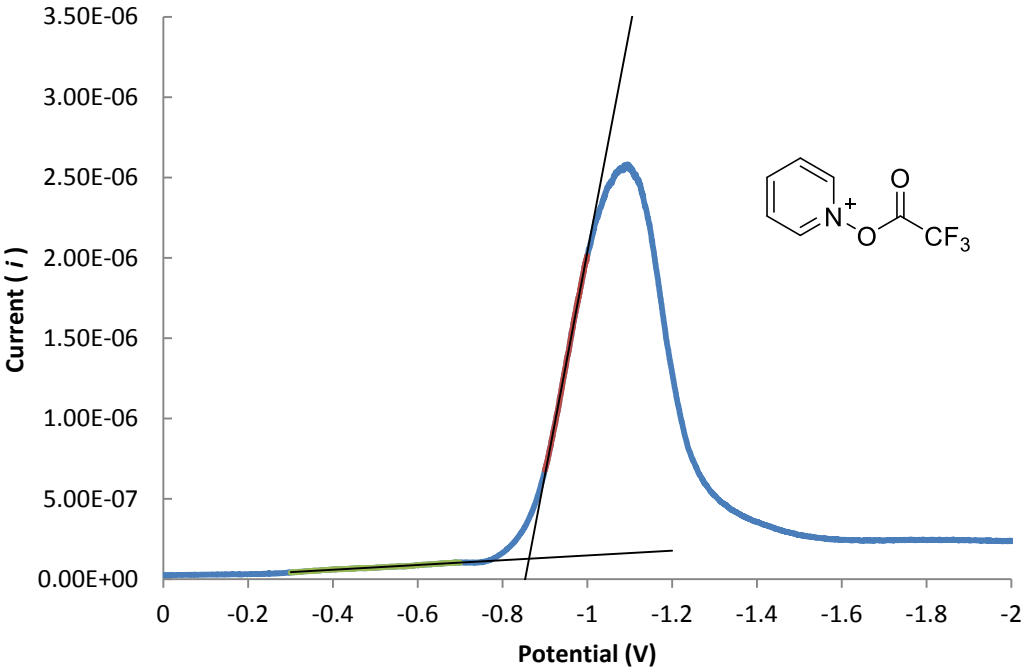

Figure S34. DPV of the pyridine *N*-oxide/TFAA adduct. Onset reduction is observed at –0.86 V vs. SCE. Peak reduction is observed at –1.10 V vs. SCE.

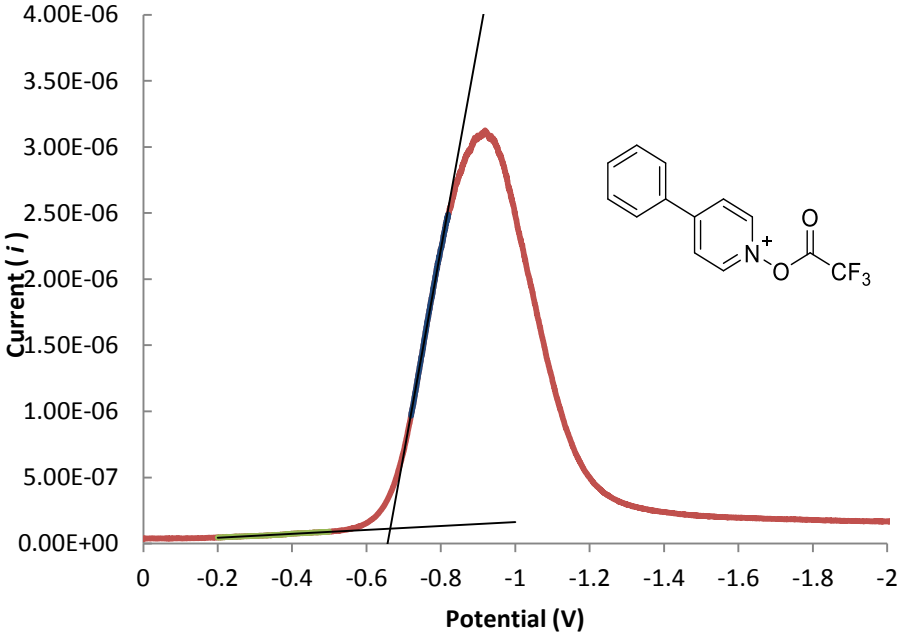

Figure S35. DPV of the 4-phenylpyridine *N*-oxide/TFAA adduct. Onset reduction is observed at –0.65 V vs. SCE. Peak reduction is observed at –0.91 V vs. SCE.

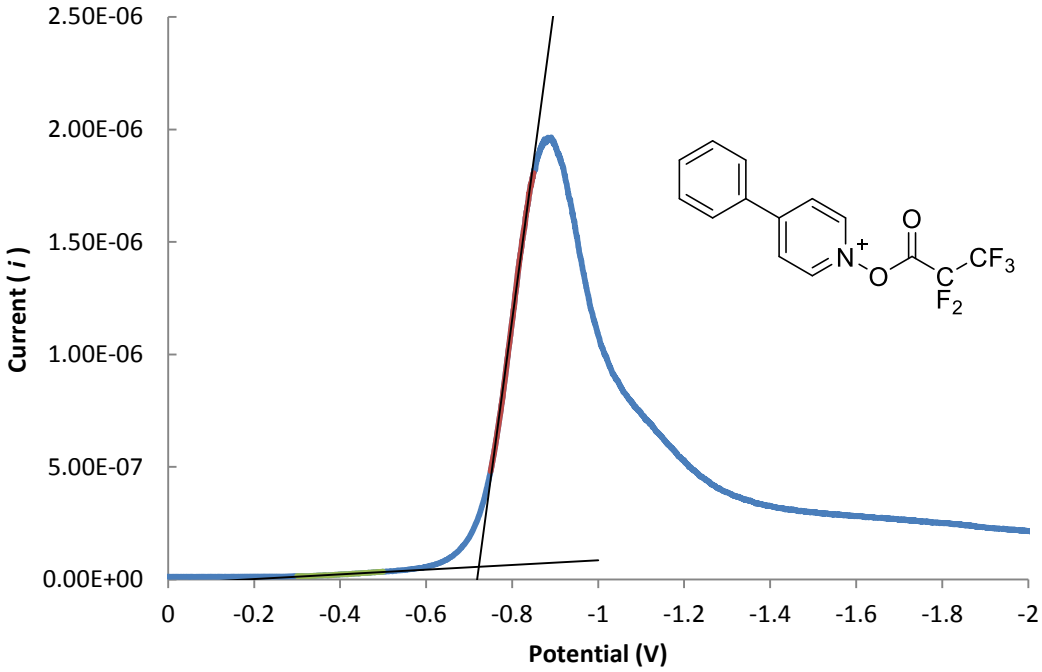

Figure S36. DPV of the 4-phenylpyridine *N*-oxide/pentafluoropropionic anhydrude adduct. Onset reduction is observed at –0.72 V vs. SCE. Peak reduction is observed at –0.88 V vs. SCE.

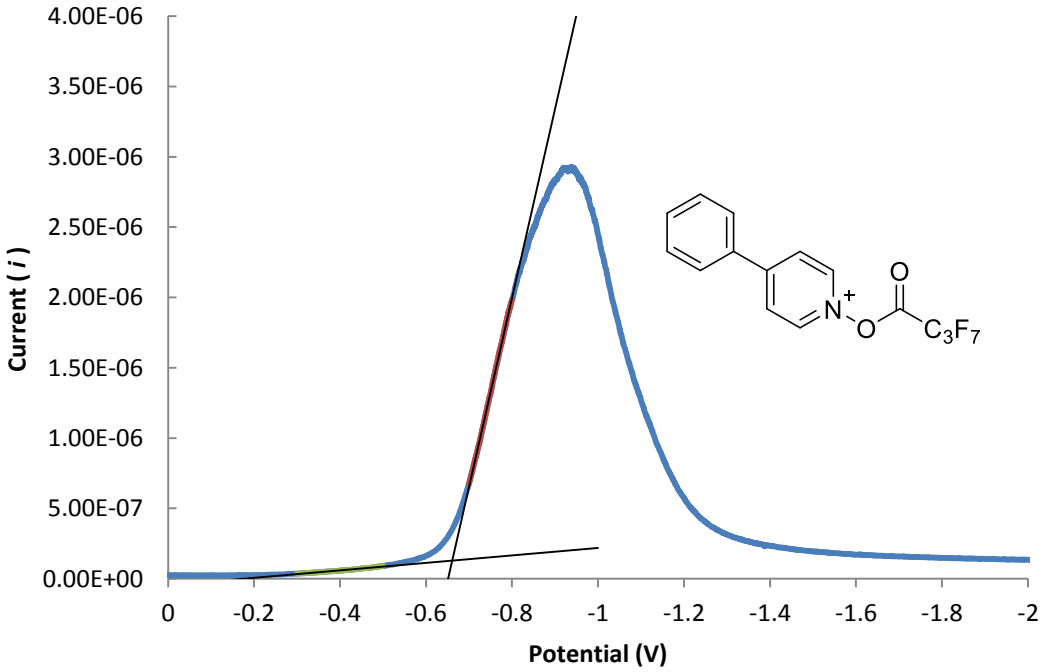

Figure S37. DPV of the 4-phenylpyridine *N*-oxide/heptafluorobutyric anhydrude adduct. Onset reduction is observed at –0.66 V vs. SCE. Peak reduction is observed at –0.93 V vs. SCE.

Fluorescence Quenching Studies:

Quenching data was obtained using a Fluoromax-2 Fluorimeter. All quenching data was recorded using a quartz cuvette with a stir bar at between 24.5 and 25.5 ˚C with $Ru(bpy)_3Cl_2$ (9.97 $x10^{-6}$ M) in dry, degassed MeCN (sparged for 5 minutes). Excitation was performed at 452 nm with emission measured at 615 nm. All values are the average of three measurements.

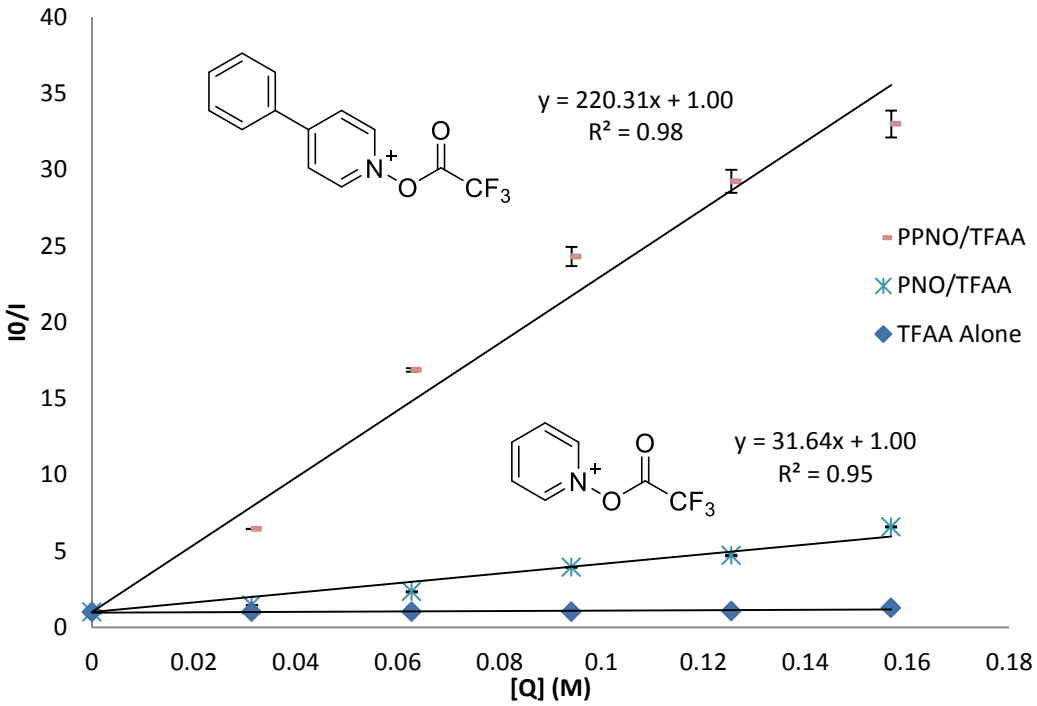

Figure S38. Stern-Volmer Quenching of $Ru(bpy)_3Cl_2$ with 4-phenylpyridine *N*-oxide (PPNO)/TFAA or with pyridine *N*-oxide (PNO)/TFAA. For each measurement the concentration of quencher refers to the concentration of the *N*-oxide, which is the limiting reagent in a ratio of 1.0:1.1 in relation to TFAA. Error bars refer to a single standard deviation, with the measurement performed in triplicate.

From the data above, quenching rates (k_q) may be extracted based on the following equation:

$$\frac{I_0}{I} = k_q \tau_0 [Q] + 1$$

Where τ_0 represents the catalyst excited state lifetime[14] at 25 ˚C in MeCN, for which we used a value of 0.87 µs.[15]

	k_q (M^{-1} s^{-1})
pyridine *N*-oxide/TFAA	$3.6x10^7$
4-Ph-pyridine *N*-oxide/TFAA	$2.5x10^8$

These rates are *not quantitatively useful*, as the quenching behavior of the PPNO/TFAA adduct does not appear to be entirely linear. Although the equilibrium constant of this reaction is not known, the increase in quencher concentration will likely shift this equilibrium towards the acylated side of the equilibrium, thus potentially explaining the non-linear trend observed above.

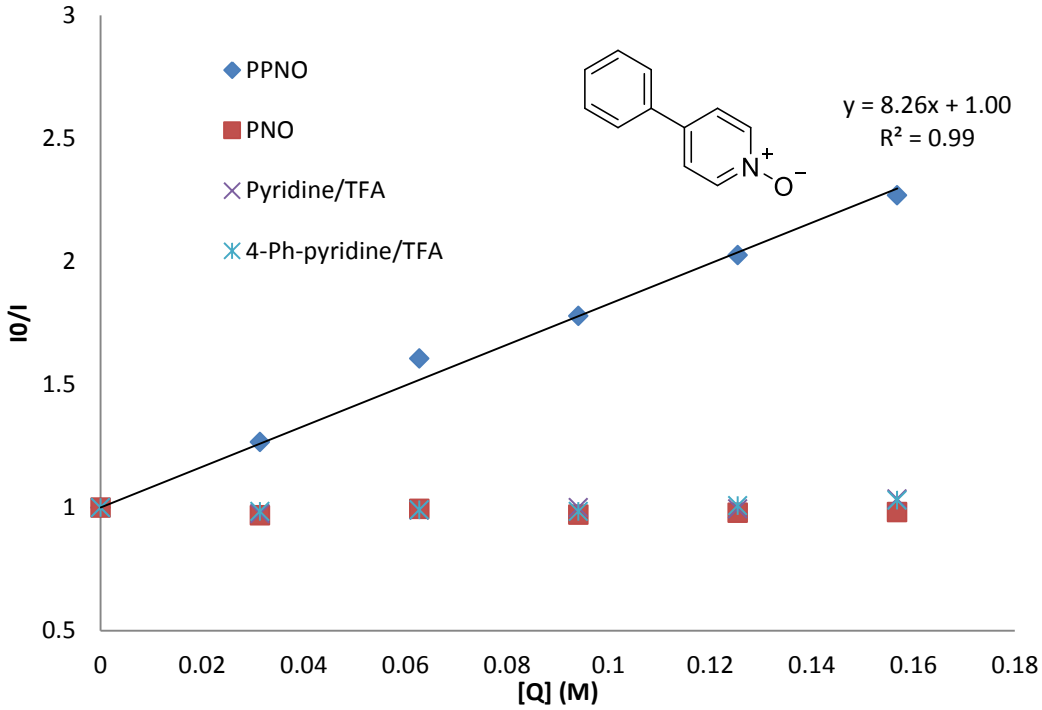

Figure S39. Stern-Volmer Quenching of $Ru(bpy)_3Cl_2$, component controls. Of the individual components of the reaction, only 4-phenylpyridine *N*-oxide (PPNO) quenched the photocatalyst, while PNO, TFAA, 4-phenylpyridinum trifluoroacetate, and pyridinium trifluoroacetate did not quench the catalyst.

Quantum Yield Measurements

Quantum yield experimental design was based on the procedure by Cismesia and Yoon.[16] Experiments were performed using a Fluoromax-2 Fluorimeter equipped with a 150 W Xenon Arc lamp. Actinometry was performed with potassium ferrioxalate trihydrate. The procedure for determining photon flux, as described by Cismesia and Yoon, is reproduced below:

> *"The photon flux of the spectrophotometer was determined by standard ferrioxalate actinometry. A 0.15 M solution of ferrioxalate was prepared by dissolving 2.21 g of potassium ferrioxalate hydrate in 30 mL of 0.05 M H_2SO_4. A buffered solution of phenanthroline was prepared by dissolving 50 mg of phenanthroline and 11.25 g of sodium acetate in 50 mL of 0.5 M H_2SO_4. Both solutions were stored in the dark. To determine the photon flux of the spectrophotometer, 2.0 mL of the ferrioxalate solution was placed in a cuvette and irradiated for 90.0 seconds at λ = 436 nm with an emission slit width at 10.0 nm. After irradiation, 0.35 mL of the phenanthroline solution was added to the cuvette. The solution was then allowed to rest for 1 h to allow the ferrous ions to completely coordinate to the phenanthroline."*

At this point, our protocol differed slightly from the published protocol. Our absorbance measurements in the 1 cm quartz cuvette at 510 nm for the Fe^{2+} phenanthroline complex were above 2.0 absorbance units, and were deemed too high for accurate quantification. Instead, we obtained the absorbance of the solutions at 510 nm after transferring some of the solution to a 1 mm (0.1 cm) path length cuvette, which provided absorbance units an order of magnitude lower. An additional sample was prepared exactly as above, was not irradiated, and upon development with the phenanthroline solution for 1 hour its absorbance was measured at 510 nm in the 1 mm path cuvette. The amount of Fe^{2+} was quantified according to the equation below.

> *"Where V is the total volume (0.00235 L) of the solution after addition of phenanthroline, ΔA is the difference in absorbance at 510 nm between the irradiated and non-irradiated solutions, l is the path length… [0.100 cm], and ε is the molar absorptivity at 510 nm (11,100 L mol^{-1} cm^{-1})."*

$$\text{mol Fe}^{2+} = \frac{\text{V} \cdot \Delta\text{A}}{\text{l} \cdot \varepsilon} = \frac{0.00235\ \text{L} \cdot 0.234009}{0.100\ \text{cm} \cdot 11{,}100\ \text{L mol}^{-1}\text{cm}^{-1}} = 4.95 \text{ x } 10^{-7}\ \text{mol Fe}^{2+}$$

Photon flux was then determined as follows:

$$\text{photon flux} = \frac{\text{mol Fe}^{2+}}{\Phi \cdot \text{t} \cdot \text{f}} = \frac{4.95 \text{ x } 10^{-7}\ \text{mol}}{1.01 \cdot 90\ \text{s} \cdot 0.99907} = 5.46 \text{ x } 10^{-9} \text{einstein s}^{-1}$$

Φ = the quantum yield of ferrioxalate at 0.15 M and λ=436 nm

f = fraction of light absorbed at λ=436 nm, which can be determined from the equation $\text{f} = 1 - 10^{-\text{A}}$. The absorbance spectrum of the non-irradiated 0.15 M ferrioxalate solution was taken and is shown on the next page. The absorbance at 436 nm was found to be 3.03186, which results in a value of 0.99907 for f.

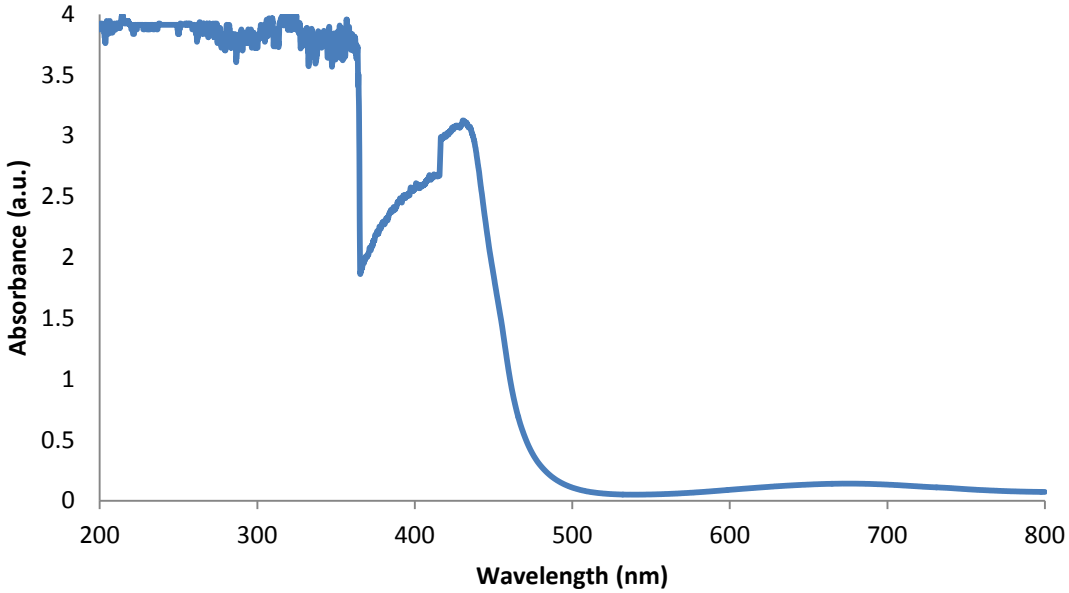

Figure S40. Optical absorbance spectrum for $K_3Fe(C_2O_4)_3$, 0.15 M in 0.05M H_2SO_4. The absorbance of the sample at 436 nm is 3.03186, which means that >99.9% of incident light is absorbed at this wavelength.

Quantum yield for the trifluoromethylation of mesitylene under standard conditions was determined as follows:

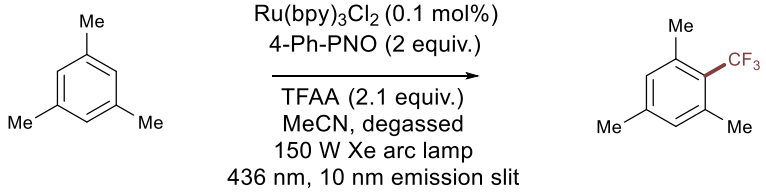

In a dark room, 4-phenylpyridine *N*-oxide (273.9 mg, 1.6 mmol, 2.0 equiv.), and mesitylene (111 µL, 96.2 mg, 0.80 mmol, 1.0 equiv.) were combined in a 1 cm path length cuvette equipped with stir bar. 500 µl of a solution 1.2 mg/ml $Ru(bpy)_3Cl_2$•$6H_2O$ in dry MeCN (0.6 mg, 0.1 mol%) was added to the cuvette, followed by 1.5 ml of dry MeCN. The solution was sparged for 30 seconds, followed by the addition of TFAA (237 µl, 353 mg, 2.1 equiv., not degassed) under a stream of nitrogen. The reaction was quickly sealed with a screw on cap, and wrapped with parafilm. Light exclusion was achieved by wrapping the reaction in foil until the reaction was placed in the fluorimeter. The sample-holder was pre-equilibrated to 35 ˚C, and the reaction sample was allowed to equilibrate to this temperature over 10 minutes. The sample was stirred and irradiated at 436 nm with a 10 nm slit width for 28,800 s (8 h). After irradiation, 0.5 ml of methanol was added to the reaction solution. After stirring for an additional 2 minutes, trifluorotoluene (98 µl, 0.8 mmol, 1.0 equiv.) was added as an internal standard, and the reaction was analyzed by ^{19}F NMR. The reaction yielded 17% (0.136 mmol) of 1,3,5-trimethyl-2-(trifluoromethyl)benzene.

The quantum yield was calculated as follows:

$$\Phi = \frac{\text{mol product}}{\text{flux}\cdot t\cdot f} = \frac{1.36\,\text{x}10^{-4}\text{mol}}{5.46\,\text{x}10^{-9}\text{einstein s}^{-1}\cdot 28800\text{ s}\cdot 1.00} = 0.87$$

Where f is the fraction of light absorbed at λ=436 nm, which can be determined from the equation $f = 1 - 10^{-A}$. The absorbance spectrum of the non-irradiated 0.15 M ferrioxalate solution was taken and is shown below. The absorbance at 436 nm was found to be 3.389282, which results in a value > 0.999 for f.

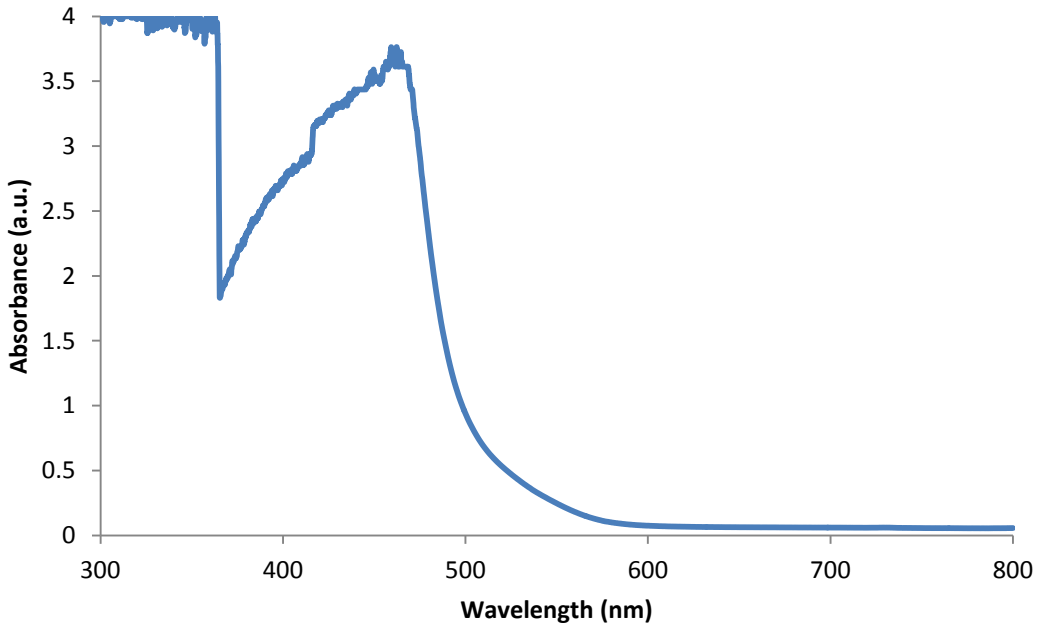

Figure S41. Optical absorbance spectrum for the full reaction mixture (0.4 M in MeCN). Reactant stoichiometry is 1.0 : 2.0 : 2.1 for mesitylene, 4-phenylpyridine *N*-oxide, and TFAA, respectively, with 0.1 mol% $Ru(bpy)_3Cl_2$. The absorbance of the sample at 436 nm is 3.389282, which means that >99.9% of incident light is absorbed at this wavelength.

Supplemental References:

1. Li, Y., Chen, T., Wang, H., Zhang, R., Jin, K., Wang, X., Duan, C. (2011) A Ligand-Free Copper-Catalyzed Decarboxylative Trifluoromethylation of Aryliodides with Sodium Trifluoroacetate Using Ag2O as a Promoter. Synlett *12*, 1713–1716.
2. Kino, T., Nagase, Y., Ohtsuka, Y., Yamamoto, K., Uragachi, D., Tokuhisa, K., Yamakawa, T. (2010) Trifluoromethylation of Various Aromatic Compounds by CF3I in the Presence of Fe(II) Compound, H2O2 and Dimethylsulfoxide. J. Fluorine Chem. *131*, 98–105.
3. Beatty, J. W., Douglas, J. J., Cole, K. P., Stephenson, C. R. J. (2015) A Scalable and Operationally Simple Radical Trifluoromethylation. Nat. Commun. *6*, 7919.
4. Wiehn, M. S., Vinogradova, E. V., Togni, A. (2010) Electrophilic Trifluoromethylation of Arenes and N-Heteroarenes Using Hypervalent Iodine Reagents. J. Fluorine Chem. *131*, 951.
5. Cui, L., Matusaki, Y., Tada, N., Miura, T., Uno, B., Itoh, A. (2013) Metal-Free Direct C–H Perfluoroalkylation of Arenes and Heteroarenes Using a Photoredox Organocatalyst. Adv. Synth. Catal. *355*, 2203–2207.
6. Li, J., Ballmer, S. G., Gillis, E. P., Fujii, S., Schmidt, M. J., Palazzo, A. M. E., Lehmann, J. W., Morehouse, G. F., Burke, M. D. Synthesis of Many Different Types of Organic Small Molecules Using One Automated Process. Science *347*, 1221–1226.
7. Kobayashi, Y., Kumadaki, I. (1980) Studies on Organic Fluorine Compounds. Part 27. Abnormal Reactions in the Trifluoromethylation of Aromatic Compounds with Trifluoromethyl Iodide and Copper Powder. J. Chem. Soc., Perkin Trans. 1. 661–664.
8. Escudero-Adan, E. C., Grushin, V. V., Martinez Belmonte, M., Tomashenko, O. A. (2011) Simple, Stable, and Easily Accessible Well-Defined CuCF3 Aromatic Trifluoromethylating Reagents. Angew. Chem., Int. Ed. *50*, 7655–7659.
9. Maleckis, A., Sanford, M. S. (2014) Catalytic Cycle for Palladium-Catalyzed Decarbonylative Trifluoromethylation Using Trifluoroacetic Esters as the CF3 Source. Organometallics *33*, 2653–2660.
10. Kholod, I., Vallat, O., Buciumas, A.-M., Neels, A., Neier, R. (2014) Synthetic Strategies for the Synthesis and Transformation of Substituted Pyrrolines as Advanced Intermediates for Rhazinillam Analogues. Eur. J. Org. Chem. 7865–7877.
11. Baar, M., Blechert, S. (2015) Graphitic Carbon Nitride Polymer as a Recyclable Photoredox Catalyst for Fluoroalkylation of Arenes. Chem. Eur. J. *21*, 526–530.
12. Lorance, E. D., Kramer, W. H., Gould, I. R. (2003) Barrierless Electron Transfer Bond Fragmentation Reactions. J. Am. Chem. Soc. *126*, 14071–14078.
13. Shulka, D., Aheard, W. G., Farid, S. (2005) Chain Amplification in Photoreactions of *N*-Alkoxypyridinium Salts with Alcohols: Mechanism and Kinetics. J. Org. Chem. *70*, 6809–6819.
14. Juris, A., Balzani, V., Barigelletti, F., Campagna, S., Belser, P., Von Zelewsky, A. (1998) Ru(II) Polypyridine Complexes: Photophysics, Photochemistry, Electrochemistry, and Chemiluminescence. Coord. Chem. Rev. *84*, 85–277.
15. Kaizu, Y., Ohta,H., Kobayashi, K., Kobayashi, H. (1985) Lifetimes of the Lowest Excited State of Tris(2,2'-bipyridine)ruthenium (II) and its Amphipathic Derivative in Micellar Systems. J. Photochem. *30*, 93–103.
16. Cismesia, M. A., Yoon, T. P. (2015) Characterizing Chain Processes in Visible Light Photoredox Catalysis. Chem. Sci. *6*, 5426–5434.